Ligne InterFaces

Instrument d'étude des Nanostructures sur Surfaces *in situ* ou *in operando* (INS)

Dans de nombreux cas, la compréhension des propriétés physiques (électroniques, magnétiques, photoniques, mécaniques …) spécifiques ou nouvelles des objets contenant des structures à l'échelle nanométrique (nanoparticules, couches minces, interfaces…) requiert la compréhension de leurs propriétés structurales, en particulier durant les différents procédés (élaboration, recuits) nécessaires à leur obtention. L'instrument d'étude des Nanostructures sur Surfaces *in situ* ou *in operando* (INS) a justement pour objectif l'étude de la structure atomique, de la morphologie et de la composition des nanostructures, des surfaces ou des interfaces, en ultra-vide, et de leur évolution soit durant la croissance, soit en fonction de la température, du temps ou du montant déposé. Cet instrument et l'équipe associée ont été pionniers de ce type d'études, en développant et couplant *in situ*, en ultra-vide, *in operando*, des techniques de diffraction aux grands angles (Diffraction en incidence rasante, GIXD, diffraction de surface, SXRD) et aux petits angles (GISAXS, réflectivité) avec la sensibilité sur la composition chimique apportée par la diffusion dite anomale [1,2]. En plus de l'optimisation de ces différentes mesures, nous avons mis un accent tout particulier sur -1- la qualité du vide de base (quelques 10^{-11} mbar), -2- la préparation (four à très haute température, bombardement ionique, recuits sous gaz) et la pré-caractérisation des surfaces (analyse chimique par spectrométrie Auger, analyse cristallographique par diffraction d'électrons), -3- les nombreuse possibilités d'élaboration de nanostructures par épitaxie par jets moléculaire (MBE), -4- l'adjonction récente de la croissance de semiconducteurs par voir chimique (UHV-CVD). Ces développements résultent en un instrument très versatile, permettant d'envisager des études très diverses telles que des transitions solide/liquide [3] ; des études de l'évolution de nanostructures catalyseurs durant une réaction de catalyse [4], ou encore la fabrication et l'étude de composants hybrides, couplant par exemple des oxydes et des semiconducteurs. Ce sont ces spécificités qui rendent encore cet instrument unique [5,6,7] comparé aux autres instruments de diffraction de surfaces sur anneaux synchrotron (comme à SOLEIL ou à l'ESRF) qui utilisent des faisceaux de rayons X plus puissants, mais sont plus limités en termes d'élaborations.

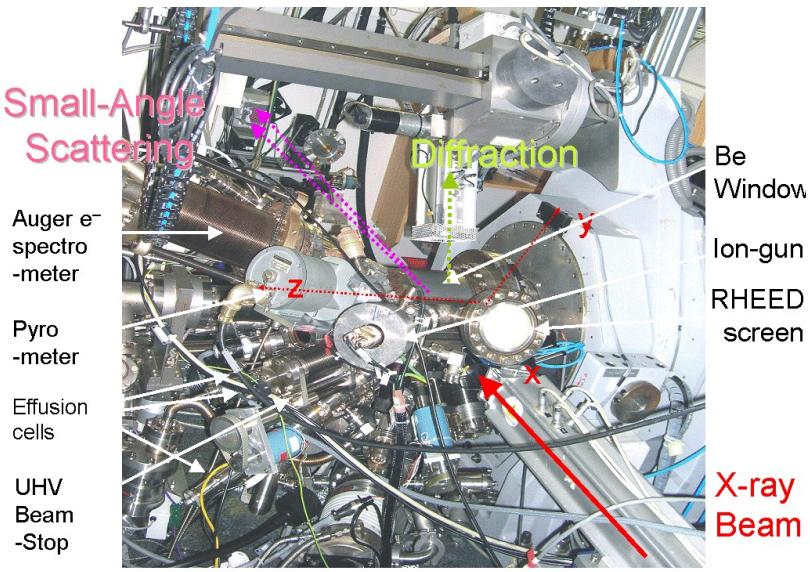

Comme on le devine sur la figure, l'instrument consiste en une chambre ultra-vide avec ses équipements de caractérisation et ses sources, couplée à un gros diffractomètre permettant d'orienter d'une part la

chambre et l'échantillon à l'intérieur de celle-ci par rapport au faisceau incident, d'autre part un détecteur bidimensionnel de dernière génération (type Pixel) sur l'hémisphère supérieure ; le tout localisé en bout de la ligne BM32.
Cet instrument a été développé au cours des années à partir d'une base construite en 1994, pour trouver récemment ses limites en termes de précision, de rapidité, mais aussi de versatilité. Ceci nous a conduit à proposer un projet d'Investissement d'avenir (EquipeX) qui a été accepté, pour remplacer cet instrument par un plus performant, permettant entre autres d'accéder à des temps caractéristiques plus court des différents processus cinétique mis en jeu.

[1] *"Real-Time Monitoring of Growing Nanoparticles*", G. RENAUD, R. LAZZARI, C. REVENANT, A. BARBIER, M. NOBLET, O. ULRICH, F. LEROY, J. JUPILLE, Y. BORENSZTEIN, C.R. HENRY, J.P. DEVILLE, F. SCHEURER, J. MANE-MANE, O. FRUCHART, ***Science* 300**, 1416 (2003).

[2] "*Probing surface and interface morphology with Grazing Incidence Small Angle X-Ray Scattering*" G. RENAUD, R. LAZZARI, F. LEROY, ***Surf. Sci. Rep.* 64,** 255-380 (2009).

[3] *"Substrate-enhanced supercooling in AuSi eutectic droplets"* T.U. SCHÜLLI, R. DAUDIN, G. RENAUD, A. VAYSSET, O. GEAYMOND AND A. PASTUREL, ***Nature*, 464**, 1174 (2010).

[4] *"Shape Changes of Supported Rh Nanoparticles During Oxidation and Reduction Cycles"*, P. NOLTE, A. STIERLE, N. Y. JIN-PHILLIPP, N. KASPER, T. U. SCHULLI, H. DOSCH, ***Science* 321**, 1654 (2008)

[5] *"Relaxation and intermixing behavior in SiGe islands grown on prepatterned Si(001) "* T. U. SCHÜLLI, G. VASTOLA, M.-I. RICHARD, A. MALACHIAS, G. RENAUD, F. UHLÍK, F. MONTALENTI, G. CHEN, L. MIGLIO, F. SCHÄFFLER, AND G. BAUER**, *Phys. Rev. Lett.* 102**, 025502 (2009)

[6] "*Controlling structure and morphology of CoPt nanoparticles through dynamical or static coalescence effects",* J. PENUELAS, P. ANDREAZZA, C. ANDREAZZA-VIGNOLLE, H.C.N. TOLENTINO, M. DE SANTIS, AND C. MOTTET ***Phys. Rev. Lett.* 100**, 115502 (2008)

[7] "*Point defect-induced strains in epitaxial graphene*" N. BLANC, F. JEAN, A. V. KRASHENINNIKOV, J. CORAUX AND G. RENAUD**, *Phys. Rev. Lett*. 111**, 085501 (2013)

Instrument de microdiffraction Laue

L'instrument [1] installé en 2006 et amélioré en 2012 est pour l'instant encore unique en Europe. Il permet d'une part d'étudier des matériaux plus proches des applications (étendant ainsi la gamme d'échantillons étudiés sur la ligne) et d'autre part de réaliser des expériences de recherche fondamentale requérant une résolution latérale sub-micronique. Il est particulièrement bien adapté à une source d'aimant de courbure à l'ESRF.

Parmi les domaines concernés on peut citer les matériaux pour l'énergie (piles à combustible de type oxyde, combustible nucléaire), les circuits intégrés complexes élaborés en microélectronique (interconnexions 2D et 3D), les matériaux de structure (superalliages pour les turbines, alliages à mémoire de forme, aciers pour les canalisations des centrales), et les matériaux en relation avec la biologie (nacre, la toxicité de l'amiante). Pour les études plus fondamentales, on peut citer les tests mécaniques *in situ* sur des micro- ou macro- objets modèles (micro-piliers métalliques découpés par FIB [2], nanofils, whiskers, bicristaux, tricristaux) pour l'étude et la modélisation des propriétés mécaniques des micro et nano objets, et des polycristaux.

La microdiffraction Laue emploie un micro-faisceau (taille inférieure à 0.5x0.5 µm) de rayons X à large spectre (bande en énergie correspondante 5-22 keV). La géométrie de détection en réflexion permet de couvrir un grand angle solide autour des angles de diffraction de 90 degrés. En déplaçant l'échantillon, sont menées des cartographies à deux dimensions de la région proche de la surface (profondeur d'analyse de quelques 10 µm à quelques mm). Le

traitement des données détermine en tout point de la cartographie l'orientation et la forme (tenseur déviatorique des déformations) de la maille cristalline. L'utilisateur peut observer et sélectionner une région particulière de l'échantillon grâce à un microscope optique (x50) et la mesure du signal de fluorescence.

L'instrument permet donc pour les matériaux polycristallins de localiser les régions où se concentrent les contraintes et les défauts cristallins qui peuvent être induits soit par les procédés d'élaboration du matériau (cristallisation, mise en forme) soit par un test réalisé *in situ* (mécanique, thermique ou électrique).

Des analyses plus fines peuvent aussi être menées en quelques points sélectionnés à l'aide de mesures complémentaires déterminant: le profil des grandeurs physiques en fonction de la profondeur dans l'échantillon (méthode à balayage d'un fil absorbant), et le volume de la maille cristalline et densité de certains défauts cristallins (méthode avec monochromateur diamant [3]).

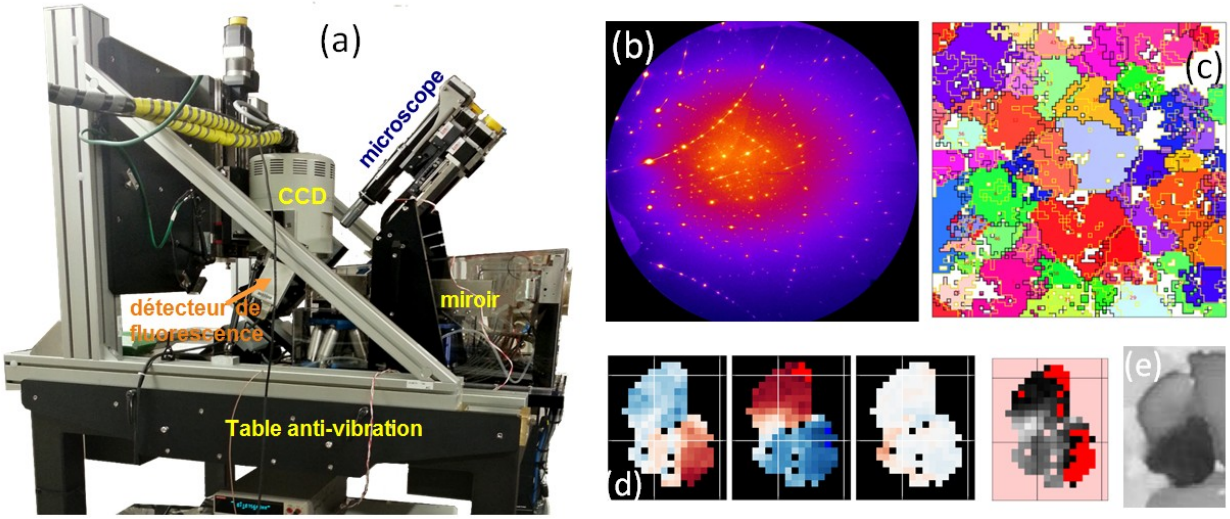

(a) Principaux éléments de l'instrument de micro-Laue. (b) Diagramme de Laue d'un polycristal (c) Cartographie d'orientation d'un polycristal (pas de 5 µm), (d) désorientations intra-grain dans un grain de CdTe, et (e) la densité de courant locale dans ce grain mesurée par EBIC (electron-beam-induced-current).

"A new white beam x-ray microdiffraction setup on the BM32 beamline at the European Synchrotron Radiation Facility", O. Ulrich, X. Biquard, P. Bleuet, O. Geaymond, P. Gergaud, J.-S. Micha, O. Robach, F. Rieutord, Rev. **Sci. Instr. 82** (2011) 033908.

"In situ µLaue: Instrumental setup for the deformation of micron sized sample", Kirchlechner C., Keckes J., Micha J.-S. and Dehm G. **Advanced Engineering Materials, 13** (2011) 837.

"A tunable multicolour 'rainbow' filter for improved stress and dislocation density field mapping in polycrystals using X-ray Laue microdiffraction", O. Robach, J.S. Micha, O. Ulrich, O. Geaymond, O. Sicardy, J. Härtwig, F. Rieutord **Acta Cryst. A. 69** (2013) 164-170, arxiv.org/pdf/1207.2868

"From metastable to stable modifications—in situ Laue diffraction investigation of diffusion processes during the phase transitions of (GeTe)nSb2Te3 (6 <= n <= 15) crystals" M. N. Schneider, X. Biquard, C. Stiewe, T. Schröder, P. Urban and O. Oeckler **Chemical Communications 48** (16) 2192-2194 (2012)

"Full local elastic strain tensor from Laue microdiffraction: simultaneous Laue pattern and spot energy measurement" O. Robach, J.-S. Micha, O. Ulrich and P. Gergaud **J. Appl. Cryst.. 44** p 688–696 (2011)

Goniomètre multi-technique (GMT)

Cet instrument robuste est en service depuis le début d'exploitation de la ligne pour l'étude des surfaces, interfaces et couches minces. Sa spécificité est son grand espace autour de l'échantillon, qui permet d'accueillir toutes sortes d'environnements construits par les utilisateurs, du plus simple (enceinte à atmosphère contrôlée) au plus complexe (réacteur pour la catalyse connecté à une chambre ultra-vide). L'utilisation de la partie haute énergie du spectre de la ligne permet l'étude des interfaces « enterrées » type solide/liquide ou solide/solide.

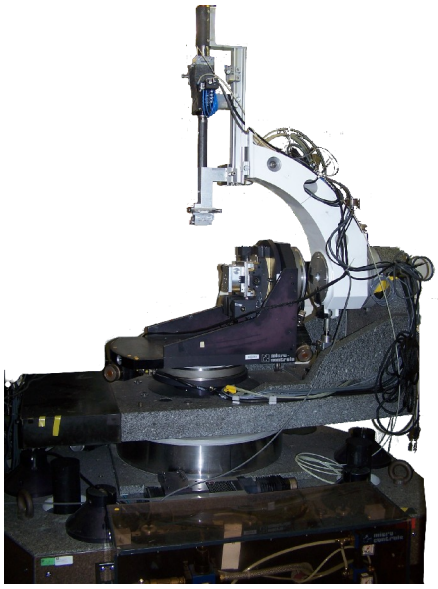

Instrument GMT

Les domaines d'application sont variés : on peut citer notamment la microélectronique (interconnexions, interfaces obtenues par collage moléculaire, couches minces de cristaux liquides, effets de l'implantation ionique), la microfluidique (interaction d'un liquide avec des micro-canaux), la catalyse (étude in operando de catalyseurs modèles formés de nanoparticules pour les réactions en phase gazeuse), et les matériaux pour l'énergie (gonflement d'une membrane polymère d'une pile à combustible, interfaces électrode/solution dans les batteries).

Des études plus fondamentales, potentiellement intéressantes pour l'agro-alimentaire, la cosmétique, la géochimie ou le nucléaire, sont également menées (compression d'une couche mince moléculaire en surface d'un liquide, modification des surfaces de minéraux en présence d'un liquide, formation de couches intermédiaires à l'interface entre deux liquides).

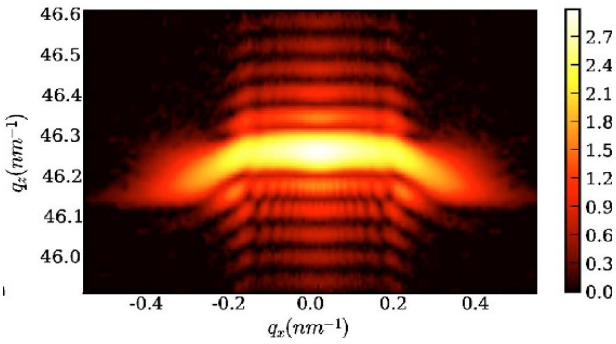

Cartographie du réseau réciproque autour du pic de diffraction (004) du silicium mesurée sur un réseau de lignes contraintes de Silicon-On-Isolator (SOI).

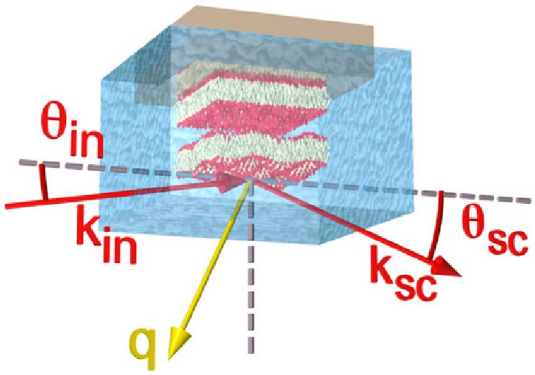

Configuration expérimentale pour les mesures de réflectivité spéculaire et hors spéculaire à haute énergie (27 keV) déterminant les grandeurs de gonflement et d'ondulation d'une membrane plongée dans une solution.

L'instrument utilise un faisceau de rayons X monochromatique de taille sub-millimétrique (0.2x0.3 mm), qui peut monter à 30keV pour l'étude des interfaces enterrées. Les rayons X envoyés sur l'échantillon éventuellement en incidence rasante pour augmenter la sensibilité à la surface sont soit : 1) réfléchis (réflectivité) fournissant épaisseurs et densités

des couches composant la structure, et la rugosité des interfaces, 2) diffusés aux petits angles (GISAXS) apportant la morphologie des couches (tailles, forme et organisation des particules), et 3) diffractés aux grands angles (XRD) permettant de déterminer la structure et l'orientation de composés cristallins ou amorphes sous forme de poudre, de film mince ou d'objets nanométriques. L'instrument peut réaliser des cartographies du réseau réciproque et mesurer la diffusion diffuse autours des pics de diffraction pour la détermination des déformations et des défauts présents dans les matériaux appliqués de la recherche amont.

"Effect of H-implantation in the local elastic properties of silicon crystals" S. Reboh, F. Rieutord, L. Vignoud, F. Mazen, D. Landru, M. Zussy, and C. Deguet Appl. **Phys. Lett. 103**, 181911 (2013)

"Controlling Interactions in supported bilayers from weak electrostatic repulsion to high osmotic pressure" A. Hemmerle, L. Malaquin , T. Charitat,, S. Lecuyer, G. Fragneto and J. Daillant **Proc. Nat. Acad. Sciences USA 109 (49)** 19938-19942 (2012)

"M-plane core-shell InGaN/GaN multiple-quantum-well on GaN wires for electroluminescent device" R. Koester, J. S. Hwang, D. Salomon, X. Chen, C. Bougerol, J.-P. Barnes, D. Le Si Dang, L. Rigutti, M. Tchernycheva, C. Durand and J. Eymery **Nano Letters 11**, p 4839-4845 (2011)

"Size and Catalytic Activity of Supported Gold Nanoparticles: An in operando Study During CO Oxidation" I. Laoufi, M.-C. Saint-Lager, R. Lazzari, J. Jupille, O. Robach, S. Garaudee, G. Cabailh, P. Dolle, H. Cruguel, A. Bailly J. **Phys. Chem. C 115** (11) pp 4673-4679 (2011)

"In situ grazing-incidence X-ray diffraction during electrodeposition of birnessite thin films: Identification of solid precursors" M. Ndjeri, S. Peulon, M.L. Schlegel, A. Chaussé **Electrochem. Commun. 13**, (5) p 491-494 (2011)

1 INTRODUCTION

En 2013 la ligne de lumière CRG/IF a délivré du temps de faisceau pour 28 expériences officielles sélectionnées par les comités de programmes français et internationaux. En plus de ces expériences d'une durée moyenne de 6 jours, 10 expériences, généralement plus courtes, pour les programmes de recherche interne, et 9 expériences pour le développement des méthodes instrumentale ont été réalisées. Cela représente environ 5000 h de fonctionnement sans panne majeure. Le chapitre 5 de ce rapport détaille l'utilisation de la ligne et en précise le contexte d'utilisation.

La production scientifique reste pratiquement constante en nombre par rapport aux années précédentes avec 20 publications, et un facteur d'impact moyen de 4.5 ; les chapitres 4 et 7 présentent respectivement la synthèse et la liste de publications.

Sur le plan technique, nous avons avancé, d'une part sur le projet EquipeX consistant à concevoir une nouvelle chambre UHV et le diffractomètre associé, et d'autre part sur l'instrument de micro-diffraction en faisceau blanc. Sur le premier projet les deux éléments principaux sont commandés et seront livrés en fin d'année, pour une mise en service et une ouverture aux utilisateurs mi-2015. Les développements sur la micro-diffraction portent eux principalement sur les techniques de mesures et d'analyse. Tout cela est développé de manière précise dans le chapitre 2 de ce rapport.

Le personnel impliqué sur la ligne reste le même que l'année précédente, et si l'on note que l'effectif pour faire fonctionner et développer l'instrument de micro-diffraction est suffisant (1 ingénieur de recherche CNRS, 1 ingénieur-chercheur CEA) il faut aussi souligner que le personnel pour exploiter et développer l'instrument UHV-CVD est nettement insuffisant (1 technicien CNRS, 1 ingénieur-chercheur CEA, ½ chercheur CNRS) vues la complexité de l'instrument et l'ampleur du projet en cours.

Afin d'illustrer l'activité de la ligne, nous présentons au chapitre 3, pour chaque instrument, un résumé de quelques expériences effectuées cette année.

2 Activité scientifique

2.1 Résumé activité goniomètre multitechnique et micro-diffraction

Le temps de faisceau d'août 2012 à octobre 2013 dans la cabane GMT a été partagé entre des expériences avec le goniomètre multitechnique et en majorité avec l'instrument de microdiffraction Laue.

Goniomètre Multitechnique

Les expériences avec le goniomètre ont été menées par deux équipes du CEA-Grenoble, animées par F. Rieutord et G. Gébel, et une équipe du CNRS de Grenoble. F . Rieutord *et al* ont déterminé l'effet de la fluence de l'implantation en ion Helium sur les déformations de wafers de Silicium. Dans le cadre général de l'amélioration du procédé smartCut, ces mesures pourraient provenir d'une modification des propriétés élastiques du matériau plutôt que de la présence de défauts cristallins (voir plus bas). Dans la thématique des batteries au lithium, comme l'année précédente, G. Gébel *et al* ont mesuré *in situ* par réflectivité des rayons X l'intercalation des atomes de lithium dans l'électrode de Si provoquant le gonflement et l'augmentation de la rugosité de la surface. D'autres investigations sur des systèmes modèles sont programmées dans le cadre du projet européen BACCARA qui a débuté officiellement en Novembre 2013. A. Bailly *et al* ont étudié l'effet de la taille et de la composition en Palladium sur l'efficacité catalytique pour l'hydrogénation du butadiène de nanoparticules d'Or-Palladium. L'équipe a utilisé la chambre à réaction catalytique spécialement conçue pour BM32 pour des mesures in situ de diffraction aux grands et aux petits angles.

Microdiffraction

L'équipe autrichienne et allemande (Kirchlechner et al), habituée à utiliser l'instrument de microdiffraction pour comprendre les propriétés mécaniques fondamentales à l'échelle micrométrique, a réalisé deux expériences cette année: l'une a consisté, lors d'un essai de fatigue plastique à suivre *in situ* l'évolution du comportement mécanique macroscopique (augmentation de la raideur et de la fragilité) et à la corréler à la localisation microscopique et la densité des dislocations. L'objectif de l'autre expérience a été de quantifier l'intensité de l'effet Bauschinger qui est la modification de la limite élastique d'un matériau polycristallin lors du changement de sens de la sollicitation, en raison d'un empilement des dislocations aux joints de grains. Pour cela, des éprouvettes modèles microscopiques ont été taillées (par faisceau d'ions) dont certaines autour d'un joint de grains. Une autre équipe française de Poitiers (P.O. Renault *et al*) s'est intéressée aux mécanismes de déformations des semiconducteurs (pour l'opto et la micro-électronique) en cartographiant des piliers d'InP dont ils avaient enregistré in situ, pendant la compression, la courbe contrainte-déformation et l'image de la surface.

Pour étudier des objets plus courants (sans préparation ni mise en forme préalable), l'équipe de T. Cornelius *et al* dans le cadre de l'ANR Mecanix a continué à développer le

système d'AFM portable (d'une ligne de lumière à l'autre) et à sélectionner et caractériser sur BM32 les les nanofils les mieux adaptés pour un futur test mécanique avec une pointe AFM.

P. Bleuet *et al* (CEA-Grenoble) ont effectué une reconstruction 3D des grains de Cuivre formant une interconnexion pour intégration verticale de la micro-électronique (TSV) par tomographie-Laue. Ils ont mis en évidence la présence d'une lacune de cuivre expliquant la baisse de fiabilité. S. Hall *et al* de l'université de Lund (Suède) ont réalisé une première expérience probante sur des whiskers d'étain en surface d'un polycristal de bronze. Ils ont validé le fait que l'utilisation de deux techniques complémentaires de microdiffraction Laue (résolution en profondeur et détermination du tenseur complet des déformations) devrait permettre de mieux comprendre la relation entre la croissance des monocristaux (par diffusion des atomes d'étain) et les gradients des déformations dans le polycristal de bronze.

2.2 Résumé de l'activité INS (In situ Nanostructure growth on Surfaces) d'étude in situ de nano-objets durant leur croissance sur des surfaces

Durant cette année 2013, l'utilisation de l'instrument d'étude *in situ* de nanoobjets durant leur élaboration sur des surfaces s'est recentrée autour de quelques thématiques principales :

-des études de GISAXS/GIXD couplées durant des réactions en voie gazeuse catalysées par des nanoparticules d'alliage AuCu déposées sur une substrat de TiO_2 ; études amont de celles réalisées à plus fortes pressions de gaz (G. Prévot et al., INSP Paris) ;

-des études de la relaxation au bord de marches de surfaces de silicium vicinales, permettant de tester les modèles théoriques correspondants (F. Leroy et al., CINAM Marseille) ;

-des études de l'équipe CNRS/INéel (Maurizio De Santis) de films ultra-minces composés d'une couche ferromagnétique et une antiferromagnétique (e.g. CoO), avec l'objectif de corréler croissance et structure observées par diffraction X sur BM32 avec les propriétés mesurés *ex situ* par rotation Kerr magnéto-optique.

-des études par l'équipe locale CEA (Gilles Renaud et Fabien Jean), en collaboration avec le CNRS/INéel (Johann Coraux) de la structure et de son évolution en température, de films de graphène épitaxiés sur surfaces métalliques (Gr/Ir(111)), et de la structure et de la morphologie de plots métalliques (Pt, CoPt, Au, Ir) organisés durant leur croissance sur graphène épitaxié ;

-dans la continuité de l'étude précédente, une collaboration entre l'équipe locale CEA-Grenoble, Institut Néel CNRS et l'Institut Lumière Matière de l'Université de Lyon a permis une première étude montrant l'organisation et l'épitaxie d'agrégats de Pt préformés sur le moiré de graphène sur Ir(111) ;

-enfin une partie significative du temps disponible a été utilisée pour poursuivre les études in operando relatives à la croissance in situ de nanofils de Ge/Si par croissance par voie chimique en ultra-vide (UHV-CVD). Le temps d'incubation entre l'exposition du catalyseur au gaz réactif et le début de la croissance a été étudié systématiquement en fonction de la taille du catalyseur, de la température et du flux gazeux, donnant des informations cinétiques. La contrainte et le profil de composition ont été étudiés dans des nanofils cœur-coquille GeSi durant la croissance de la coquille (Ge cœur Si ou coquille Si cœur Ge).

Afin d'illustrer l'activité scientifique sur l'instrument INS, nous avons sélectionné quelques résultats, présentés ci-dessous.

Remarquons que les études sur l'instrument INS ont fait l'objet d'un article de vulgarisation dans un numéro des Reflets de la Physique (couplé avec un numéro du Bulletin des professeurs de Physique/Chimie), dédié aux études à l'aide du rayonnement synchrotron. La page de garde ci-dessous montre une photographie du coeur de l'instrument INS actuel, avant donc sa rénovation dans la cadre du projet EquipEX INS-2.

3 Publications

Nombre de publications (avec comité de lecture) par année, avec en moyenne un facteur d'impact supérieur à 3.

2013	20	[4.5]
2012	23	[3.3]
2011	25	[3.6]

Articles publiés depuis trois ans (2011-2013) classés par leur facteur d'impact (>2) sur les cinq dernières années:

Acta Cryst. A	30.6	1
Nano Letters	14.1	1
Proc. Nat. Acad. Sci. USA	10.6	1
Phys. Rev. Lett.	7.4	1
Chem. Comm.	6.2	1
J. Phys. Chem	**5.2**	**3**
Elect. Comm.	5.0	1
J. Appl. Cryst.	**4.5**	**4**
Acta Mater.	**4.4**	**3**
Faraday Disc.	4.1	2
Nanotechnology	4.0	1
Appl. Phys. Lett.	**3.8**	**8**
Phys. Rev. B	**3.4**	**11**
J. Elect. Soc.	**2.8**	**3**
Nanoscale Res. Lett	2.5	1
Eur. Biophys. J.	2.4	1
J. Appl. Phys.	**2.2**	**8**

Articles les plus cités depuis 5 ans

[22.3] (138) *Probing surface and interface morphology with Grazing Incidence Small Angle X-Ray Scattering*
G. Renaud, R. Lazzari and F. Leroy
Surf. Sci. Rep. 64 pp 255-380 (2009)

[7.4] (59) Enhanced Relaxation and Intermixing in Ge Islands Grown on Pit-Patterned Si(001) Substrates
T. U. Schülli, G. Vastola, M.-I. Richard, A. Malachias, G. Renaud, F. Uhlik, F. Montalenti, G. Chen,
L.Miglio, F. Schäffler, G. Bauer
Phys. Rev. Lett. 102, 025502 (2009)

[4.0] (41) Nucleation mechanism of GaN nanowires grown on (111) Si my molecular beam epitaxy
O. Landré, C. Bougerol, H. Renevier and B. Daudin
Nanotechnology 20 415602 (2009)

[5.2] (27) *Size and Catalytic Activity of Supported Gold Nanoparticles: An in operando Study During CO Oxidation*
I. Laoufi, M.-C. Saint-Lager, R. Lazzari, J. Jupille, O. Robach, S. Garaudee, G. Cabailh, P. Dolle, H. Cruguel, A. Bailly
J. Phys. Chem. **C 115** (11) pp 4673-4679 (2011)

[36.2] (26) *Substrate-enhanced supercooling in AuSi eutectic droplets*
T.U. Schülli, R. Daudin, G. Renaud, A. Vaysset, O. Geaymond and A. Pasturel,
Nature **464**, 1174 (2010)

[3.4] (23) Adhesion of growing nanoparticles at a glance: Surface differential reflectivity spectroscopy and grazing incidence small angle x-ray scattering
R. Lazzari, G. Renaud, C. Revenant , J. Jupille and Y. Borensztein
Phys. Rev. B 79, 125428 (2009)

Articles les plus cités depuis 3 ans:

[5.2] (27) *Size and Catalytic Activity of Supported Gold Nanoparticles: An in operando Study During CO Oxidation*
I. Laoufi, M.-C. Saint-Lager, R. Lazzari, J. Jupille, O. Robach, S. Garaudee, G. Cabailh, P. Dolle, H. Cruguel, A. Bailly
J. Phys. Chem. **C 115** (11) pp 4673-4679 (2011)

[1.5] (15) *Dislocation storage in single slip-oriented Cu micro-tensile samples: New insights via X-ray*
microdiffraction
C. Kirchlechner, D. Kiener, C. Motz, S. Labat, N. Vaxelaire, O. Perroud, J. -S. Micha, O. Ulrich, O.
Thomas, G. Dehm, and J. Keckes
Phil. Mag. **91** (7-9) Special Issue p 1256-1264 (2011)

[5.2] (11) *Competition between polar and nonpolar growth of MgO films on Au(111)*
S. Benedetti , N. Nilius, P. Myrach, P. Torelli, G. Renaud, H.-J. Freund, S. Valeri
J. Phys. Chem. **C 115,** 23043 (2011)

[1.7] (11) *A new white beam x-ray microdiffraction setup on the BM32 beamline at the European Synchrotron Radiation Facility*
O. Ulrich, X. Biquard, P. Bleuet, O. Geaymond, P. Gergaud, J. S. Micha, O. Robach, and F. Rieutord
Rev. Sci. Instrum. **82**, 033908 (2011)

[2.2] (8) *Structural and optical analyses of GaP/Si and (GaAsPN/GaPN)/GaP/Si nanolayers for integrated photonics on silicon*

T. Nguyen Thanh, C. Robert, W. Guo, A. Letoublon, C. Cornet, G. Elias, A. Ponchet, T. Rohel, N. Bertru, A. Balocchi, O. Durand, J.-S. Micha, M. Perrin, S. Loualiche, X. Marie and A. Le Corre
J. Appl. Phys. **112**, 053521 (2012)
Publisher erratum: J. Appl. Phys. **112**, 079904 (2012)

4 Statistiques d'utilisation du temps de faisceau

Les données présentées sont relatives aux expériences allouées sur BM32 sur les périodes couvertes par les comités de programmes d'octobre 2012 et avril 2013 et donc planifiées entre le 01/03/2013 et le 28/02/2014. Le comité Français a alloué 240 shifts de 8 heures et le comité international de l'ESRF 145 shifts.

La figure 1 présente le nombre de shifts demandés et alloués sur la période d'exploitation. Le rapport du temps demandé sur le temps attribué est de 1.3 sur le comité français et 3.3 sur le comité international, pour un taux de pression global de 2.1. La tendance est à une stagnation de la pression sur le comité français et une augmentation sur le comité international. La répartition du temps de faisceau sur les trois instruments est donnée sur la figure 2. On constate l'équilibre entre les deux cabanes d'expérience INS et GMT, cette dernière accueillant le goniomètre multi-technique et l'instrument de micro-diffraction en faisceau blanc.

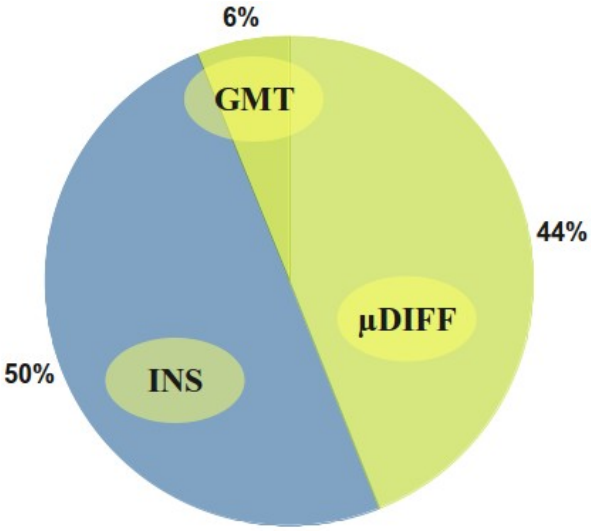

Figure 1 : Nombre de shifts demandés et alloués par les comités de programmes du 10/2012 et 4/2013

Figure 2 : Répartition par instrument des shifts alloués par les comités GMT : goniomètre multi-technique, INS : In Situ nanostructure Surface, µdiff : micro diffraction Laue.

La répartition par comité de programme (figure 3) indique toujours la prépondérance des sciences des Surfaces et Interfaces (SI) pour lesquelles la ligne BM32 est optimisée. Si

100% des expériences sur l'instrument INS concernent ce domaine, le goniomètre multi-technique de par sa flexibilité, reçoit lui des expériences plus variées retenues par les comités SI et MA (Engineering Matériaux appliqués). L'installation de micro-diffraction répond uniquement à des problématiques de MA (mécanique fondamentale, métallurgie) grâce sa capacité à mesurer des déformations à l'échelle sub-micronique.

Figure 3 : Répartition par comité de programme (équivalent ESRF) des expériences réalisées sur BM32 CRG-IF

SI: Surface and Interface

MA: Applied Materials Engineering + Instrumental

Figure 4 : Répartition du temps de faisceau par le laboratoire d'origine des utilisateurs pour les expériences réalisées sur BM32 CRG-IF.

CEA : DEN+DRT+DSM

CNRS/Univ :CNRS + Université,

UE : International (Allemagne, Autriche, Suède).

La figure 4 présente l'origine des utilisateurs classée selon 3 catégories. La part internationale, très majoritairement de l'Union Européenne, prouve une fois de plus la pertinence des choix faits sur BM32 ces dernières années pour développer une instrumentation performante. L'instrument de micro-diffraction en faisceau blanc reste à ce jour unique en Europe et attire une majorité de groupe de recherche étrangers. Le cloisonnement entre CEA et CNRS n'est qu'apparent puisque plusieurs équipes mixtes ont été accueillies cette année. Enfin pour compléter, le figure 6 montre l'ancrage de la ligne Interface dans le milieu grenoblois, avec une utilisation majoritaire de 50 % (CEA/INAC, LITEN, LETI, CNRS/Institut Néel).

Ligne InterFaces

1 INTRODUCTION

En 2013 la ligne de lumière CRG/IF a délivré du temps de faisceau pour 28 expériences officielles sélectionnées par les comités de programmes français et internationaux. En plus de ces expériences d'une durée moyenne de 6 jours, 10 expériences, généralement plus courtes, pour les programmes de recherche interne, et 9 expériences pour le développement des méthodes instrumentales ont été réalisées. Cela représente environ 5000 heures de fonctionnement sans panne majeure. Le chapitre 5 de ce rapport détaille la répartition du temps de faisceau en fonction des thématiques scientifiques et de l'origine des utilisateurs.

La production scientifique reste pratiquement constante en nombre par rapport aux années précédentes avec 20 publications, et un facteur d'impact moyen de 4.5 ; les chapitres 4 et 7 présentent respectivement la synthèse et la liste de publications.

Sur le plan technique, nous avons avancé, d'une part sur le projet EquipeX consistant à concevoir une nouvelle chambre UHV et le diffractomètre associé, et d'autre part sur l'instrument de micro-diffraction en faisceau blanc. Sur le premier projet les deux éléments principaux sont commandés et seront livrés en fin d'année, pour une mise en service et une ouverture aux utilisateurs mi-2015. Les développements sur la micro-diffraction portent eux principalement sur les techniques de mesures et d'analyse. Tous les développements sont précisés dans le chapitre 2 de ce rapport.

Le personnel impliqué sur la ligne reste le même que l'année précédente, et si l'on note que l'effectif pour faire fonctionner et développer l'instrument de micro-diffraction est suffisant (1 ingénieur de recherche CNRS, 1 ingénieur-chercheur CEA) il faut aussi souligner que l'effectif du personnel en charge d'exploiter et développer l'instrument UHV-CVD est nettement insuffisant (1 assistant ingénieur CNRS, 1 ingénieur-chercheur CEA, ½ chercheur CNRS) compte tenu de la complexité de l'instrument et l'ampleur du projet en cours.

Afin de décrire l'activité de la ligne, nous présentons au chapitre 3, pour chaque instrument, un résumé de quelques expériences effectuées cette année.

2 Développements techniques

2.1 Projet EquipeX CRG/F : INS2

Un élément majeur du projet EquipeX CRG/F, nommé INS-2, consiste à développer un nouvel ensemble diffractomètre + chambre ultra-vide pour remplacer le cœur de l'instrument INS. L'équipe projet est constituée de Gilles Renaud et Olivier Ulrich du CEA/INAC; de Dominique Grand et Philippe Jeantet du CNRS/SERAS, et de Olivier Geaymond et Maurizio de Santis, de l'Institut Néel / CNRS.

Les principes guidant ce projet sont:

-1- Une chambre ultra-vide plus versatile, se rapprochant encore plus d'une MBE, comportant un grand nombre de sources et d'instruments de caractérisation, permettant de minimiser les ouvertures/étuvages et offrant de nouvelles possibilités d'élaboration;

-2- Une conservation des trois techniques principales (GISAXS, GIXD et Réflectivité) couplées pour caractériser les nanomatériaux durant leur élaboration, en les améliorant;

-3- Une possibilité d'accélérer les mesures afin d'étudier des croissances (de boîtes quantiques, de nanofils etc.…) par MBE ou CVD en temps réel, à l'échelle de la seconde, c'est-à-dire 10 à 100 fois plus rapidement qu'actuellement.

La pré-étude, démarrée au printemps 2012, s'est terminée en juillet 2013 par les appels d'offre de la chambre et du diffractomètre.

Nous avons dans un premier temps cherché des solutions complètement nouvelles, pour finalement aboutir à un projet similaire sur le principe à l'instrument actuel, mais comprenant un grand nombre d'améliorations.

Parmi celles-ci, la fenêtre de béryllium d'entrée (Fig. 2a) est à présent fixe, monocristalline et éloignée de la chambre (Fig. 1), ce qui devrait permettre de pratiquement annuler le bruit de fond induit par la diffusion aux petits angles par cette fenêtre. Elle est suivie de fentes en ultra-vide pour parfaire l'élimination du fond diffus, puis d'un long soufflet (Fig. 2a), permettant d'accommoder le mouvement de définition de l'angle d'incidence (Fig. 2b). Deux fenêtres de béryllium sont prévues en sortie, l'une pour la diffraction aux grands angles ; l'autre pour la diffusion aux petits angles (GISAXS et réflectivité). Cette dernière fenêtre est également éloignée de la chambre, ce qui permet d'éloigner le « puits» d'arrêt du faisceau direct, diminuant ainsi drastiquement l'angle mort de part et d'autre de l'origine, et donc d'augmenter significativement la taille des objets étudiés.

La plupart des sources d'épitaxie par jets moléculaires et des instruments développés au cours des années précédentes peuvent être montés simultanément sur la chambre ultra-vide, plus grande que la précédente, de même que des outils supplémentaires, tels que des écrans pour le faisceau X diffusé ou pour les jets moléculaires, des pyromètres couvrant toute la gamme de température de 500 K à 1800 K ou encore des outils de polarisation de l'échantillon. Nous réutiliserons le four développé ces dernières années, qui donne entière satisfaction.

La chambre ultra-vide (voir figure 1) avec ses fenêtres de béryllium soudées par bombardement électronique, cœur de l'instrument, a été commandée en octobre à la firme

Matrion/Electrofusion en Californie, seule à maîtriser les technologies requises pour la soudure d'une feuille mince de béryllium sur une enceinte aussi complexe.

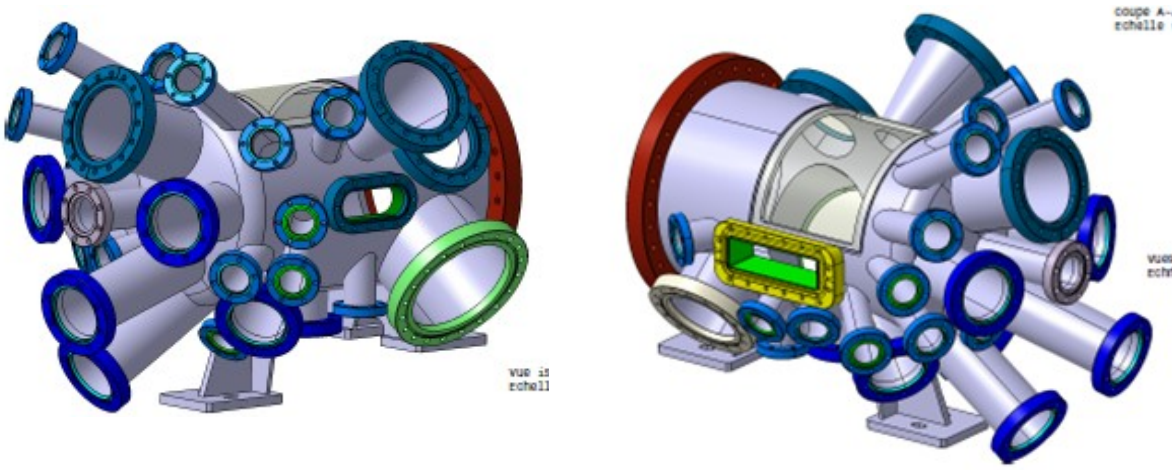

Figure 1 : Chambre ultra-vide en cours d'étude

L'appel d'offre pour le diffractomètre a également été conclu en octobre 2013 par le choix de la firme française Symétrie, spécialiste des hexapodes. Le support et l'alignement de l'échantillon sont justement réalisés par un hexapode, qui doit en sus entrainer un passage tournant à pompage différentiel permettant de transmettre en ultra-vide une rotation azimuthale de l'échantillon de haute précision. La proposition de Symétrie l'a emporté sur cette de Microcontrôle principalement du fait d'un bien meilleure prise en compte des spécificités de cet instrument, telles qu'un accès aisé à la chambre ultra-vide et à ses équipements.

L'ensemble chambre ultra-vide et goniomètre est représenté en figure 2 sur laquelle certains éléments sont indiqués.

L'année 2014 sera consacrée à l'étude détaillée de l'ensemble ainsi qu'à l'ajout de certains éléments essentiels.

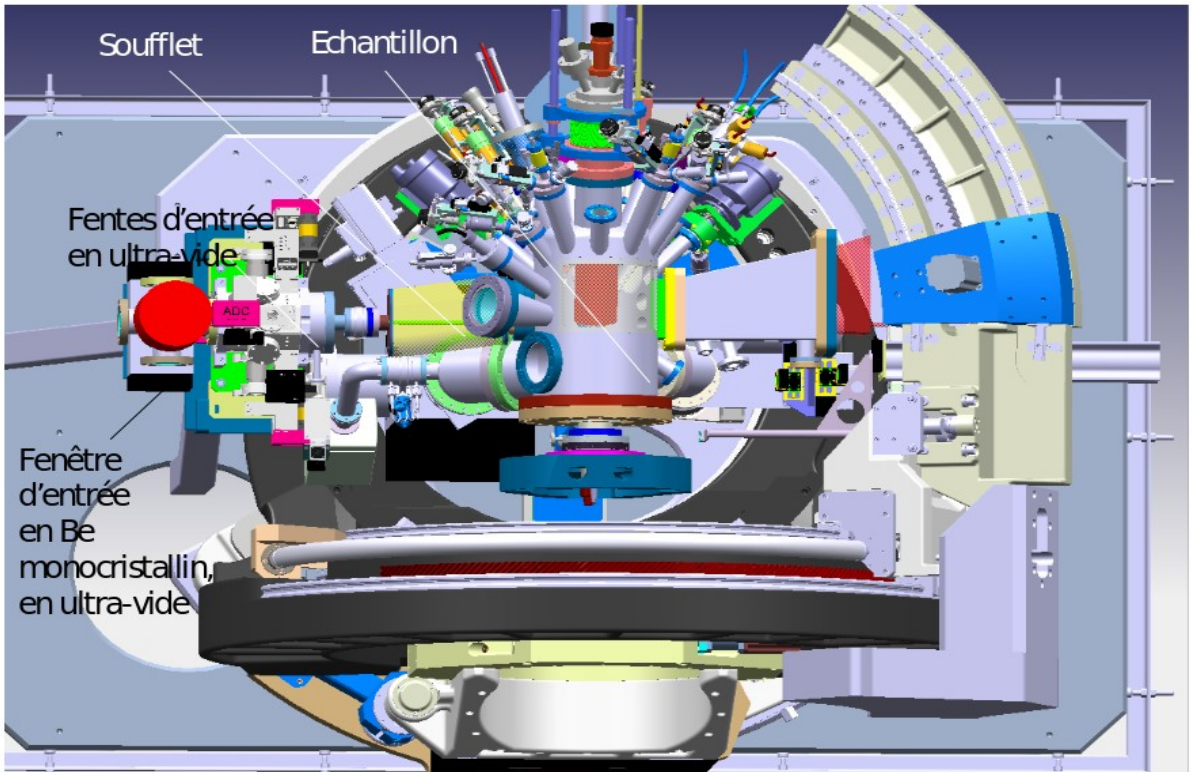

Figure 2a : Représentation 3D de l'ensemble INS-2 vu du dessus. Elle fait apparaître à gauche les fenêtres et fentes d'entrée et au centre la chambre ultra-vide avec ses fenêtres de béryllium. Cette chambre ultra-vide est équipée de nombreux instruments de caractérisation parmi lesquels un RHEED (diffraction d'électrons de haute énergie en incidence rasante), un spectromètre Auger (pour l'analyse chimique de la surface), et des sources d'élaboration par voie gazeuse ou par évaporation physique. Les rayons X diffractés aux grands angles sortent de la chambre par la grande fenêtre de Be soudée dessus, alors qu'une seconde fenêtre de Be, plus éloignée de l'échantillon, permet des mesures aux petits angles optimisées.

L'échantillon est entraîné en rotation par un cercle d'axe horizontal portant un hexapode (dont seul le plateau côté chambre est représenté) portant lui-même l'échantillon. Ce cercle est amovible grâce à un système de pivot, permettant ainsi un accès facilité à la chambre pour les maintenances.

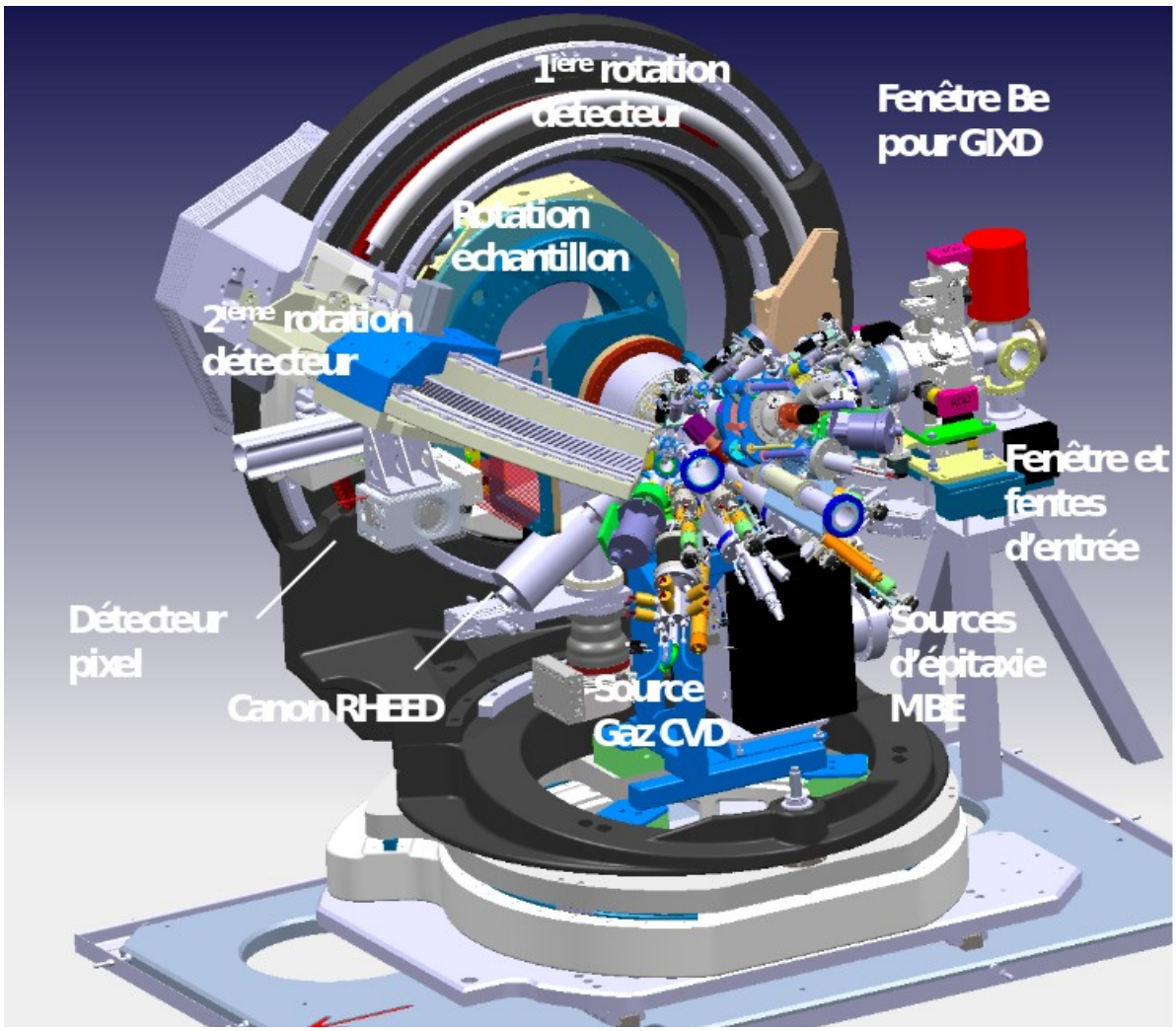

Figure 2b : Vue en 3D de l'ensemble INS-2 faisant apparaître la chambre ultra-vide équipée, et intégrée au goniomètre. Celui-ci possède quatre mouvements principaux : une rotation de l'ensemble autour d'un axe vertical pour définir l'angle d'incidence du faisceau par rapport à la surface verticale de l'échantillon. Cette rotation emporte une rotation de l'échantillon autour d'un axe horizontal et 2 rotations du détecteur.

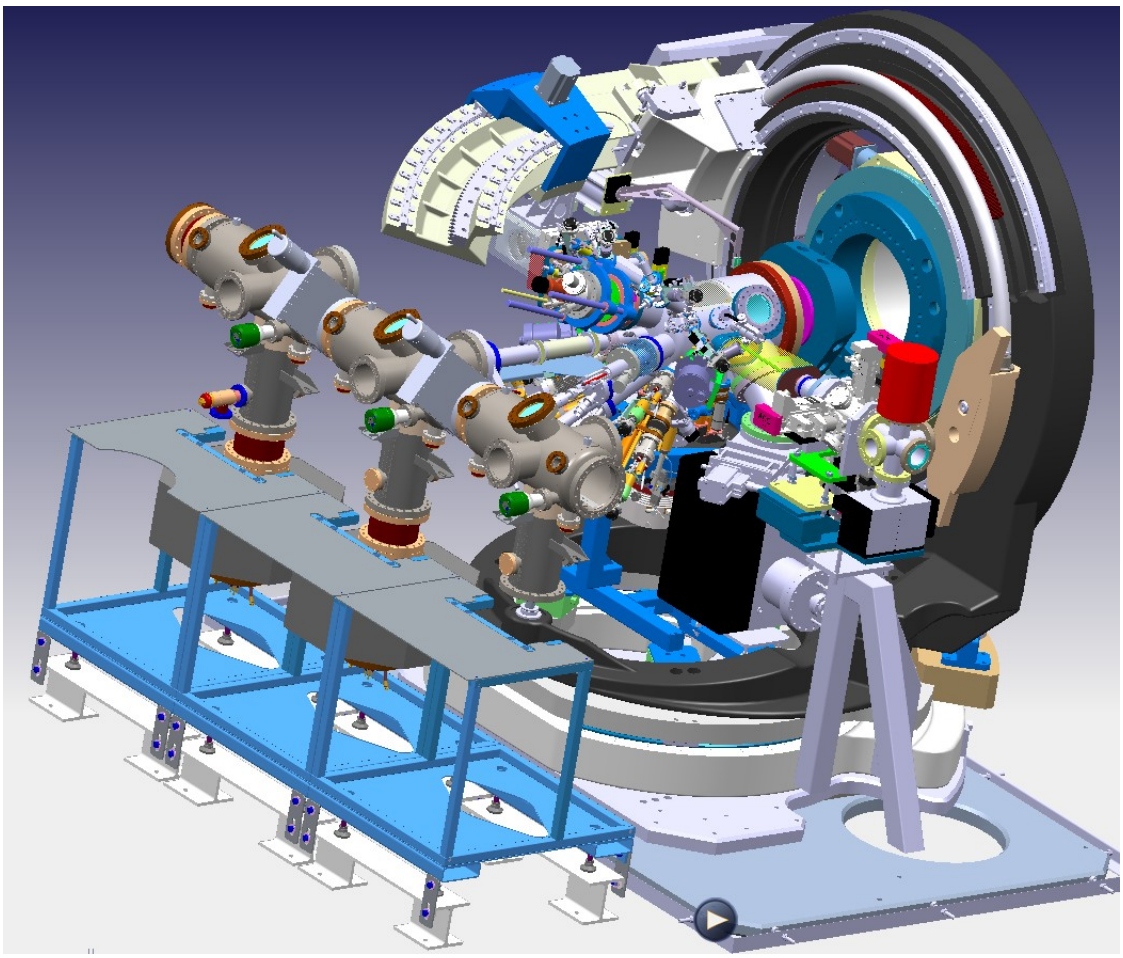

Figure 2c :Vue en 3D de l'ensemble INS-2 avec son système d'introduction d'échantillons.

2.2 Micro-Diffraction en faisceau blanc

Développement instrumental et techniques de mesure

Au cours de l'année 2013 le développement de deux techniques auxiliaires du micro-Laue ont été poursuivis:

- Résolution 3D en profondeur grâce au balayage d'un fil
- Détermination du tenseur complet des déformations par la mesure d'énergie des pics de diffraction au moyen d'un "monochromateur inversé" en diamant.

De plus, nous avons travaillé à la résolution des dérives et des instabilités du système de focalisation. Grâce à un nouveau système de régulation sensible et rapide mis en place en été 2013, l'instrument de microdiffraction est très performant :le faisceau est stable en position (±0.2 microns) et sa taille est constante et minimale (à ± 0.1 microns) pendant 12h, période bien supérieure au temps de collections de données usuelles.

Développements logiciels

introduction

Depuis 2006, lors de l'ouverture aux utilisateurs de l'instrument de microdiffraction, nous avons entrepris de concevoir un logiciel souple et adapté aux besoins de la communauté scientifique. Nous maintenons ainsi un code opensource écrit en langage python permettant de développer efficacement et rapidement des modules de traitement de données. Nous adoptons autant que possible une démarche conforme à celle suivie par le développement logiciel , notamment en conservant une trace de toutes les modifications et de toutes les versions du projet. Le paquetage peut être déployé facilement et gratuitement sur n'importe quel système d'exploitation propre aux utilisateurs (Windows, linux, MacOS) et n'exige pas de matériels informatiques particuliers.

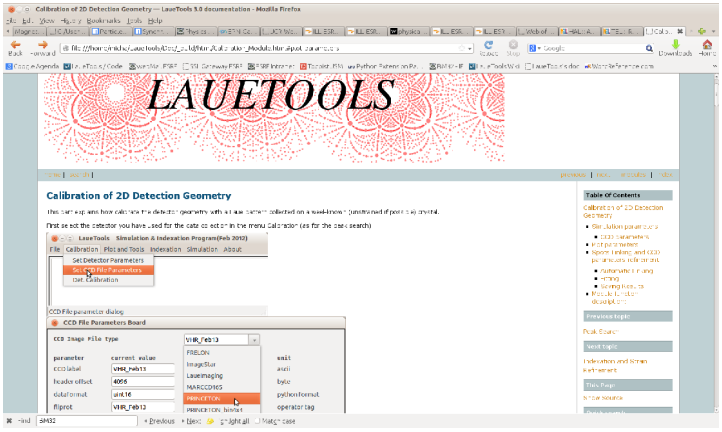

Figure 1 : Documentation hypertexte de LaueTools comprenant des captures d'écrans, enrichie des détails sur les fonctions et les modules, le code source, un récapitulatif des étapes d'analyse, un index des modules, fonctions et mots clés. (élaborée avec Sphinx)

Formation et documentation

Deux journées de formation à l'utilisation du code LaueTools développé par la ligne (http://www.sourceforge.net/projects/lauetools) ont été organisées en juin 2013 pour les utilisateurs de l'instrument. Il est prévu de continuer sur ce rythme cette année. L'objectif est de simplifier l'analyse des données de microdiffraction par les utilisateurs des laboratoires extérieurs. Nous les formons aux principes théoriques de la diffraction et de l'analyse des diagrammes Laue. Nous mettons à disposition des outils logiciels sous plusieurs formes (scripts, interface graphique). Une documentation (hypertexte en format html et pdf) comporte d'une part des captures d'écrans pour un premier usage des logiciels et pour s'initier à la technique de microdiffraction, et d'autre part, une description détaillée de toutes les procédures ou classes utiles aux utilisateurs avancés et aux développeurs.

Ces journées permettent de décrire les dernières fonctionnalités mises en place et d'interagir avec les utilisateurs pour définir les besoins, préparer les nouvelles fonctionnalités et améliorer l'ergonomie de celles déjà existantes.

Nouvelles fonctionnalités

Nous avons cette année mis en place les outils permettant de visualiser rapidement pendant l'expérience la position et la forme des objets à étudier (figure 2), et le signal de diffraction (figure 3). D'autres interfaces permettent de suivre en temps réel l'intensité des pics de diffraction appartenant soit à un grain, soit à partir d'une liste de pics fournie par l'utilisateur, ou sélectionnée directement à l'aide d'une interface graphique.

Les outils précédents permettent une pré-analyse qualitative rapide. Celle-ci est beaucoup moins longue et complexe que l'analyse complète à mener en définitive après l'expérience par l'utilisateur de retour à son laboratoire. L'analyse automatique complète de plusieurs milliers d'images peut maintenant être lancée de manière ergonomique, grâce à une interface graphique conçue pendant le stage de licence de Tiphaine Cerba,. Elle comporte plusieurs étapes successives et indépendantes de manières à pouvoir revenir facilement en arrière. Cette analyse peut désormais profiter pleinement du calcul parallèle pour optimiser notablement le temps d'analyse sur les ordinateurs multicoeurs aujourd'hui très répandus.

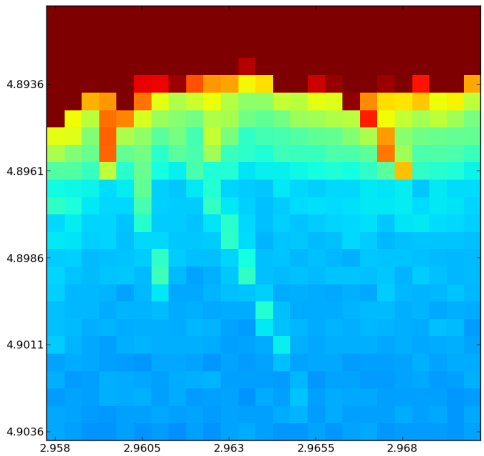

Figure 2: Cartographie (pas de 0.5 µm) du signal de fluorescence de l'or mettant en évidence des nanofils droits d'or (diamètre moins de 200 nm, longueur plusieurs microns).

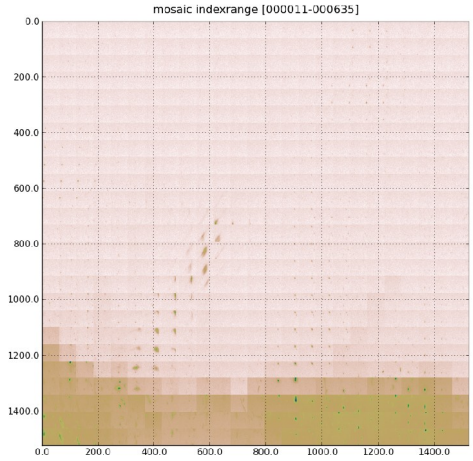

Figure 3: Cartographie formée par la mosaïque de pavés comportant une même région des images collectées entourant un pic de diffraction appartenant à un nanofil d'or. Les forts déplacements du pic par rapport au centre des pavés, lorsque le faisceau se déplace le long du nanofil, indiquent un vrillage de l'axe de croissance de celui-ci. La largeur du pic observée augmente avec la densité de défauts (dislocations).

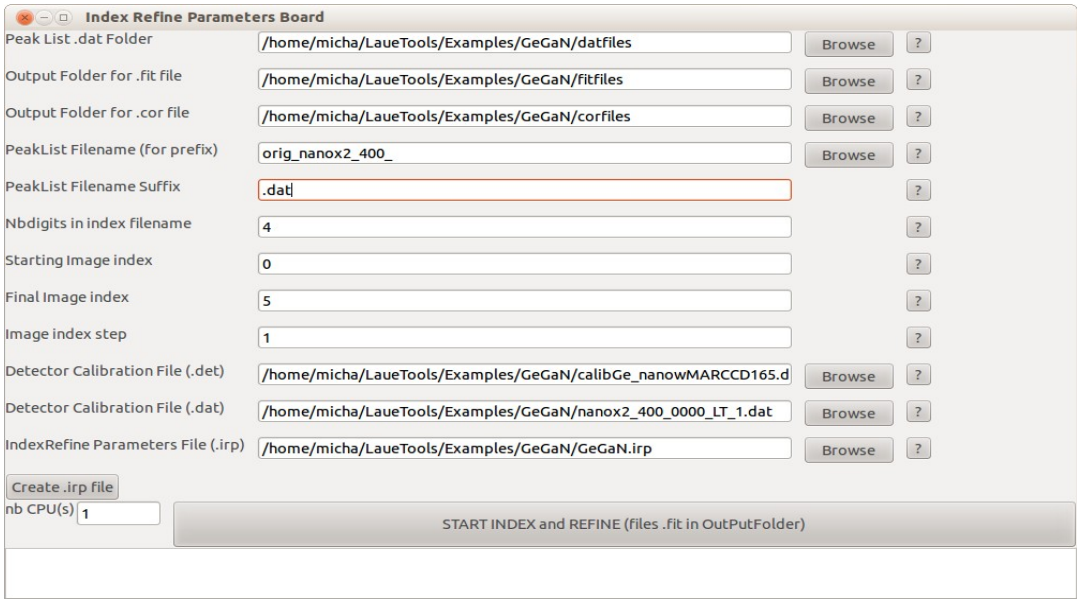

Figure 4: Nouvelle interface graphique de LaueTools déclenchant l'analyse des diagrammes de Laue contenus dans une série d'images.

Post-traitement des données

Nous concentrons aussi beaucoup nos efforts sur le traitement des résultats de l'analyse d'une grande quantité d'images collectées lors de la cartographie d'un échantillon.

De nouvelles fonctionnalités dans LaueTools permettent de traiter un grand volume d'information et d'en visualiser les grandeurs physiques pertinentes :

- position, forme et frontière de chaque grain
- orientation, déformation et contrainte en chaque point de l'échantillon
- désorientations intra-grain

La fiabilité de ces mesures peut être quantifiée et visualisée en chaque point par des critères de qualité (nombre de pics ajustés par grains et écart résiduel après ajustement entre les positions théoriques et expérimentales des pics de diffraction). Nous avons aussi commencé à mettre les résultats d'analyse sous forme d'une grande base de données à accès et interrogation rapide.

La figure 1 montre par exemple les cartographies des rotations de la maille cristallographique locale au sein d'un même grain dans plusieurs grains d'un film polycristallin de CdTe. Celle-ci peut être directement confrontée avec des cartographies de densité de courant induit (EBIC) mesurées dans un microscope électronique à balayage. Grâce à ces résultats d'analyses, des grains bicolores en EBIC pourraient ainsi être associés à la présence de sous-joints particuliers à l'intérieur des grains à l'origine de certaines hétérogénéités de rendement dans les imageurs de rayons X à base de CdTe.

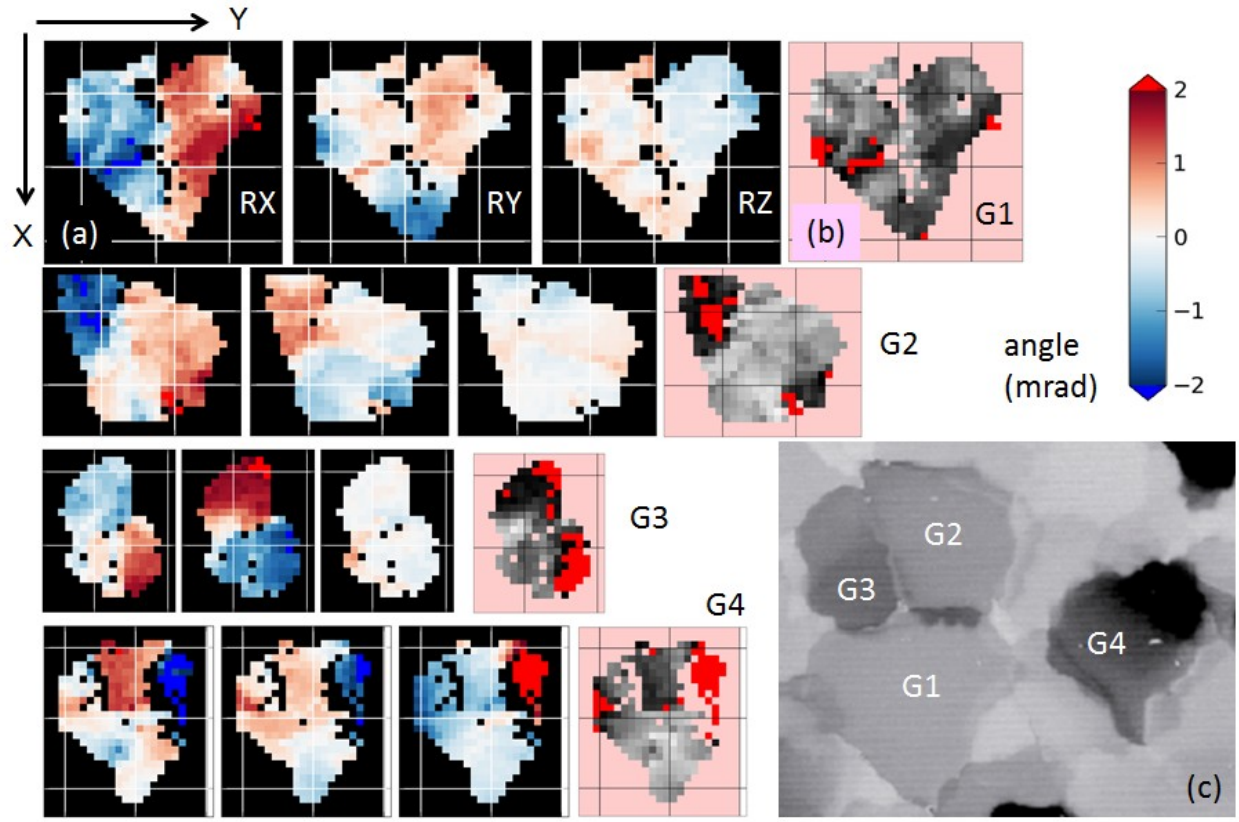

Figure 1 : (a) cartographies des rotations intra-grain dans quatre grains d'un film de CdTe destiné aux imageurs de rayons X. De gauche à droite : composante de rotation autour des axes x, y et z. L'axe z est perpendiculaire au film et à la figure. Les désorientations sont calculées par rapport à l'orientation moyenne du grain. (b) cartographie de l'angle de rotation total. Blanc = 0, noir = 2 mrad, rouge > 2 mrad. (c) cartographie par EBIC de la densité de courant locale dans le même film de CdTe. Cette technique fournit une mesure du rendement local du capteur. La frontière entre les zones plus claires et plus sombres des grains G4 et G3 dans (c) coïncide approximativement avec la frontière entre deux zones très désorientées dans (a).
(V. Consonni et al. Phys. Rev. B vol 89)

3 Activité scientifique

3.1 Résumé activité goniomètre multitechnique et micro-diffraction

Le temps de faisceau d'août 2012 à octobre 2013 dans la cabane GMT a été partagé entre des expériences avec le goniomètre multitechnique et en majorité avec l'instrument de microdiffraction Laue.

Goniomètre Multitechnique

Des expériences avec le goniomètre ont été menées par deux équipes du CEA-Grenoble, animées par F. Rieutord et G. Gébel, et une équipe du CNRS de Grenoble. F .

Rieutord *et al* ont déterminé l'effet de la fluence de l'implantation en ion Helium sur les déformations de wafers de Silicium. Dans le cadre général de l'amélioration du procédé smartCut, ces mesures pourraient indiquer que l'implantation provoquerait plus une modification des propriétés élastiques du matériau que la création de défauts cristallins. Dans la thématique des batteries au lithium, comme l'année précédente, G. Gébel *et al* ont mesuré *in situ* par réflectivité des rayons X l'intercalation des atomes de lithium dans l'électrode de Si provoquant le gonflement et l'augmentation de la rugosité de la surface. D'autres investigations sur des systèmes modèles sont programmées dans le cadre du projet européen BACCARA qui a débuté officiellement en Novembre 2013. Enfin, A. Bailly *et al* ont étudié l'effet de la taille et de la composition en Palladium sur l'efficacité catalytique pour l'hydrogénation du butadiène de nanoparticules d'Or-Palladium. L'équipe a utilisé la chambre à réaction catalytique spécialement conçue pour BM32 pour des mesures *in situ* de diffraction aux grands et aux petits angles.

Microdiffraction

L'équipe autrichienne et allemande (Kirchlechner et al), habituée à utiliser l'instrument de microdiffraction pour comprendre les propriétés mécaniques fondamentales à l'échelle micrométrique, a réalisé deux expériences cette année: l'une a consisté, lors d'un essai de fatigue plastique à suivre *in situ* l'évolution du comportement mécanique macroscopique et à la corréler à la localisation microscopique des dislocations et à leur densité. L'objectif de l'autre expérience a été de quantifier l'intensité de l'effet Bauschinger correspondant à la modification de la limite élastique d'un matériau polycristallin lors du changement de sens de la sollicitation, en raison d'un empilement des dislocations aux joints de grains. Pour cela, des éprouvettes modèles microscopiques ont été taillées (par faisceau d'ions) dont certaines autour d'un joint de grains. Une autre équipe française de Poitiers (P.O. Renault *et al*) s'est intéressée aux mécanismes de déformations des semiconducteurs (pour l'opto et la micro-électronique) en cartographiant des piliers d'InP dont ils avaient enregistré au préalable , lors de la compression, la courbe contrainte-déformation et l'image de la surface.

Pour étudier des objets plus divers (notamment ceux ne nécessitant pas de préparation ni de mise en forme préalable), l'équipe de T. Cornelius *et al (CNRS-IM2NP, Marseille)* dans le cadre de l'ANR Mecanix a continué de développer le système d'AFM portable (d'une ligne de lumière à l'autre) et de sélectionner et caractériser sur BM32 les nanofils les mieux adaptés pour un futur test mécanique avec une pointe AFM.

P. Bleuet *et al* (CEA-Grenoble) ont effectué une reconstruction 3D des grains de cuivre formant une interconnexion pour l'intégration verticale en micro-électronique (TSV) par tomographie-Laue. Ils ont mis en évidence la présence d'une lacune de cuivre expliquant la baisse de fiabilité. S. Hall *et al* de l'université de Lund (Suède) ont réalisé une première expérience probante sur des whiskers d'étain croissant à la surface d'un polycristal de bronze. Ils ont validé le fait que l'utilisation de deux techniques complémentaires de microdiffraction Laue (résolution en profondeur et détermination du tenseur complet des déformations) devrait permettre de mieux comprendre la relation entre la croissance des monocristaux (par diffusion des atomes d'étain) et les gradients des déformations dans les grains de bronze.

ANR-AMOS : *(coordinateur : Jean-Luc Rouvière, CEA/INAC)*
Mesure des Orientations et des Déformations dans des nanostrutures
Début : décembre 2010 ; Durée 3 ans
Le projet vient de se terminer fin 2013.

Le budget alloué à ce projet a été utilisé pour acquérir plusieurs équipements pour l'instrument de microdiffraction : hexapodes des miroirs focalisant (2012), table anti-vibration active (2012), platines motorisées de rotation et translation et tête goniométrique pour le système de diamant tournant (2013) et détecteur de fluorescence rapide (2013).

La méthode du diamant a ainsi bénéficié d'une installation améliorée pour mesurer les déformations dans des matériaux appliqués:

- *Matériaux pour l'énergie* : Etude des contraintes locales dans les grains (5 µm) de ZrO_2 formant la couche électrolytique solide des piles à combustible SOFC (collaboration avec O. Sicardy, CEA/LITEN).
- *Métallurgie et résistance des matériaux* : Etude de l'effet de l'implantation d'atomes d'Azote sur la résistance de surface d'un polycristal de Ni (taille de grain 50 µm) (collaboration avec A. Leineweber, MPI Stuttgart)
- *Matériaux pour la microélectronique* : Etude des propriétés mécaniques de wafers de silicium comportant des trous cylindriques (Through-Silicon-Via TSV) par des mesures de déformation locale.

Ces expériences et leur préparation ont été l'occasion d'ajouter des outils logiciels pour le traitement de données pendant l'acquisition et d'améliorer les outils d'analyse liés à la méthode du diamant.

ANR MICROSTRESS *(coordinateur O. Castelnau, ENSAM Paris)*
Hétérogénéités du champ de contraintes à l'échelle du (sub)micromètre dans les polycristaux élasto-plastiques
Début : janvier 2012 ; Durée 4 ans

2013 a vu la suite du développement de la technique en micro-Laue permettant d'obtenir une résolution dans la profondeur de l'échantillon, et le début de l'emploi de la corrélation d'image optique (DIC Digital Image Corrélation) pour la mesure des champs de déplacement lors des tests mécaniques.

Le code d'analyse des diagrammes de micro-Laue collectés au cours du balayage du fil a été mis en place (travail de postdoc de F. Grennerat). Il permet :

- de déterminer la position et la taille en profondeur d'un grain à partir de quelques pics de diffraction masqués lors du balayage du fil.
- de reconstruire les diagrammes de Laue provenant de différentes profondeurs dans un même un grain dans le but de déterminer les profils en profondeur des déformations de la maille cristalline.

Deux matériaux modèles ont été caractérisés avec cette technique: polycristal d'UO_2 implanté en surface (fig. 2) (chaque grain comporte une partie déformée en surface) et deux nanofils monocristallins (1 µm de diamètre) de GaN posés l'un sur l'autre sur un wafer de Ge.

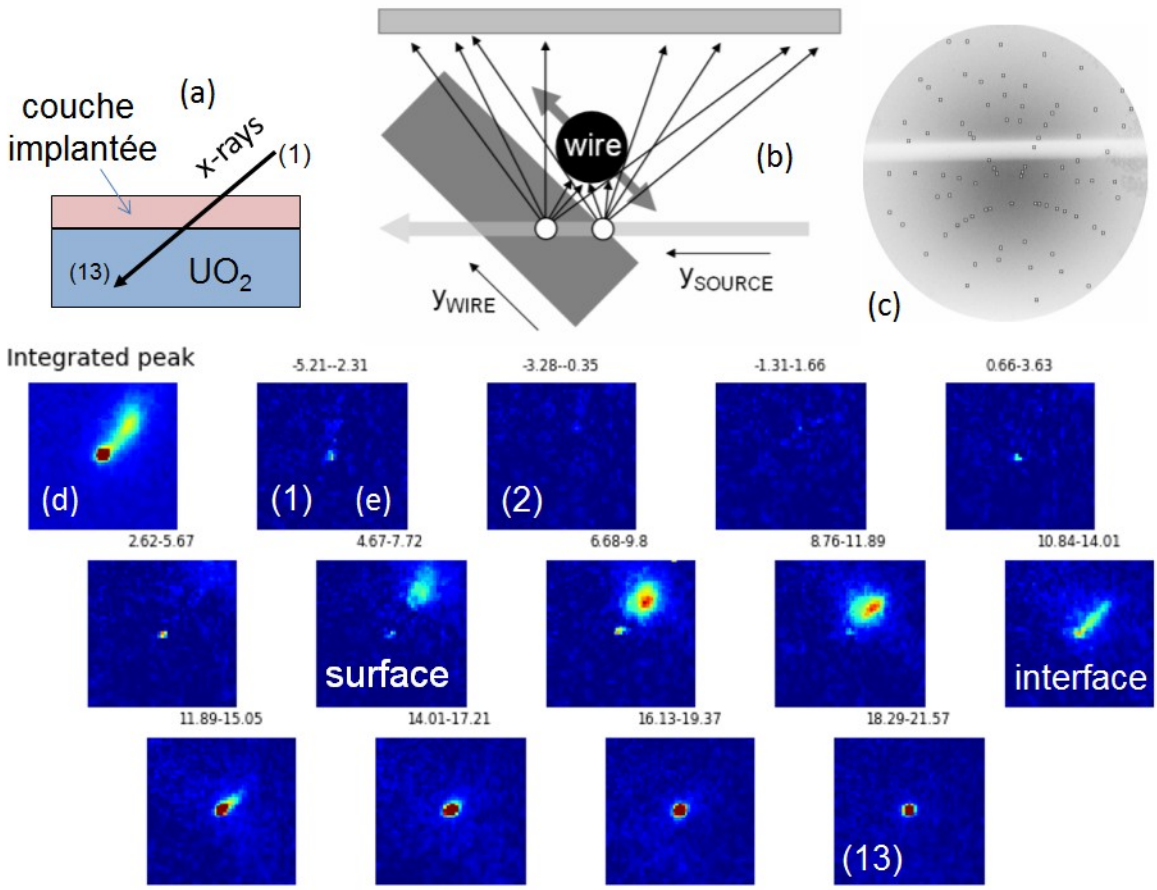

Figure 1 : (a) Schéma du substrat d'UO2 et de la couche implantée, et direction du faisceau incident. (b) Principe de la méthode du fil. (c) Un des 400 diagrammes de Laue collectés pendant le balayage du fil. (d) Gros plan sur un des spots du diagramme de Laue de l'UO_2, montrant le spot étroit du substrat et le satellite large provenant de la couche de surface. (e) Images reconstruites à différentes profondeurs à partir du masquage des différents pixels de l'image (d) lors du balayage du fil.

Une expérience acceptée par le comité de programme international et considérée comme prioritaire par l'ESRF sur des whiskers d'étain (cf. rapport d'expérience Hall *et al*) devrait bénéficier pleinement des avancées instrumentales et logicielles réalisées.

Dans le cadre de l'ANR, trois campagnes d'expériences (acceptées par le comié de programme) ont été menées contribuant au travail de de thèse de E. Plancher (EDF-Mines de St-Etienne), J.B. Marijon et F. Zhang (ENSAM-Paris).

- Comparaison des techniques Laue-DIC et EBSD à haute résolution angulaire par des mesures *in situ* des profils de déformation élastique à plusieurs étapes de flexion sur la tranche d'éprouvettes de plusieurs matériaux (Ge, Si, acier 316L).

- Mesures résolues en profondeur et *in situ* avec la nouvelle machine de flexion (développée par l'ENSAM). L'emploi de 4 fils de tungstène au lieu d'un a été par ailleurs testé afin de réduire le temps de mesure. Le mode opératoire et les outils logiciels sont en cours de développement.

- Combinaison de cartographies de déformation élastique à l'échelle microscopique (Laue) et de cartographies de déformation totale par DIC optique à plusieurs étapes de chargement, sur des 'éprouvettes d'acier 316L, courbées dans le domaine élastique puis dans le domaine plastique.

Probing Sn whisker growth mechanisms

S. Hall, J. Hektor, M. Ristinmaa, H. Hallberg, S. Iyengar, Lund University Sweden

This experiment investigated the use of 2D and 3D (by wire-scanning: differential aperture x-ray microscopy, DAXM) Laue diffraction to measure grain distributions and grain strains around “tin whiskers” growing from a tin layer over a copper substrate. The objective was to understand the driving forces for tin whisker growth to subsequently advance the concurrent developments of a theoretical material model of such systems. Measurements were performed on a sample of tin-plated copper that had been aged for about 5 weeks such that tin

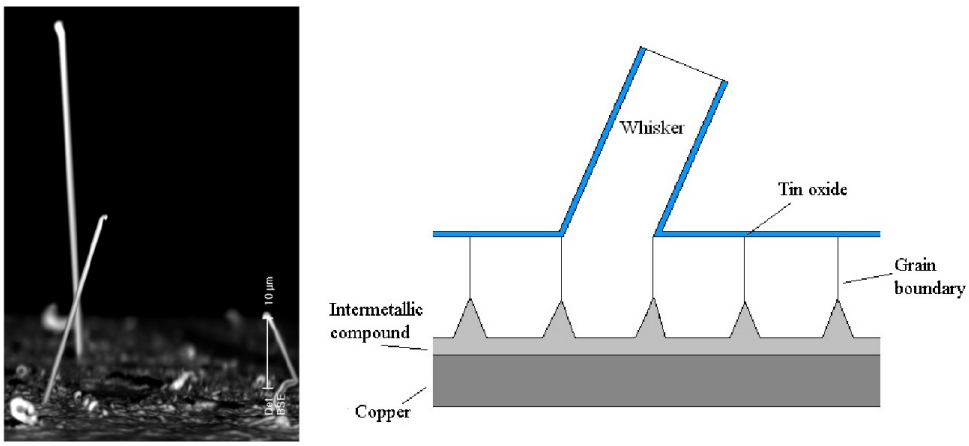

Figure 1: (left) Tin whiskers on a tin-coated copper surface; (right) A model for whisker growth on tin coated copper

whiskers (single crystal tin “protrusions” from the sample surface) could be observed under an optical microscope. A region of the sample containing a single evident tin whisker was identified for investigation using the optical microscope on the BM32 measurement stage. Using a 0.5 x 0.5 μm^2 beam, an area of 10x12 μm^2 around the whisker was scanned using 2D Laue diffraction to provide an initial mapping of the crystal structure.

From the resultant data at each point, it was demonstrated that clear Laue diffraction patterns could be measured through the thickness of the tin layer down to, and including, the copper substrate. Furthermore, initial analyses showed that the Laue patterns associated with the tin grains could be identified and fitted for the local cell parameters. Figure 2 shows a map of the c-axes of the tin grains in this region, based on fitting of the Laue patterns (using LaueTools software) to the strongest intensity family of diffraction spots (making the assumption that the strongest intensities correspond to the grain nearest the surface of the sample at each point).
Figure 3 shows the principal grain-strains at each of these points corresponding to the fitted cell parameters relative to an ideal unit cell. Clear regions of consistent c-axis orientations can be seen that probably reflect the tin grain structure at the surface. Furthermore, the strain maps show correlations of the strain field with the grain shapes in the c-axis plot and in some cases strain gradients can be seen within grains. These strain gradients could be related to the formation of a tin whisker (the approximate position of the main whisker is at (x,y)=(6, 4) µm).

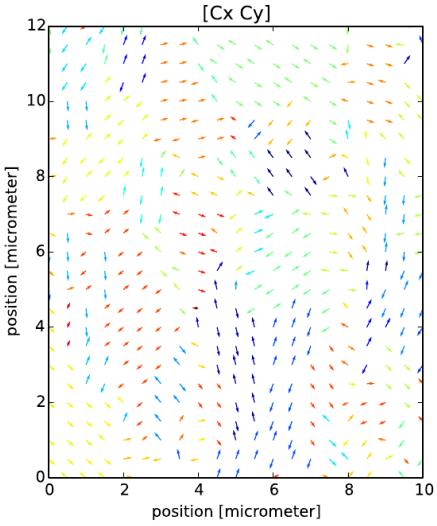

Figure 2: plot of the c-axis orientations (colors indicate the out of plane angle) from the analysis of 2D Laue map.

The strongest intensity family of diffraction spots (based on a preliminary assumption that these correspond to the grain nearest the surface) is considered for fitting, using LaueTools, to determine the tin cell orientation and lattice parameters at each spatial location.

The results described above are preliminary, but already indicate that Laue Diffraction can be used to
investigate the crystallography and strain through the thickness of the tin layer down to the copper substrate. Furthermore, indications of the intermetallic compound that forms between the copper and the tin could be seen in the diffraction data, which suggests that this interface might be mapped, in future experiments, and its topography could then be related to the strains in the tin grains (however full crystallographic and strain information may be difficult to extract for this phase).

In addition to the 2D mapping, two 3D-Laue wire scanning line scans were made (one in the y-direction, 10 μm length with 1 μm spacing, and one in the x-direction, 10.5 μm length at 0.7 μm spacing through the centre of the images in Figure 2). This wire scanning took approximately 1 hour/point. Analysis of the 3D crystallography and strains based on these data is under way; early results suggest that depth resolved information can be derived to correctly separate the signals from different depths (including separating the diffractions from whiskers from those from the grains in the sample).

The described 3D-Laue wire scanning can only provide the deviatoric strains in the sample, but the
phenomenon of interest is strongly linked to volumetric changes with the formation of the intermetallic
compound. Therefore it is desirable to quantify the volumetric strain component of the deformation. It is foreseen to use the new technique developed recently (with the diamond monochromator) to obtain this information.

Whilst promising results were achieved from this experiment, the experiment also revealed the complexity of the sample, a complexity that makes for a more difficult interpretation of the 3D resolved crystal strain and strain-gradient data in relation to whisker growth. This complexity is due to the fact that a significant number of whiskers appear to have formed and, whilst a zone with a relatively isolated whisker has been selected, a more in-depth analysis will be facilitated by ensuring that there are minimal interactions between whiskers. Analysis of the optical microscopy and x-ray diffraction data suggests that this complexity might arise from the grain size in the copper substrate and also from the tin-surface preparation. For future experiments the sample preparation will be optimized, based on the current results and insight gained, to provide samples with spatially isolated whiskers. With such samples it should be possible to develop a clear picture of the strain fields around individual whiskers (the existing data have proven the experiment concept and the possibility of extracting good crystallographic and strain results from the Laue diffraction data, but greater insight to the processes requires a simplification of the mechanical system). Furthermore, measurements of the volumetric +strain must be made, as this is an essential part of the phenomena of interest.

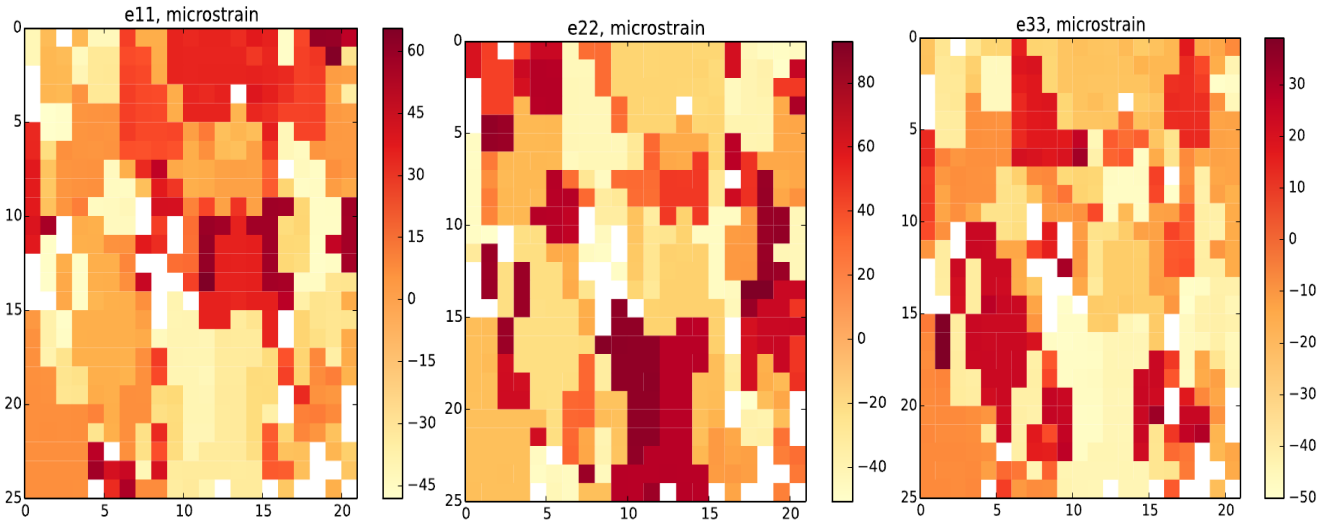

Figure 3: principal deviatoric strain components determined et each scan point.

Qualification of local strain measurements by HR-EBSD and Laue microdiffraction

J. Petit, O. Castelnau, J.B. Marijon, E. Plancher, O. Robach
ENSAM/PIMM Paris
CRG-IF BM32
ANR-Microstress

Strain heterogeneity develops at the micron scale in polycrystalline metals during mechanical deformation, often leading to annoying back stresses. In order to reproduce this phenomenon through numerical simulation, one should pay attention at the constitutive laws used to describe intragranular behavior.
Our current research, funded by the French ANR project "microstress", focuses on collecting trustworthy data required for parameter identification of some 316L steel constitutive laws. Especially, we try to assess scale elastic strains (or stresses) and total (or plastic) strains fields at the micron scale. Total strains are usually obtained by the well-established digital image correlation technique. Hence efforts concentrate on asserting the quality of elastic strain measurements, in our

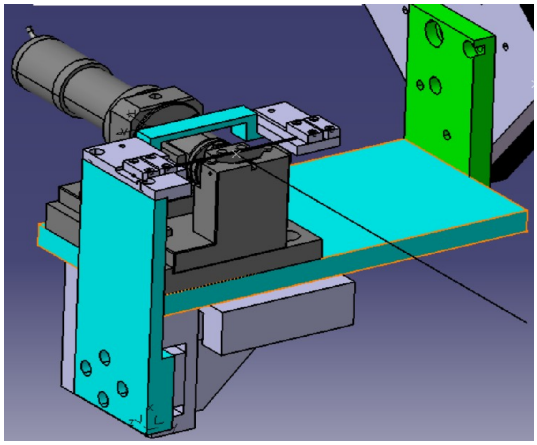

Four points bending machine (dark grey) specifically designed to be mounted on BM32 microdiffraction setup allowing local in situ strain measurements and wire-scanning for 3D resolution (light grey motorized translation stages and wire holders)

case obtained by two promising techniques: synchrotron-based Laue microdiffraction and SEM-based HR-EBSD.
One of our previous concerns was to determine the surface characteristics needed for acquiring reliable HR-EBSD data. In order to compare the in-depth strain information of Laue microdiffraction (>10µm) with the near-surface information of HR-EBSD (<50nm), we suggested to manufacture standards from Si, 316L (Fe-Cr-Ni) and W single crystals, with controlled surface preparation. A preliminary experiment, performed at BM32 in February 2013, was carried out on a 316L single crystal with optimal preparation (flat surface, roughness <1µm, no back stress).
It turns out that even in this optimal case, comparison of HR-EBSD and Laue microdiffraction datasets remains a challenge. In particular, this preliminary work enlights insufficient accuracy of the alignment procedure in the SEM when performing HR-EBSD and issues of noise coming from image processing. As we are currently addressing these issues, working with only few 316L standard samples, with optimal preparation, seemed relevant.
We thus redirected part of our work on acquiring both Laue microdiffraction (elastic strain evaluation) and proper optical images for image correlation analysis (total strain measurements), on two 316L single crystals deformed in a four points bending machine. Coupling the two fields must lead to more efficient identification ways of constitutive laws parameters.

During the experiment two types of specimens were scanned:

- Two 316L single crystals used as reference samples for HR-EBSD and Laue microdiffraction in different states: (i) stress free and (ii) already deformed. Theses sample were carefully embedded in mounting resin, prepared to obtain a flat surface, small roughness (<1µm) and without back stress (coming from polishing).
- Two 316L single crystals in the shape of four points bending samples (30*5*0.5mm). First sample has a ([100],[010],[001]) orientation compared the sample axes linked with its long and narrow surface, second has a ([110],[1-10], [001]) orientation. Both sample were prepared with a flat and stress-free surface on which a speckle pattern of Mo particles was created (in order to get suitable contrast in optical images for DIC).

Thanks to the improved microdiffraction setup, a stable beam of size 500 x 280 nm² (HxV) was achieved. The CCD detector was ~60mm far from the sample. An optical microscope with low lenses distortions was installed close to the diffraction setup. We used a dedicated four points bending device to strain the samples. The machine is equipped with an easy-removal system, which allows its transportation between the microscope and the diffraction setup.
The experiment on bent samples runs as follows:

- The sample is inserted in the bending device, unstrained. Three lines scans of 300 Laue patterns are acquired. The setup geometry is calibrated as usual on an unstrained Ge single crystal and the beam size is checked at the sharp edge of a gold micro-block.
- The bending device is brought under the microscope. Images are recorded before, during the loading, and after. We take care to ensure images are focused and unsaturated.

- While the displacement is kept constant, the machine is carried to the diffraction setup and three scans are acquired.
- Respectively 8 and 10 loading steps are carried out, including 3 to 4 steps in the elastic regime and one in the relaxed state.

The diffraction patterns recorded are of good quality, with almost circular spots. All the data is being processed with the open source software LaueTools, developed at BM32, and will probably be analyzed with the new Laue-DIC method. Optical images have a contrast suitable for the digital correlation technique. We plan to use EDF's in-house code to process the data.

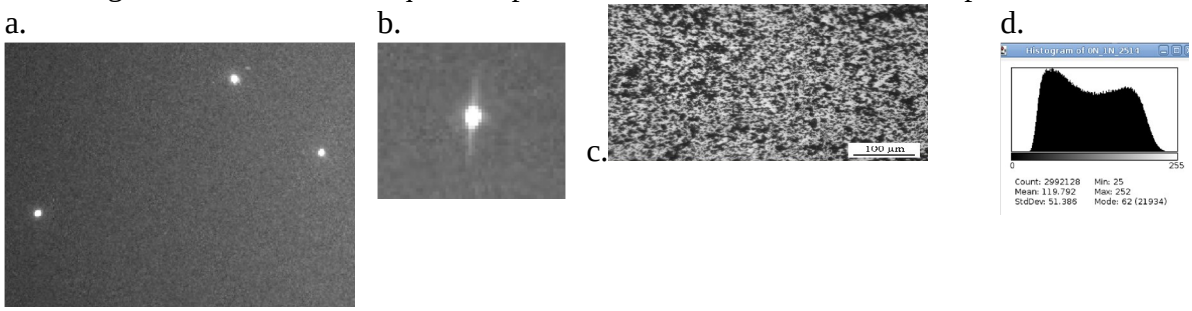

(a) Three diffraction spots from the dataset acquired on a stainless steel single crystal. (b) Diffraction peaks with an elongated tailt from Ge calibration data. (c) Speckle pattern used for digital image correlation and (d) corresponding pixel intensity distribution.

We should be able, for the first time, to evaluate stress and plastic strain fields on two single crystals during deformation. The use of both information seems to be a promising way to improve parameters identification procedures of constitutive laws. We are planning to extend this experimental procedure to a more realistic case by bending bi-crystals, in order to observe heterogeneous fields. The grain boundary effect on the deformation would then be measured.

This work is a key part in the PhD of Emeric Plancher. Publications will be submitted when final conclusions and comparisons with a finite element model will be reached.

Implantation d'hydrogène dans le silicium

François Rieutord, Shay Reboh
CEA-INAC, CEA-LETI

L'implantation d'atomes dans un semi-conducteur est à la base de nombreux procédés industriels tels que dopage, amorphisation et/ou procédés de fragilisation (type SmartCut™). Nous avons étudié l'effet de la dose implantée d'hydrogène sur la déformation d'une matrice de silicium. Typiquement, la diffraction des rayons X est utilisée pour obtenir le profil de déformation, par cartographie à haute résolution du réseau réciproque (Fig.1).

Ces mesures sont complétées par des mesures annexes comme par exemple des mesures de courbure de plaque qui permettent d'obtenir la valeur de la contrainte globale dans la zone implantée. En combinant ces deux techniques, pour différentes doses et différentes orientations du substrat, on peut donc suivre l'évolution de certains coefficients élastiques (ex: module de cisaillement) en fonction de la dose. Nous avons effectués de telles mesures dans

le cas du silicium. Sans surprise, on mesure au delà d'une certaine dose une diminution des constantes élastiques avec l'endommagement du matériau.(Fig. 2)

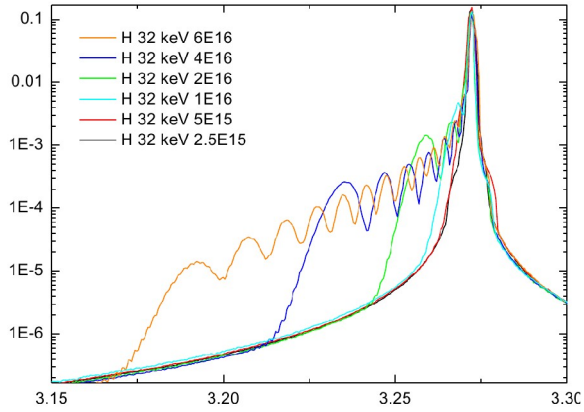

Fig. 1. Figure de diffraction X autour de la raie (220) du substrat Si (orienté (110)). Le matériau a été implanté à différentes fluences indiquées dans la légende.

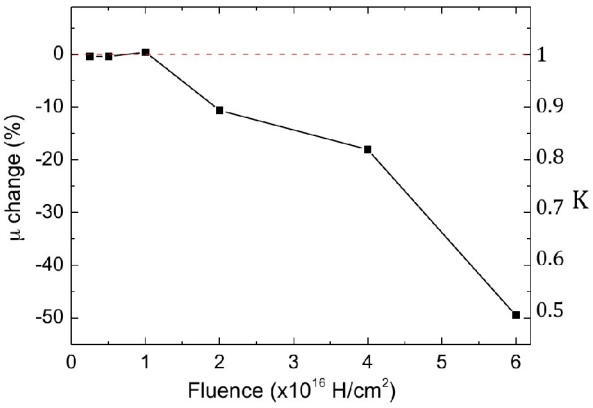

Fig. 2. Evolution du module de cisaillement μ avec la dose implantée. L'axe de droite indique le rapport du module mesuré au module du silicium vierge.

Ces mesures nous ont ensuite permis d'analyser la seule dépendance de la déformation avec la dose implantée. Nous avions constaté (comme d'autres équipes sur d'autres systèmes) que la déformation z variait plus vite que linéairement avec la dose, au contraire d'effets de saturation attendus. (Fig.3).

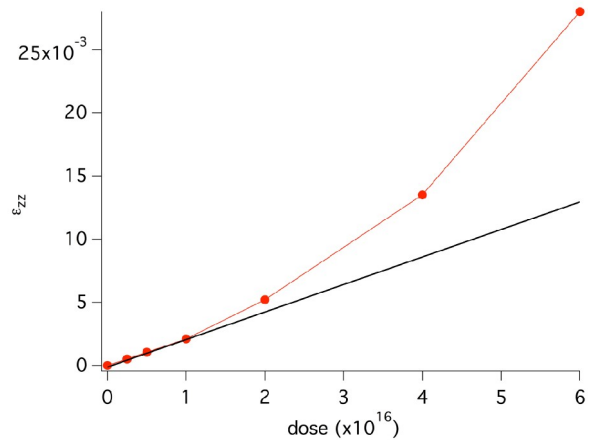

Fig.3 : Dépendance de la déformation ε_{zz} (normale à la surface) avec la dose implantée. De façon contre-intuitive, la déformation évolue de façon supra-linéaire.

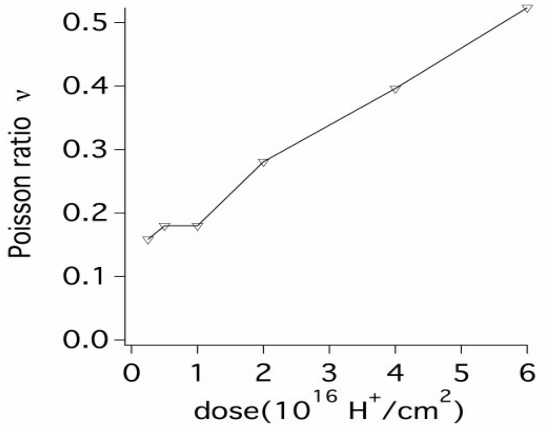

Fig.4 Dépendance avec la dose du coefficient de Poisson permettant d'expliquer la variation de ε_{zz} avec la dose à partir d'un volume par espèce implantée constant

Plusieurs interprétations de ce phénomène sont possibles, incluant par exemple le rôle des défauts ponctuels (lacunes, interstitiels). Nos études privilégient plutôt une dépendance régulière du volume par espèce implantée avec la dose, la variation observée de la

déformation serait alors associée à une évolution du coefficient de Poisson (qui relie déformation mesurée et gonflement volumique du matériau) (Fig.4).

Cu Through Silicon Via characterization by Laue X-ray microdiffraction

P. Bleuet, D. Sanchez, P. Gergaud
CEA-Grenoble/LETI

In the frame of the ANR-AMOS project, it is proposed to investigate and develop the micro Laue diffraction tomography technique for the characterization of copper Through Silicon Via

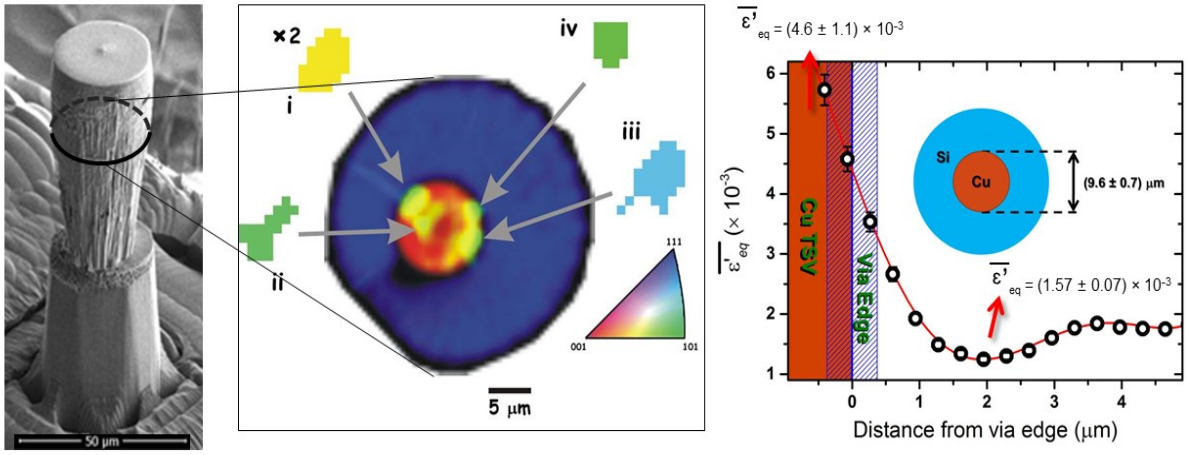

TSV sample prepared by FIB (left), reconstruction of Si and Cu grains (middle) with their corresponding orientation and (right) strain profile through the silicon.

(TSV) features, such as size, shape, orientation and lattice deformation of copper grains and strain profile in the silicon matrix. Those characteristics are very important to understand, since process-induced stresses in the TSVs by the thermal treatments and also by the Si wafer thinning and chip-packing interactions as well as around the TSVs in the Si matrix, raise serious reliability issues (Si cracking and performance degradation of 3D integrated circuit devices). For this purpose, a cylindrical shaped sample from ST-Microelectronics has been prepared using Focused Ion Beam (FIB) with one single Cu TSV-middle (10 µm of diameter and 80 µm of depth) surrounded by 10 to 15 µm the original crystalline Si matrix. In this context, a Laue Tomography (LT) experiment has been performed in March 2013 at the BM32 beamline.

Using the Laue Tools software package, developed at BM32, we could manage to adapt and apply the code for the analysis of LT, so that we could reach the original goal of the project:

(i) obtain the strain profile in the surrounding silicon around the TSV
(ii) the shape, size and orientation of the Cu grains in the TSV.

To go even further, with the interaction of the process team at CEA-LETI, who provided new TSVs samples, we have prepared new samples with more TSVs (2, 4 and 6), to investigate and understand the dependence of the strain in the silicon matrix, as well in the TSVs, on several parameters:

(i) surface density of TSVs in Si matrix
(ii) distances between them
(iii) manufacturing processes (thermal treatments and barriers material)
(iv) presence of voids in TSVs.

Thanks to the close interactions of CEA-LETI and the beamline BM32 at the ESRF, we already had the opportunity to perform two new experiments (September 2013) on two different samples:

1 – One with four TSVs with voids, where we could measure 2 different regions, one with voids and another without, in order to compare the effect of the voids on the strain profile in Si nm matrix.

2 – One with 6 TSVs, with a TiN barrier (different of the Ta barrier used in the other samples, Figure 2).

Applying the same methodology we were able to obtain the silicon strain profile on these new samples (a paper is expected to be submitted early 2014).

Influence of stacking fault energy of fatigue at the micron scale

C. Kirchlechner, C. Motz and G. Dehm
Max-Planck-Institut für Eisenforschung, Düsseldorf, Germany
Universität Saarbrücken, Germany

The aim of the proposed experiment was to investigate the fatigue behavior of micron sized single crystalline bending beams by *in situ* µLaue diffraction. The experiment should serve for comparison of the previously performed deformation of copper samples with the newly deformed silver samples exhibiting a much lower stacking fault energy.

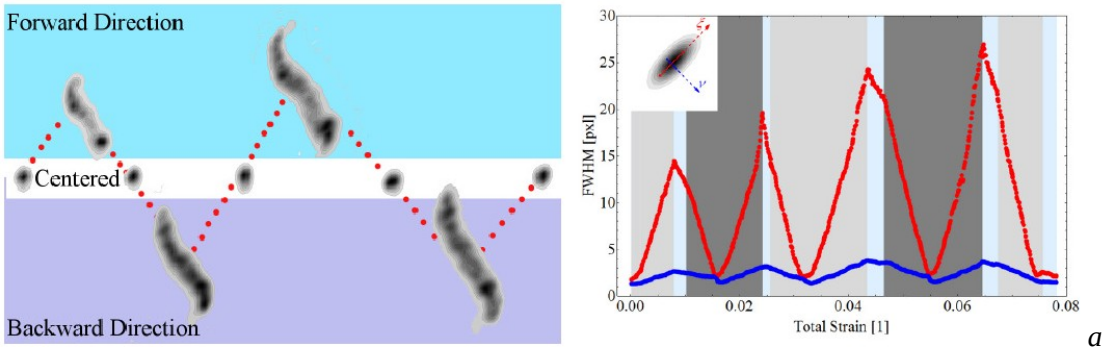

a

a) Evolution of the diffraction peak shape during bending of a 6µm sized copper sample during two cycles. b) analysis of the peak widths during four cycles. Note that the red and blue curve always come back to the bottom line which represents the values of the virgin sample.

Due to the change of stacking fault energy the cross-slip probability changes significantly which will alter the amount of reversible dislocation plasticity.

10 silver samples with a size of 7x7x35µm were produced in our home facility by focused ion beam (FIB) milling. The samples were oriented for single slip.

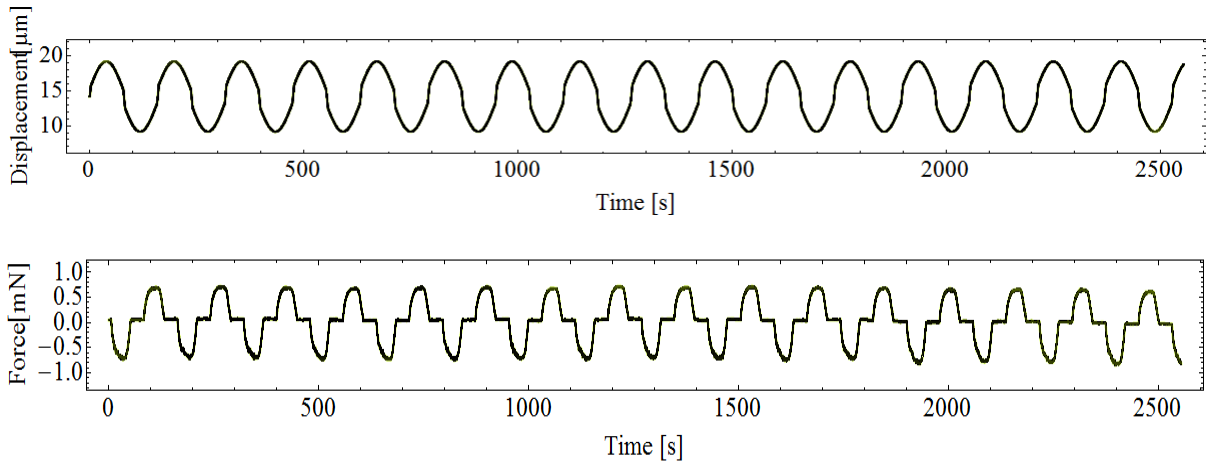

Displacement time and force time curve of a silver sample deformed in situ at CRG-IF @ BM32. Due to the good stability of the setup during the experiment we were able to perform several hour lasting fatigue tests during nights.

The initial microstructure of the sample was analyzed by high resolution raster scans with a stepsize of 500nm. Subsequently, the X-ray beam was focused on one spot of interest and displacement was sinusoidal applied. Force, displacement and diffraction images were continuously recorded in order to correlate changes in the mechanical behavior with the underlying dislocation structure.

The evaluation of diffraction data is still ongoing and at this date still no thorough conclusive results can be presented. However, the data quality is impressive and mainly shows that the streaking of Laue spots is less sharp, but rather more blurry. This fits with the classical expectations, but still needs to be quantified.

In addition we were able to perform two *ex situ* experiments on gold wires and magnesium pillars. Both experiments are used to test the abilities of the new setup and open new perspectives for proposals at BM32.

Bauschinger Effect at a single interface

C.Kirchlechner, C. Motz, W. Grosinger, J. Keckes and G. Dehm
Erich Schmid Institut for Material Science , Leoben, Austria
Max-Planck-Institut für Eisenforschung, Düsseldorf, Germany
Universität Saarbrücken, Germany

The aim of the proposed experiment was to investigate at the micron scale by *in situ* µLaue diffraction the Bauschinger effects.

In single crystalline bending samples dislocations can partly pass through the neutral axis which acts as strain interface. During unloading dislocations of the pile-up show reversible back motion (see Kirchlechner et al. Phil Mag. 2012) being responsible for the observed Bauschinger effect in single crystalline micro bending beams.
By producing a sample with grain boundary (the grainboundary matches the neutral plane) the dislocations are hindered and the pile-up is confined in size, leading to possible higher pile-up stresses and a more pronounced Bauschinger effect.
In contrast, by milling a slit in the neutral fiber one can avoid the dislocation pile up and switch off the Bauschinger effect.

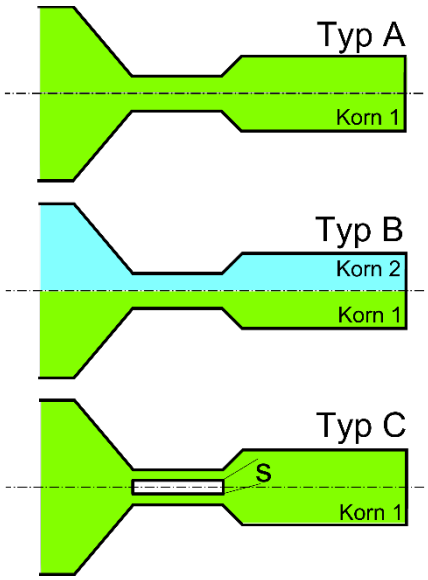

Fig. 1 Used sample geometries ("korn" stands for "grain")

15 samples (5 single crystalline, 5 bi-crystalline and 5 single crystalline with slit) have been prepared by focused ion beam (FIB) milling in our home facility.

During the experiment, we were able to use the new setup at BM32 providing a submicron sized polychromatic x-ray beam. The µLaue station (including beam shape recovery after thermal drift) is very user friendly and well designed.

The in situ µLaue experiment allowed for a quantification of the Bauschinger effect and the corresponding pile-up in micron sized samples, which would not have been possible with alternative methods.

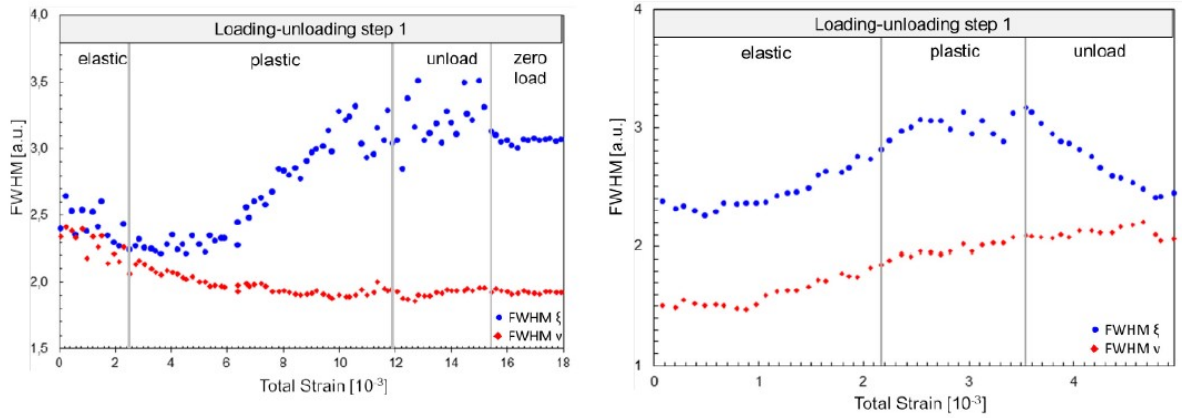

Fig. 2 Peak width evolution during the first loading step in a single crystalline sample and single crystalline with slit. In case of the single crystalline sample the peak width significantly decreases during unloading; in case of the slit it stays constant.

Based on the experiments within MA1696 on BM32 it is our strong belief, that the role of pile-ups for Bauschinger effects in micro bending cantilevers is clear. We are looking forward to a publication in Philosophical Magazine.

3.2 Résumé de l'activité INS (In situ Nanostructure growth on Surfaces) d'étude in situ de nano-objets durant leur croissance sur des surfaces

Durant cette année 2013, l'utilisation de l'instrument d'étude *in situ* de nanoobjets durant leur élaboration sur des surfaces s'est recentrée autour de quelques thématiques principales :

-des études de GISAXS/GIXD couplées durant des réactions en voie gazeuse catalysées par des nanoparticules d'alliage AuCu déposées sur une substrat de TiO_2 ; études amont de celles réalisées à plus fortes pressions de gaz (G. Prévot et al., INSP Paris) ;

-des études de la relaxation au bord de marches de surfaces de silicium vicinales, permettant de tester les modèles théoriques correspondants (F. Leroy et al., CINAM Marseille) ;

-des études de l'équipe CNRS/INéel (Maurizio De Santis) de films ultra-minces composés d'une couche ferromagnétique et une antiferromagnétique (e.g. CoO), avec l'objectif de corréler croissance et structure observées par diffraction X sur BM32 avec les propriétés mesurés *ex situ* par rotation Kerr magnéto-optique.

-des études par l'équipe locale CEA (Gilles Renaud et Fabien Jean), en collaboration avec le CNRS/INéel (Johann Coraux) de la structure et de son évolution en température, de films de graphène épitaxiés sur surfaces métalliques (Gr/Ir(111)), et de la structure et de la morphologie de plots métalliques (Pt, CoPt, Au, Ir) organisés durant leur croissance sur graphène épitaxié ;

-dans la continuité de l'étude précédente, une collaboration entre l'équipe locale CEA-Grenoble, Institut Néel CNRS et l'Institut Lumière Matière de l'Université de Lyon a permis une première étude montrant l'organisation et l'épitaxie d'agrégats de Pt préformés sur le moiré de graphène sur Ir(111) ;

-enfin une partie significative du temps disponible a été utilisée pour poursuivre les études in operando relatives à la croissance in situ de nanofils de Ge/Si par voie chimique en ultra-vide (UHV-CVD). Le temps d'incubation entre l'exposition du catalyseur au gaz réactif et le début de la croissance a été étudié systématiquement en fonction de la taille du catalyseur, de la température et du flux gazeux, donnant des informations cinétiques. La contrainte et le profil de composition ont été étudiés dans des nanofils cœur-coquille GeSi durant la croissance de la coquille (Ge cœur Si ou coquille Si cœur Ge).

Remarquons que les études sur l'instrument INS ont fait l'objet d'un article de vulgarisation dans un numéro des Reflets de la Physique (couplé avec un numéro du Bulletin des professeurs de Physique/Chimie), dédié aux études à l'aide du rayonnement synchrotron. La page de garde ci-dessous montre une photographie du coeur de l'instrument INS actuel, avant donc sa rénovation dans la cadre du projet EquipEX INS-2.


reflets de la PHYSIQUE
n°34-35
juin 2013
Revue de la Société Française de Physique
www.refletsdelaphysique.fr
La lumière synchrotron
au service de la science et de la société
www.sfpnet.fr
udppc
www.udppc.asso.fr

Growth, strain and organisation of Graphene on Ir(111)

F. Jean[1,2], J. Coraux[1], N. Blanc[1,2] and G. Renaud[2]
1 Institut Néel, CNRS Grenoble
2 INAC/SP2M CEAGrenoble

Within the framework of the ANR project NMGEN (NanoMagnétisme sur Graphène Epitaxié sur Métaux), several experiments were carried out in the INS ultra high vacuum (UHV) setup. They were performed under two guidelines, a better understanding of the structure of graphene on iridium and the growth and study of nanoparticles (NPs) on top.

Two-dimensional crystals hold promises for future applications in nanotechnology. Their most famous representative, graphene, has attracted a lot of attention. Graphene is a 2D monoatomic carbon sheet and presents exceptional properties (electronic, mechanical, optical...). There are diverse means to obtain it, mechanical exfoliation of graphite or growth on different substrate. Graphene on Ir(111) is grown *in-situ* in the UHV setup by a chemical vapor deposition process (CVD) of ethylene on the surface of an iridium single crystal. The substrate is cleaned previously by a combination of ion bombardment and annealing at high temperature under oxygen.

Graphite's negative thermal expansion coefficient (TEC) below 500 K has been known for a long time. Graphene, a single layer of graphite, has been predicted to exhibit negative TEC as well, below 300 K, with a unique dependence of its lattice parameter with temperature due to the out-of-plane vibration modes, which its membrane-like topography allows. This prediction was tested on both suspended graphene, in electromechanical resonators, and on supported graphene, for graphene exfoliated from graphite and transferred to SiO_2/Si. The loose contact between graphene and SiO_2 presumably explains why graphene does not follow the TEC of the support. Which TEC graphene exhibits under the influence of a support with which it forms a good contact is of fundamental interest and an open question in any future application operating at variable temperature. The answer to this question is indeed, as we shall see, related to the formation of defects and strain, which are both known to modify the properties of graphene.

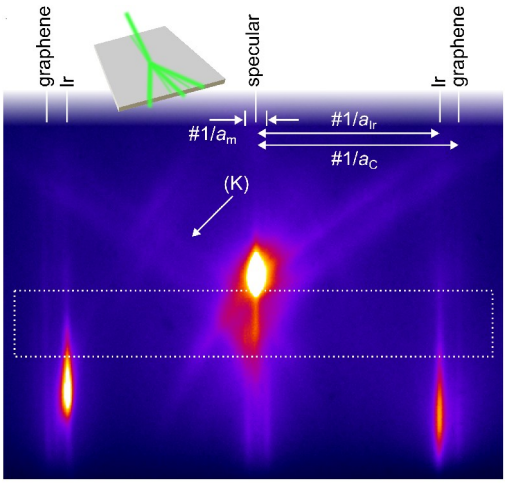

Figure RHEED patterns of graphene on Ir(111)

The evolution of the graphene lattice parameter was studied *in operando* using the RHEED (reflection high energy electron diffraction) technique available in the INS UHV chamber, either during the *in situ* growth of graphene, or during annealing under oxygen, or ion bombardment of a full one monolayer thick graphene sheet. On the first hand, during the growth at high temperature, it has been observed that the graphene shift between different commensurate phases, as the flakes become larger and larger. On the other hand, strains up to 2.2% in the graphene were uncovered during the ion bombardment when the density of

defects is high (less than 1nm between defects). These results have been published in the Physical Review Letters [1], see highlight below.
The effects of the temperature on the structure of a single layer of graphene on Ir(111), has been investigated *in situ*, in the growth chamber, by grazing incidence X-ray diffraction, between 10 and 1300 K. In addition, the effect of two growth temperatures has been studied. The graphene lattice parameter of the main, non-rotated phase, displays a characteristic hysteresis whose lower and upper branches correspond to phases in which integer numbers $(m,n)_{Ir}$ of Ir lattice parameters match integer numbers $(p,q)_{Gr}$ of graphene lattice parameters, *i.e.* commensurate phases, $(19,0)_{Ir}\times(21,0)_{Gr}$ and $(9,0)_{Ir}\times(10,0)_{Gr}$, respectively. With a higher growth temperature, graphene presents, in addition to a main non-rotated, incommensurate phase, domains with a small rotation (2.37°) relative to the substrate, corresponding to a $(7,2)_{Ir}\times(8,2)_{Gr}$ commensurate phase. Despite the weak interaction between graphene and iridium, the thermal expansion coefficient of graphene is positive at all temperatures, even at liquid helium temperature contrary to free-standing graphene, and is close to the iridium thermal expansion, presumably because of the tendency to form commensurate phases, which creates a strong link between the graphene and substrate lattices. These results have been published in the Physical Review B [2].

Two more weeks of experiment were devoted to the graphene on Ir(111) system. The first was to complete an experiment done previously. Graphene on iridium presents a moiré that is used to grow organized nanoparticles (NPs) of different materials by self-organized growth. Platinum and cobalt were deposited by molecular beam epitaxy (MBE) in the UHV chamber on a full graphene layer to obtain pure platinum and cobalt/platinum alloy particles. In situ capping of the resulting sample sample with amorphous carbon to make it air-protected was performed, allowing to perform complementary laboratory measurements such as magneto-optic Kerr effect. All the samples were characterized with a combination of SXRD and crystalline truncation rods (CTRs) measurements. The data are still under analysis using the homemade program PyRod (see below).

[1] "*Point defect-induced strains in epitaxial graphene*"
N. Blanc, F. Jean, A. V. Krasheninnikov, J. Coraux and G. Renaud,
Phys. Rev. Lett. **111**, 085501 (2013)
[2] Different commensurabilities and 10-1300 K thermal expansion of graphene on Ir(111) as a function of preparation"
F. Jean, T. Zhou, N. Blanc, J. Coraux AND G. Renaud,
Phys. Rev. B, **88**, 165406 (2013).

Strains Induced by Point Defects in Graphene on a Metal

Nils Blanc,[1,2] Fabien Jean,[1] Arkady V. Krasheninnikov,[3] Gilles Renaud,[2] and Johann Coraux[1,*]
[1]*Institut NÉEL, CNRS and Université Joseph Fourier, BP166, F-38042 Grenoble Cedex 9, France*
[2]*CEA-UJF, INAC, SP2M, 17 rue des Martyrs, 38054 Grenoble Cedex 9, France*
[3]*Department of Applied Physics, Aalto University, Post Office Box 11100, Aalto FI-00076, Finland and Department of Physics, University of Helsinki, Post Office Box 43, Helsinki FI-00014, Finland*
(Received 13 February 2013; published 20 August 2013)

Strains strongly affect the properties of low-dimensional materials, such as graphene. By combining *in situ*, *in operando*, reflection high-energy electron diffraction experiments with first-principles calculations, we show that large strains, above 2%, are present in graphene during its growth by chemical vapor deposition on Ir(111) and when it is subjected to oxygen etching and ion bombardment. Our results unravel the microscopic relationship between point defects and strains in epitaxial graphene and suggest new avenues for graphene nanostructuring and engineering its properties through introduction of defects and intercalation of atoms and molecules between graphene and its metal substrate.

DOI: 10.1103/PhysRevLett.111.085501 PACS numbers: 81.05.ue, 61.72.J−, 68.60.Bs, 81.15.Gh

Strain engineering, sometimes referred to as "straintronics," is a powerful method for tuning the properties of bulk and two-dimensional materials [1]. Graphene, as an atomically thin membrane with unprecedented mechanical strength [2], offers unique possibilities in this respect. While large compressive stresses applied to this material are readily relieved by wrinkle [3] and nanobubble [4] formation, tensile or small in-plane compressive strains can be stabilized by interaction with a substrate. Strain-induced changes in the vibrational properties [5,6], electronic band gaps [4,7], as well as variations of the local [8] and macroscopic electronic conductivity [9,10], have been reported. Strains are also expected around defects in graphene [11], and their role should be considered wherever defects are involved, for instance, when engineering electronic [12] or magnetic [13] properties using plasma etching or irradiation. Interactions between point defects have been predicted to be attractive or repulsive, depending on their relative orientation and separation [14], which could lead to the buildup of extended strains from local ones.

The experimental exploration of the interplay between defects in graphene and strains has started recently, with atmospheric condition Raman spectroscopy of ion-bombarded exfoliated graphene [15]. A step forward are *in situ* investigations, which we report in this Letter, while the defects are created (or healed) under ultraclean conditions (ultrahigh vacuum). This minimizes the effects of the contamination of graphene with highly reactive defects by molecular species present in air.

Here, we report on the determination of the average strain, with a relative accuracy better than 10^{-3}, during the growth of graphene on Ir(111), its bombardment with ions, and its etching with oxygen, using *in situ*, *in operando* reflection high-energy electron diffraction (RHEED). By combining the observations with *ab initio* density functional theory (DFT) calculations, we show that the global tensile strains stem from local ones around point defects which are formed during O_2 etching at high temperature and ion bombardment, or healed during chemical vapor deposition (CVD). Such strains are found to influence the epitaxy between graphene and the metal and can be used for nanostructuring epitaxial graphene and engineering its properties.

CVD of graphene on Ir(111) under ultrahigh vacuum with ethylene as a carbon precursor [16] at 850 °C started with a 9×10^{-2} μm^{-2} density of nucleation centers, as determined *ex situ* by atomic force microscopy (AFM) under ambient conditions [Fig. 1(a)] [16]. The determination of graphene coverage based on a set of AFM images allowed one to calibrate the ethylene dose. Indeed, coverage increases with dose following a modified Langmuir model without any free parameter [17]. In Fig. 1(b), we show the average coverage of the sample, 24% ± 5%, which allows deducing the ethylene dose by using this model. From the average graphene island density, the average island radius is estimated to be ~1 μm for the

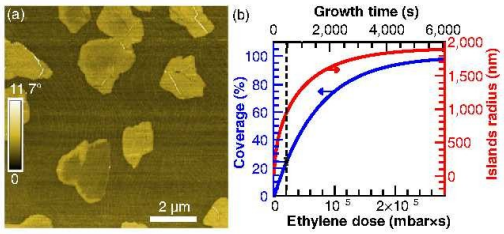

FIG. 1 (color online). (a) AFM phase image of graphene islands (24% coverage) grown on Ir(111) at 850 °C with ethylene. (b) Graphene coverage and average island radius (mainly relevant before ≃ 25%, when coalescence starts) as a function of ethylene dose and growth time. The vertical line corresponds to the ethylene dose for (a).

sample grown at 850 °C, assuming evenly sized, disk-shaped islands.

The growth of graphene was studied with RHEED in real time at two growth temperatures. A typical RHEED pattern is shown in Fig. 2(a) [16]. As expected for a flat crystalline surface, it displays streaks perpendicular to the surface. Two groups of streaks are visible on each side of the specularly reflected beam. Each comprises two streaks. The outer one only appears during graphene growth, and it is roughly 10% farther away from the center of the pattern than the inner one. This streak is ascribed to graphene, whose lattice parameter is ~10% smaller (the distance from the corresponding streak to the center of reciprocal space is thus 10% larger) than the Ir(111) one. We measured the distance between Ir and graphene peaks as a function of ethylene dose [16]. The distance between the Ir streaks served as a reference for lattice parameters, which are tabulated as a function of temperature [18]. Figure 2(b) shows an overall decrease of about 1.6% of a_C, the surface projection of the lattice parameter in graphene, until steady values, of $a_C = 2.4705 \pm 0.0020$ Å at 850 °C and $a_C = 2.4723 \pm 0.0020$ Å at 950 °C, are reached, for graphene coverages above 50% [19]. These values are about 0.6%–0.7% larger than those calculated for freestanding graphene [20], suggesting the presence of a residual tensile strain even in (almost) defect-free graphene. The a_{Ir} surface lattice parameter of Ir(111) (2.7319 and 2.7343 Å at 850 °C and 950 °C) is a fractional number (21/19) times a_C; i.e., graphene and Ir(111) are commensurate. This implies a local periodic C-Ir interaction, giving rise to an energy gain, presumably overcoming the cost associated with the tensile strain energy. Note that no significant increase in a_C is expected as arising from stress relief at the island edges [21] because of the large size (> 100 nm) of the islands.

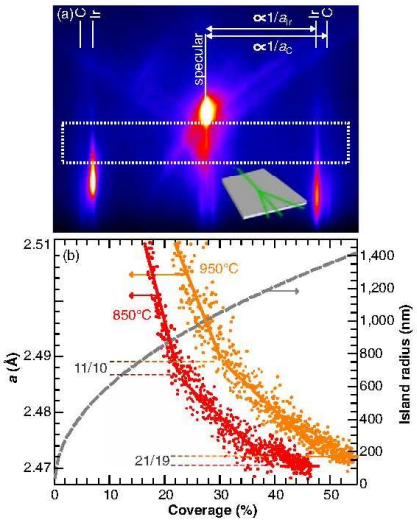

FIG. 2 (color online). (a) RHEED pattern measured with 10 keV energy electrons along the [$\bar{2}$11] direction of Ir(111), for a full graphene layer grown at 850 °C on Ir(111). The distances from the central streak to the other streaks are inversely proportional to the lattice parameters of graphene (a_C) and Ir (a_{Ir}) [16]. The dotted line frame is the region used for determining the position of the various streaks as a function of ethylene dose. (b) Lattice parameter of graphene as a function of graphene coverage, for two growth temperatures (colored lines are guides for the eyes), and average radius of the graphene islands for the sample grown at 850 °C (mainly relevant before ≃ 25% when coalescence starts).

We now discuss the possible origins of the observed decrease in a_C with graphene coverage. The reduction of the graphene-metal interaction as the island size increases due to the decreasing contribution of edge atoms [22], which would relieve heteroepitaxial stress in graphene, can only be marginal, given the fraction of edge atoms in the large islands considered here. The coalescence of neighboring islands, having different registries on Ir(111), implies the accommodation of one substrate interatomic distance over the distance between island nucleation centers ~1 μm, i.e., a negligible ~0.03% strain. More relevant are the numerous vacancies of various sizes that are trapped inside graphene at the growth front. At a 30% coverage, their density is several 0.1 nm^{-2} [17], and a_C is several 0.1% larger than the value at the end of growth. Our DFT calculations [16] for a defect density of 0.2 nm^{-2} reveal that single, di-, and tetravacancies in graphene/Ir(111) are surrounded by a tensile strain field [Fig. 3(a) and Fig. S3 of the Supplemental Material [16]], from a few to several 0.1% depending on the configuration, usually longer ranged for larger vacancies (unless their location allows a close-to-perfect match between the positions of C dangling bonds and Ir atoms). These values are different from those expected in freestanding graphene [23] due to the strong interaction between C and metal atoms at vacancy edges [24] [Fig. 3(a)]. Even though this interaction reduces formation energies of vacancies [25], their migration barriers are high (3–8 eV, depending on the position in the moiré pattern and size of the vacancy), so that the agglomeration of vacancies, a situation reported to be energetically favorable for other types of defects in graphene [26], is hindered, especially for large defects like tetravacancies. Calculations of RHEED profiles from the atomic position optimized with DFT calculations qualitatively confirm the relevance of vacancy-induced strains (Fig. S4 of the Supplemental Material [16]).

The progressive filling of vacancies during growth and the thermally activated diffusion of small vacancies that are annihilated upon reaching the edges of graphene are expected to decrease tensile strains and thus to account for the decrease of a_C. Because of the short lifetime of

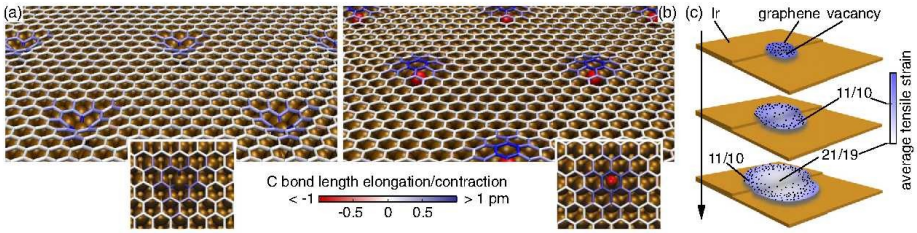

FIG. 3 (color online). Structure of graphene on Ir(111) in the presence of (a) single vacancies and (b) intercalated Ar atoms. Ir and Ar atoms are represented with ochre and red spheres, respectively; C-C bonds are colored according to their length with regard to bonds in pristine graphene (see the color bar). Insets are top views. (c) Sketch of tensile strain (blue shades) in growing graphene islands resulting from the tensile strain due to vacancies (dark dots). Salient points match 11/10 and 21/19 commensurate structures (see the text).

ethylene on graphene at the growth temperature, the filling of the vacancies must be less and less efficient as their size decreases, which agrees with the slower decrease in a_C at larger doses.

Moreover, the decrease in a_C is accompanied by a series of surface phase transitions: it shows salient points at 23% and 31% coverage for 850 °C and 950 °C growth temperatures, respectively, at $a_C = 2.487$ and 2.489 Å, corresponding to a commensurate phase with 11 C rings on 10 Ir atoms (first-order commensurability). Eventually, at 850 °C and 950 °C, a_C reaches 2.4705 and 2.4723 Å steady values, both corresponding to 21 C rings on 19 Ir atoms, a superstructure corresponding to a second-order commensurability similar to the one reported at room temperature in graphene/Ru(0001) [27]. The change of the slope of a_C vs dose points to a tendency of graphene to adopt the 11/10 phase, presumably because it maximizes the interaction between C and Ir. This implies, before the salient point, the coexistence of a 11/10 central region with a more strongly strained region around, where the vacancy density is higher [Fig. 3(c)]. After the salient point, the opposite situation is expected, with a decreasing vacancy density at the center of the graphene island, eventually leading to a 21/19 phase, and a 11/10 region around the center of the island [Fig. 3(c)]. How the slopes of a_C vs dose change with temperature is a tradeoff between vacancy diffusion, healing, and incorporation at edges, and thus a complex balance between vacancy diffusion length (larger at higher temperature), intervacancy distance (likewise, larger at higher temperature), and graphene island radius (whose first time derivative, the growth rate of the islands, is smaller at higher temperature). An additional mechanism can be invoked: the first salient point coincides with the onset of coalescence, above which the graphene-free edge length rapidly decreases. Micrometer-scale slippage of graphene on Ir(111) [28], which would promote the formation of a strained 11/10 phase stabilized by periodic C-Ir interactions, would then be hindered above this point and the slope of the a_C vs dose would decrease.

We now consider two other processes which are known to induce defects in graphene: ion bombardment and etching with oxygen. Once grown at 950 °C and cooled down to room temperature, graphene covering ~100% of the surface was bombarded with 200 eV Ar^+ ions. Such ions are expected to yield prominently single atom vacancies and Ar^+ ions trapped below graphene (referred to as interstitials in the following), with a yield close to unity [29], and to leave Ir(111) essentially nondamaged. The average distance between defects, from a few nanometers to below one nanometer in the ion dose range explored, is smaller than between defects at initial stages of graphene growth. During bombardment, the graphene streaks shift toward the center of reciprocal space, broaden, and loose intensity [Fig. 4(a)]. For an ion dose of about 2×10^6 ions/μm^2, a_C is increased by as much as 2.2% and the FWHM of the graphene streaks is multiplied by 2 before they vanish. Ir streaks only lose intensity but do not move or broaden. This intensity decrease upon increase of the graphene-free area, during graphene etching, is an effective roughness effect, stemming from variations of the graphene coverage at length scales below the coherence length of the electron beam.

The a_C increase can be interpreted as the buildup of tensile strain induced by the formation of single atom vacancies and interstitials, in agreement with our DFT calculations. The increase goes beyond the strain obtained by DFT for an isolated defect. This is a possible signature of the interaction between defects through the strain fields they create. In graphene/SiO_2/Si, much smaller strains were detected with Raman spectroscopy. About 20 cm^{-1} shifts of the 2D vibration mode were found [15], corresponding to 0.3% strains at most under the assumption of biaxial strain [5].

What is the origin for the seven times larger strains measured in graphene/Ir(111)? In graphene/SiO_2/Si, the contact between graphene and its substrate is only local due to a relatively high substrate corrugation, at the protruding points of the substrate, and graphene is

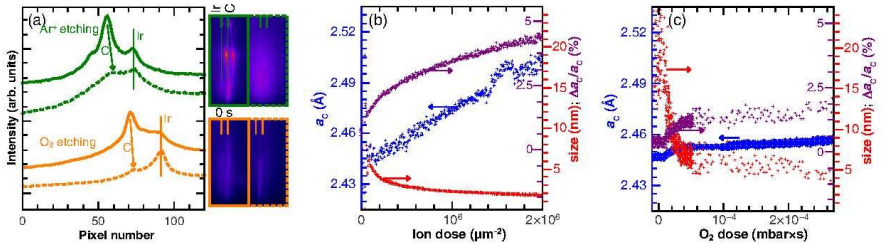

FIG. 4 (color online). (a) RHEED pattern profiles at room temperature before and after Ar^+ bombardment with 200 eV ions (solid and dotted green lines, respectively) and at 950 °C before and at the end of O_2 etching (solid and dotted orange lines, respectively). RHEED patterns close to the first-order graphene and Ir streaks are shown aside before (0 s) and after O_2 etching and Ar^+ bombardment. (b),(c) a_C, size of structurally relevant domains, and relative distribution $\Delta a_C/a_C$ of the lattice parameter as a function of (b) ion and (c) O_2 doses (see the text for a discussion about the relevance of the $\Delta a_C/a_C$ and size estimates).

freestanding elsewhere [30]. Interstitials may be trapped without distorting graphene below these freestanding regions. In contrast, the contact between graphene and Ir(111) is rather intimate, characterized by a 3.4 Å average distance [31]. Strong steric effects are thus expected for interstitials, which should induce noticeable strain fields, in agreement with our DFT calculations [Fig. 3(b)]. In addition, the loose graphene/SiO_2 contact is favorable to nanorippling, rather than bond length compression, in the case of interaction between vacancies or interstitials through their strain fields. In graphene/Ir(111), much less freedom exists for nanorippling due to the nonvanishing graphene-metal interaction, so that C bond contraction must play an important role.

The broadening of the graphene streaks arises from strain fields, the finite size of structurally coherent domains, and/or a roughening of graphene. The first two effects can be estimated from the inverse of the FWHM of the streaks [Fig. 4(b)]. The third effect, resulting from the increasing corrugation around the defects or displaced C atoms not escaping the surface, is more difficult to assess. At low doses, finite size effects are not actually relevant, as the coherence length of electrons (typically 10 nm) sets the apparent size of the structurally coherent graphene domains. At larger doses the estimated size falls below this coherence length, indicating that small domains could be present. Strain fields, typically a few 1% FWHM, are also relevant in this regime. All effects are consistent with large defect densities and a tendency to graphene gradual amorphization under irradiation.

The effects of oxygen etching on a full layer of graphene, which is efficient only at elevated temperatures (here 950 °C), are rather peculiar [Fig. 4(c)]: first, a_C rapidly increases by only 0.4%, then very slowly, and graphene streaks only slightly broaden even before vanishing, after a 2.5×10^{-4} mbar × s O_2 dose. This dose is close to that corresponding to the total removal of graphene, 3×10^{-4} mbar × s, as determined by *in situ* imaging during etching with low-energy electron microscopy in other experimental setups (data not shown). The rapid a_C increase is interpreted as the buildup of strain fields around defects present in low density, vacancies of various sizes, created at the vacancies left in graphene after growth, and/or heptagon-pentagon pairs found at grain boundaries, where local bending and thus reactivity are stronger. Once a critical defect density is reached, O_2 etching most likely occurs at the edges of existing vacancies without the need for creating new ones, presumably by graphene decomposition with intercalated oxygen as an intermediate step [32,33]. Unlike the case of ion bombardment at the highest ion dose explored, qualitative estimates of the size of the structurally coherent graphene domains indicate that they never are below the coherent length of the electrons. The average distance between defects is hence larger than in the case of ion bombardment, and the streak broadening is ascribed to strains around defects, typically in the range of 1%.

In conclusion, we have shown that vacancies formed during CVD, ion bombardment, and high temperature oxygen etching, as well as atoms trapped between graphene and its substrate, all induce significant strains in epitaxial graphene. When the system is close to complete amorphization, with defect separation of less than 1 nm, tensile strains in graphene on Ir(111) reach 2.2%, a value much larger than in graphene on SiO_2. Graphene goes through a series of commensurate phases with its substrate as the vacancy density varies. Besides the strong local perturbations of the properties of graphene due to missing atoms (vacancies), this change of epitaxy is expected to give rise to the changes of the graphene-support interaction. The observed defect-induced strains are, e.g., candidates for engineering the electronic properties of graphene in a straintronics approach, not only around vacancy defect sites [24] but also where the carbon lattice is not disrupted, in between vacancies and around intercalated atoms or molecules. An analog to a zero-energy Landau level, predicted in nanorippled graphene [34], could indeed develop in the regions where strains vary. This hallmark for the

Dirac-fermion-like nature of charge carriers in graphene is, for instance, expected to strongly enhance graphene's chemical reactivity and opens the way to strain-promoted experiments. The effects we observed are also expected to take place during the preparation and processing of a wealth of related systems, for instance, the actively investigated graphene/Cu and BN/metal interfaces.

F. J., G. R., and J. C. acknowledge financial support from the Agence Nationale de la Recherche through Contract No. ANR-2010-BLAN-1019-NMGEM and from EU through GRENADA Contract No. NMP3-SL-2010-246073. A. V. K. acknowledges the Academy of Finland for the support through Projects No. 218545 and No. 263416. Valuable help from Y. Curé and O. Ulrich is gratefully acknowledged. A. K. V. thanks CSC Finland for generous grants of computer time.

*johann.coraux@grenoble.cnrs.fr

[1] K. S. Novoselov and A. H. C. Neto, Phys. Scr. **T146**, 014006 (2012).
[2] C. Lee, X. Wei, J. W. Kysar, and J. Hone, Science **321**, 385 (2008).
[3] W. Bao, F. Miao, Z. Chen, H. Zhang, W. Jang, C. Dames, and C. N. Lau, Nat. Nanotechnol. **4**, 562 (2009).
[4] N. Levy, S. A. Burke, K. L. Meaker, M. Panlasigui, A. Zettl, F. Guinea, A. H. C. Neto, and M. F. Crommie, Science **329**, 544 (2010).
[5] T. M. G. Mohiuddin *et al.*, Phys. Rev. B **79**, 205433 (2009).
[6] F. Ding, H. Ji, Y. Chen, A. Herklotz, K. Dorr, Y. Mei, A. Rastelli, and O. G. Schmidt, Nano Lett. **10**, 3453 (2010).
[7] F. Guinea, M. I. Katsnelson, and A. K. Geim, Nat. Phys. **6**, 30 (2009).
[8] M. L. Teague, A. P. Lai, J. Velasco, C. R. Hughes, A. D. Beyer, M. W. Bockrath, C. N. Lau, and N.-C. Yeh, Nano Lett. **9**, 2542 (2009).
[9] M. Huang, T. A. Pascal, H. Kim, W. A. Goddard, and J. R. Greer, Nano Lett. **11**, 1241 (2011).
[10] X.-W. Fu *et al.*, Appl. Phys. Lett. **99**, 213107 (2011).
[11] O. Cretu, A. V. Krasheninnikov, J. A. Rodríguez-Manzo, L. Sun, R. M. Nieminen, and F. Banhart, Phys. Rev. Lett. **105**, 196102 (2010).
[12] L. Zhao *et al.*, Science **333**, 999 (2011).
[13] R. R. Nair, M. Sepioni, I.-L. Tsai, O. Lehtinen, J. Keinonen, A. V. Krasheninnikov, T. Thomson, A. K. Geim, and I. V. Grigorieva, Nat. Phys. **8**, 199 (2012).
[14] J. Kotakoski, A. V. Krasheninnikov, and K. Nordlund, Phys. Rev. B **74**, 245420 (2006).
[15] E. H. M. Ferreira, M. V. O. Moutinho, F. Stavale, M. M. Lucchese, R. B. Capaz, C. A. Achete, and A. Jorio, Phys. Rev. B **82**, 125429 (2010).
[16] See Supplemental Material at http://link.aps.org/supplemental/10.1103/PhysRevLett.111.085501 for details about surface preparation, graphene growth and etching, details about characterizations, analysis of RHEED patterns, experimental details, DFT calculation framework, and additional DFT results.
[17] J. Coraux, A. T. N'Diaye, M. Engler, C. Busse, D. Wall, N. Buckanie, F.-J. Meyer zu Heringdorf, R. van Gastel, B. Poelsema, and T. Michely, New J. Phys. **11**, 023006 (2009).
[18] R. T. J. Wimber, J. Appl. Phys. **47**, 5115 (1976).
[19] Cooling from a growth temperature of 950 °C to room temperature further decreases a_C to 2.4470 ± 0.0020 Å; in other words, epitaxial graphene on Ir(111) has a positive thermal expansion coefficient, unlike that predicted for freestanding graphene in this temperature range [20].
[20] K. V. Zakharchenko, M. I. Katsnelson, and A. Fasolino, Phys. Rev. Lett. **102**, 046808 (2009).
[21] J. Massies and N. Grandjean, Phys. Rev. Lett. **71**, 1411 (1993).
[22] P. Lacovig, M. Pozzo, D. Alfè, P. Vilmercati, A. Baraldi, and S. Lizzit, Phys. Rev. Lett. **103**, 166101 (2009).
[23] A. V. Krasheninnikov and R. M. Nieminen, Theor. Chem. Acc. **129**, 625 (2011).
[24] M. M. Ugeda, D. Fernández-Torre, I. Brihuega, P. Pou, A. J. Martínez-Galera, R. Pérez, and J. M. Gómez-Rodríguez, Phys. Rev. Lett. **107**, 116803 (2011).
[25] L. Wang, X. Zhang, H. L. W. Chan, F. Yan, and F. Ding, J. Am. Chem. Soc. **135**, 4476 (2013).
[26] M.-T. Nguyen, R. Erni, and D. Passerone, Phys. Rev. B **86**, 115406 (2012).
[27] D. Martoccia *et al.*, Phys. Rev. Lett. **101**, 126102 (2008).
[28] A. T. N'Diaye *et al.*, New J. Phys. **11**, 113056 (2009).
[29] J. R. Hahn and H. Kang, Phys. Rev. B **60**, 6007 (1999).
[30] V. Geringer, M. Liebmann, T. Echtermeyer, S. Runte, M. Schmidt, R. Rückamp, M. Lemme, and M. Morgenstern, Phys. Rev. Lett. **102**, 076102 (2009).
[31] C. Busse *et al.*, Phys. Rev. Lett. **107**, 036101 (2011).
[32] P. Sutter, J. T. Sadowski, and E. Sutter, J. Am. Chem. Soc. **132**, 8175 (2010).
[33] E. Starodub, N. C. Bartelt, and K. F. McCarty, J. Phys. Chem. C **114**, 5134 (2010).
[34] F. Guinea, M. I. Katsnelson, and M. A. H. Vozmediano, Phys. Rev. B **77**, 075422 (2008).

Structure, morphology and ordering of preformed size-selected Pt-based nanoclusters deposited on graphene/Ir moire patterns

S. Linas,[1] F. Tournus[1], L. Bardotti,[1] F. Jean[2,3] and G. Renaud[3]
1 Institut Lumière Matière, Université de Lyon
2 2Institut Néel, CNRS Grenoble
3 3 INAC/SP2M CEA-Grenoble

The aim of this experiment was to determining the structure, epitaxial relationships, lattice relaxation, shape, organization and possibly locations of preformed Pt-based nanoparticles deposited on the moiré pattern of graphene/Ir(111). We had planned to consider 1.5 nm diameter Pt and FePt particles, for two different surface coverages, and follow the evolution of the system with the annealing temperature (up to 300°C). The purpose was to gain insight on both the cluster/cluster and cluster/surface interactions (diffusion, pinning, ordering, coalescence). This proposal is part of the NMGEM ANR project which aims to explore nanomagnetism on graphene/metals. Due to the original behaviour of size-selected Pt clusters deposited on graphite (where a local hexagonal self-organization is observed with a ~1 nm interparticle separation), [1] we expected to observe a self-organization of the Pt nanoparticles on the moiré lattice (periodicity of 2.5 nm).

Three samples have been studied. For each sample, a graphene monolayer has been grown on the (111) surface of an Ir single crystal following the procedure described in ref. 2, and characterized by x-ray diffraction. The sample has then been transferred, under UHV, to the PLYRA platform of Lyon university for cluster deposition (LECBD technique). Size-selected Pt clusters, with a diameter around 1.3 nm have been soft-landed (random deposition) on the moiré pattern. The three samples correspond to different coverages: ~9% for S1, ~15% for S2 and ~4.5% for S3. It should be noted, that given the particle size and the moiré lattice parameter (2.5 nm), a full occupation of each site corresponds to a coverage ~25%. Samples S1 and S2 have unfortunately been exposed to air **after** deposition (problem of sample fixation) while S3 has been prepared and characterized fully in UHV conditions. However, at this point, no major differences were detected between S2 and S3. S1 has been annealed during the x-ray measurements, at a moderate temperature (~200°C), while S3 has been annealed up to 600°C.

As shown in Fig. 1 (sample S1), the GISAXS pattern indicates that the Pt particles are located on the moiré hexagonal lattice. This implies that they have been able to diffuse on the surface and self-organize at room temperature. Some particles must however be almost isolated (no neighbours on the nearest moiré lattice sites) so that the form factor of the Pt clusters is apparent on the GISAXS pattern. This is due to the low coverage used for S1. The GIXRD measurements also indicate that the Pt particles could be in a (111) epitaxy over the Ir crystal (see Fig. 1): this is visible as a shoulder at the bottom of the Ir 110 and 111 diffraction peaks. However, the difference between Pt and Ir lattice parameter is very small (~2%).
Another indication of the location of Pt particles on the moiré lattice is visible on the GIXRD measurements. As shown in Fig. 2, the moiré peaks are more pronounced when Pt particles have been deposited on top of the graphene/Ir substrate. This effect has also been observed in the case of Pt particles obtained by atomic deposition [2]. Interestingly, the intensity of these moiré peaks decreases upon annealing and vanishes between 270°C and 320°C (see Fig. 2). At the same time, the Pt nanoparticle organization evolution has been followed, up to 600°C.

As shown in Fig. 3, while the particle coalescence is limited, the lattice organization remains visibleup to around 500°C. The results still need to be analyzed in details and further experiments with bi-metallic particles should be very fruitful!

[1] D. Tainoff et al., J. Phys. Chem. C 112, 6842 (2008).
[2] N. Blanc et al., Phys. Rev. B 86, 235439 (2012).

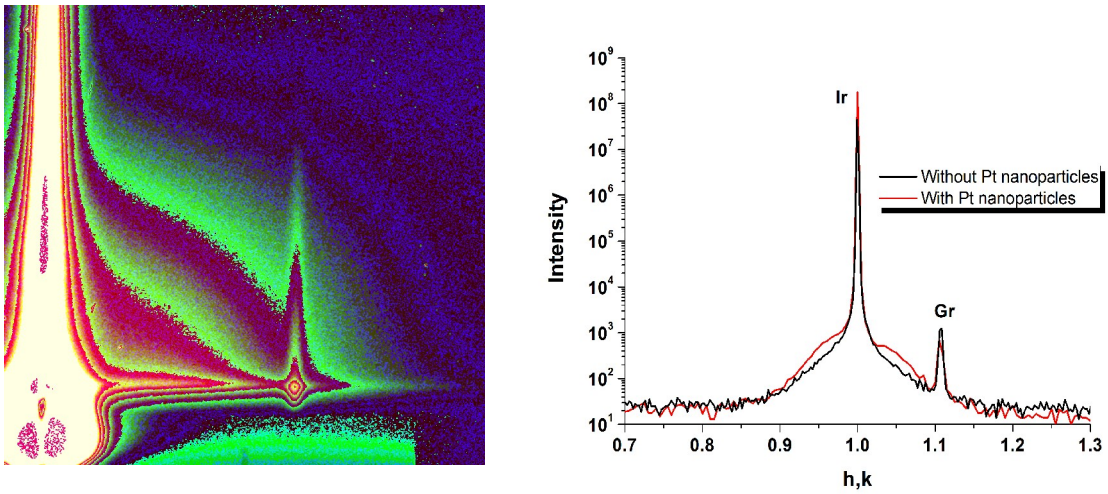

Fig. 1: (Left) GISAXS pattern at room temperature for sample S1. The peak corresponding to the moiré superlattice is clearly visible. (Right) GIXRD measurements for sample S1 around the Ir (110) peak. A shoulder is visible after Pt nanoparticle deposition.

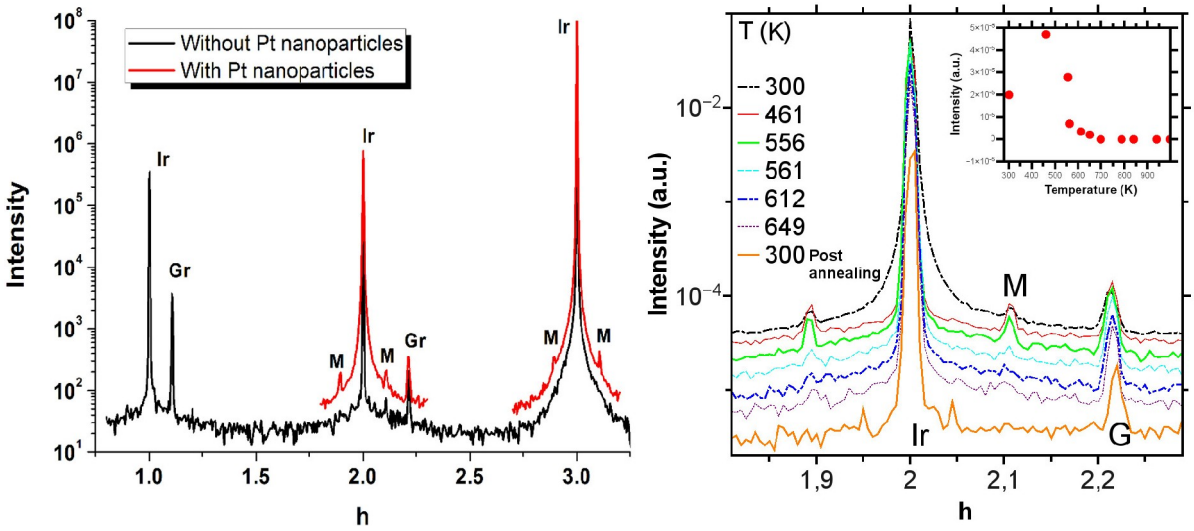

Fig. 2: (Left) Comparison of the GIXRD peak intensities, along the (h00) direction, before and after Pt nanoparticle deposition (sample S3). The moiré peaks are labelled by the letter "M". (Right) Evolution upon annealing of the GIXRD peak intensities, in the (h00) direction, for sample S3.

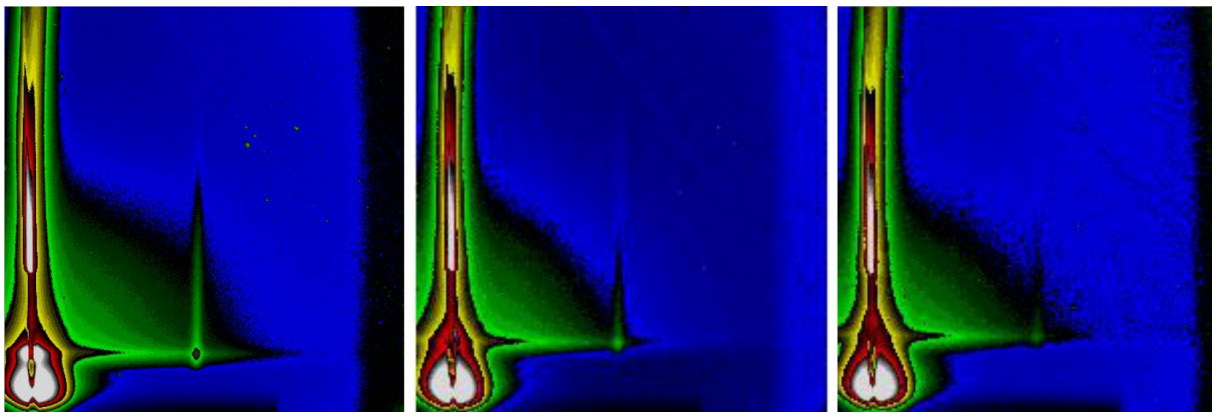

Fig. 3: Evolution of the GISAXS pattern for sample S3 upon annealing. From left to right, the temperature is room temperature, 300°C and 490°C. The peak corresponding to the moiré lattice organization decreases.

In situ X-ray scattering investigations of the Vapour-Liquid-Solid growth of Si nanowires on Si(111) substrates

T. Zhou[1], O. Geaymond[2], O. Ulrich[1] and G. Renaud[1]
1 INAC/SP2M CEA-Grenoble
2 Institut Néel, CNRS Grenoble

In 2013, we have moved from growing mono-element nanowires (*i.e.* Si or Ge) to growing heterostructure nanowires (Fig. 1). Our primary focus was the Ge/Si coreshell NW due to its high yield, homogeneity, its possession of larger strain compared to axial heterostructures and feasibility of carrying out *in situ* experiments.

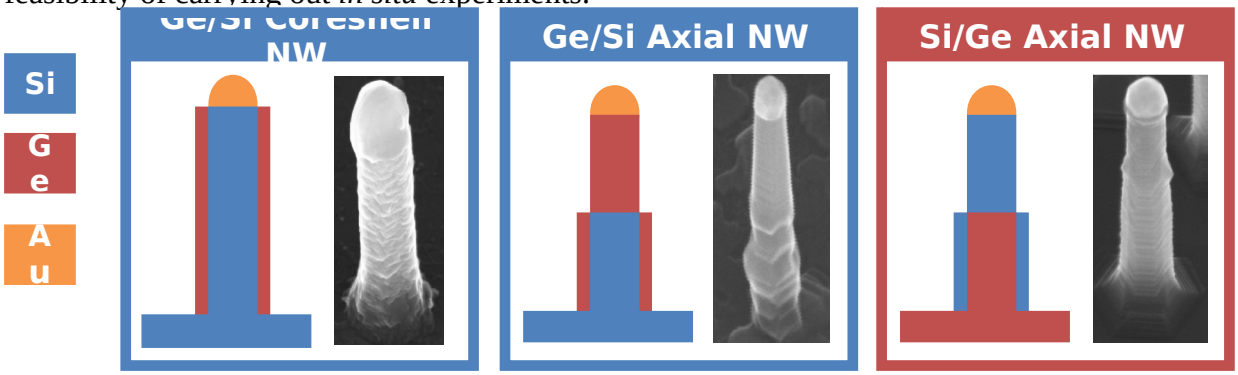

Figure 1 : List of heterostructure nanowires grown at the BM32 beamline with the UHV-CVD instrument.

The objective is to measure the strain relaxation during growth of the Ge shell deposited on the sidewall of the Si NWs. However, due to our large beam size (300µm*400µm), we also expect signals from other objects such as the Si/Ge islands formed on the sample surface as illustrated in Figure 2 (top left).
Our way to filter the unwanted signals involves the growth of a reference sample (Figure 2 top right) which has everything but the coreshell NWs. We did it by depositing only 1ML of gold, enough to form the wetting layer, but insufficient for the formation of AuSi catalyst islands which are indispensable to the growth of NWs.
Immediately after the first injection, we observe on sample 1 a signal having an atomic spacing in between that of bulk Si and bulk Ge (Figure 2 bottom left) whereas on the reference sample nothing was observed. This indicates that the signal must come from the NW sidewall and hence is the object what we intend to study. Further study reveals that these SiGe alloy islands on the NW sidewall has an average atomic spacing that is 3.1% larger than that of bulk Si, and has an average size of around 37 nm.
To understand the composition of the aforementioned mixed signal, we turn to multi-wavelength anomalous scattering techniques. The result as well as our interpretation is shown below. The calculated Ge composition Ge% sits right on the green dashed line (Figure 3 left) which corresponds to a fully relaxed alloy while its value suggests a gradually increasing Ge % from 40% at the Ge/Si interface to 100% at the NW sidewall surface (Erreur : source de la référence non trouvée 3 right).
Other studies carried out with the UHV-CVD instrument in the past year include the study of strain in doped Ge NWs with different dopant concentration (a collaboration with researchers

from the CEA), our own research on the bending of NWs by MBE deposition, both of which are yet to be analyzed.

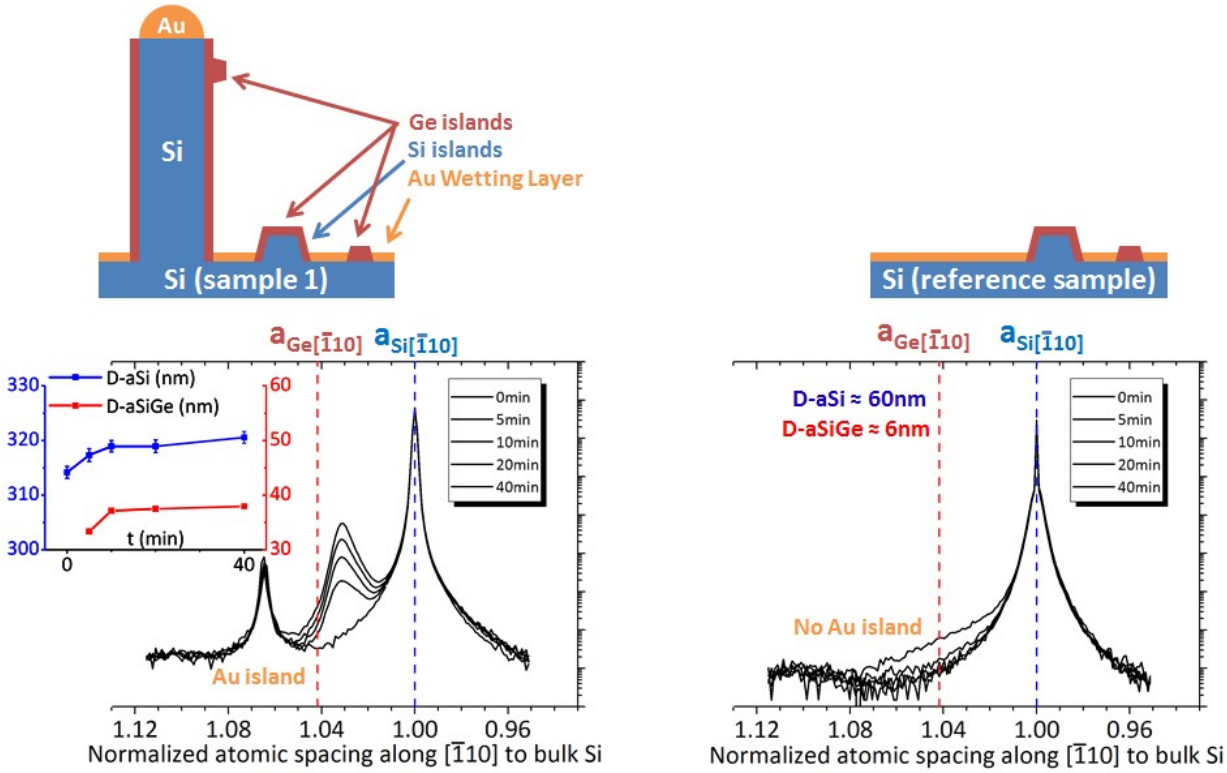

Figure 2 : Top left : illustration of the nano-objects found at the sample surface which includes the SiGe coreshell NW as well as some Si/Ge islands. Top right : only the unwanted islands can be found on the reference sample surface. Bottom left : Measured intensity of a radial scan along the [-110]$_b$ direction at different growth stage The three peaks from left to right are Au peak, mixed SiGe peak and Si Bragg peak. Inset: rocking scans on both the Si peak (blue) and on the mixed SiGe peak (red) reveal the size of the nano-objects. Bottom right: The same measurement on the reference sample.

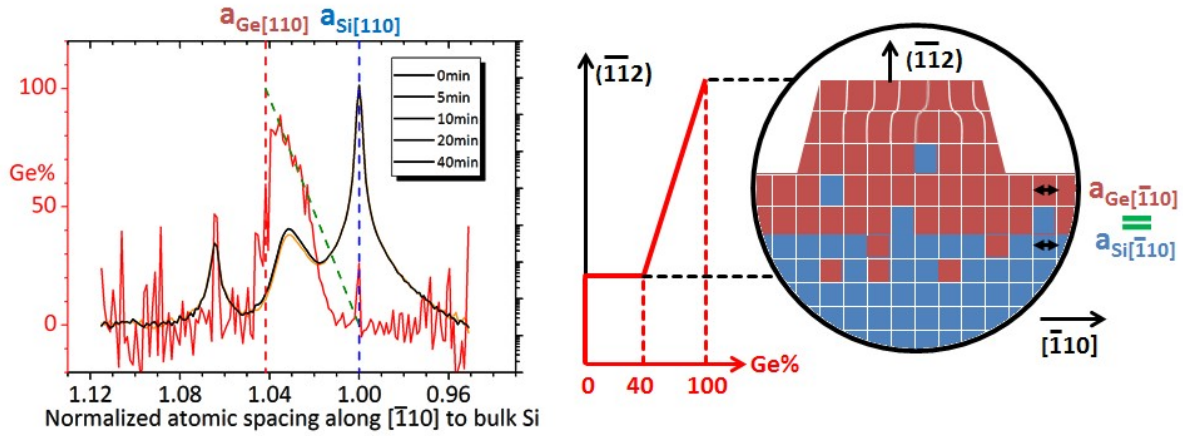

gure 3 : (left) Calculated Ge concentration with anomalous scattering measurements after 20min of injection. (right) Graphical illustration of our interpretation of the data.

Development of Data Visualization, Analysis, Simulation Software PyRod

T. Zhou
INAC-SP2M CEA-Grenoble

A multi-platform software has been developed on BM32 as part of the PhD project of Tao Zhou. The python powered software, codenamed PyRod, is dedicated to the visualization, analysis, simulation of surface diffraction data acquired with the new generation two dimensional detectors. The source code (which runs under Windows, Linux, Mac OS X, given that the required packages are properly installed) and a standalone executable (Windows only) can be found at http://zhoutao.eu/PyRod.

Owing to the lack of a unified standard of how data are named and stored, the use of PyRod is currently limited to data acquired on the two surface diffraction beamlines, ID03 and BM32 at the ESRF. Nevertheless, the software has been subjected to extensive beta tests thanks to beamline co-workers Fabien Jean, Nils Blanc and Gilles Renaud.

Visualization

The first part allows the user to visualize easily, for a given point measured, the corresponding 2D image (Figure 1). Moreover, rather than collecting data from just a series of “points” in the reciprocal space, the 2D detector actually covers a three dimensional volume with a single scan. Additional operations (V-Cut and H-Cut) are implemented to further explore the scanned 3D space in different ways, thus providing a more comprehensive view of the experimental data.

In addition, PyRod can also perform data pretreatment and generate input file for the program IsGISAXS used to simulate and fit GISAXS data.

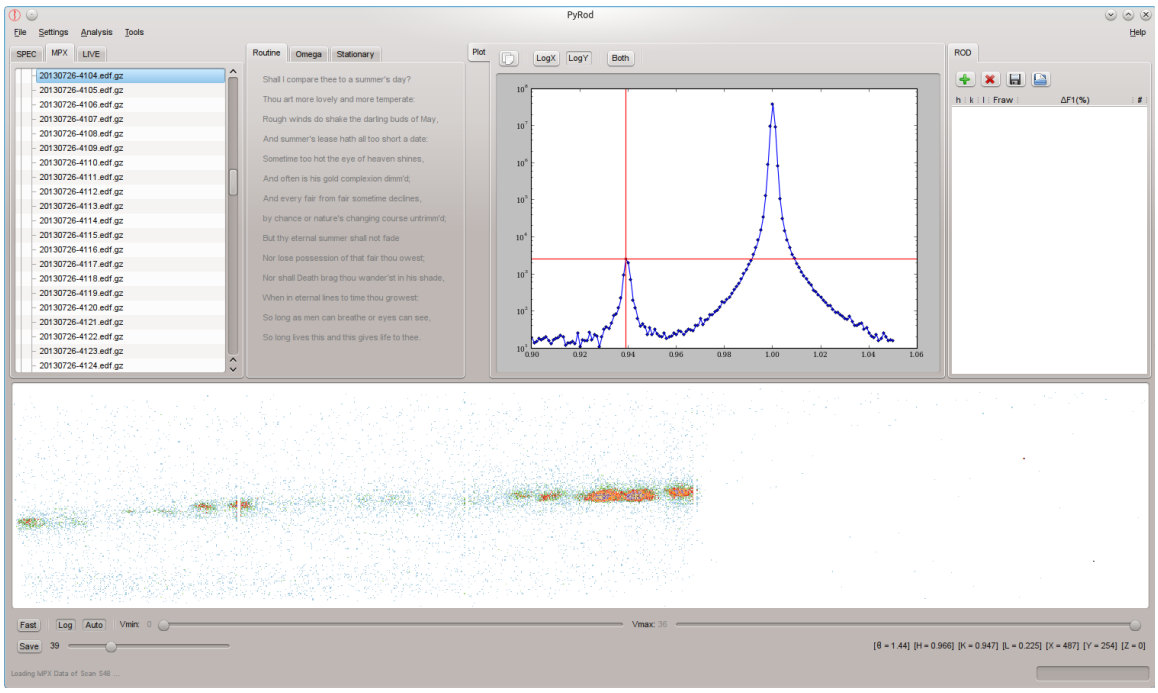

Figure 1 : For a given point chosen (red cross-hair, upper figure), the corresponding 2D image is displayed (lower figure) as well as the name of the file (upper-left panel).

Analysis

The second part operates in a similar way as the ANA-AVE project i.e. the integrated intensity is first calculated, to be subtracted by the background intensity, before applying various correction factors. However, it offers a more flexible user interface and supports various techniques unique to 2D detectors. These techniques, co-published recently by members of the ID03 beamline and us (Drnec, Zhou *et al.* Journal of Applied crystallography, accepted), can dramatically accelerate data acquisition speed (by an estimated factor of 20 to 80).

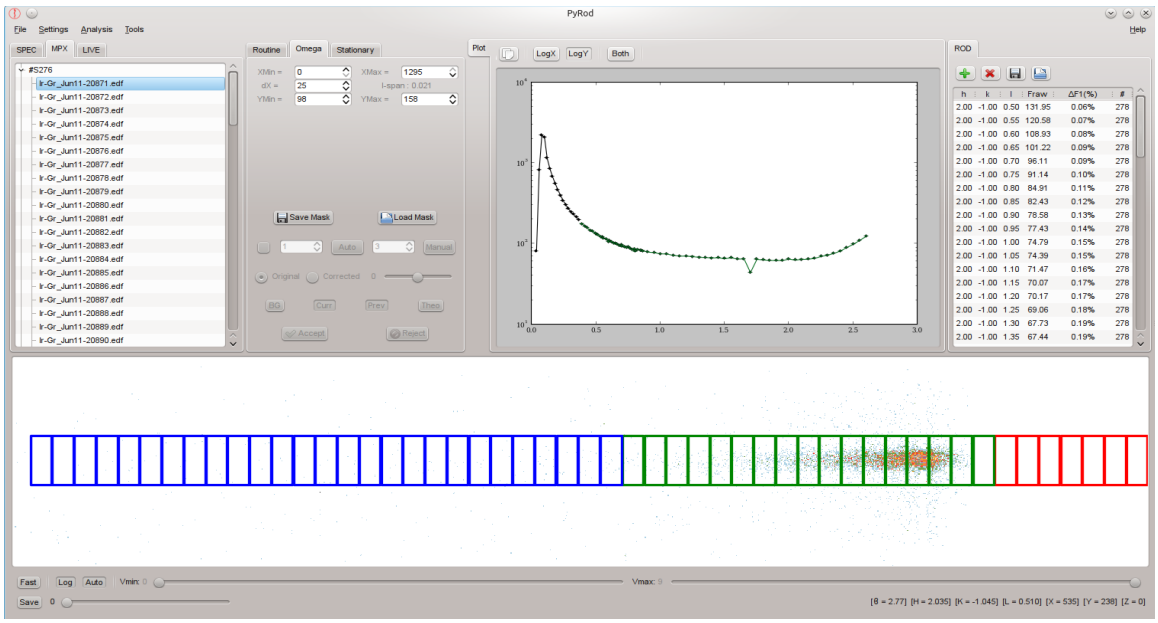

Figure 2 : Data analysis in the "omega-scan mode". Lower figure: Sections of data rejected (red), accepted (green) and to be analyzed (blue). Upper figure: the calculated structure factor from three different scans on the same rod. Right panel: Output file of the calculated structure factor.

Simulation

The third part is basically a rewrite of the popular surface data analysis package ROD, but boasts a more user friendly interface and better flexibility on the parameterization. Ongoing efforts are being made to use this unique feature to analyze Graphene on Ir(111) data measured previously.

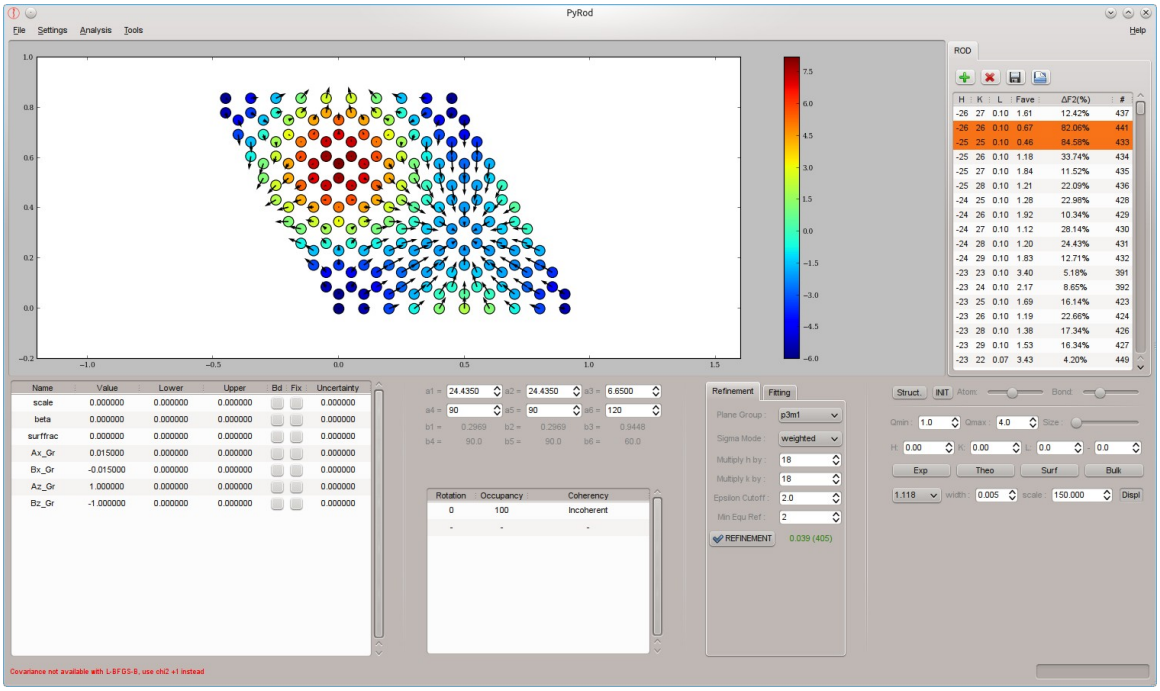

Figure 1: Top figure: the fitted structure model. The displacement perpendicular to the plane of paper is indicated by the false color scale while that parallel to plane of paper is indicated by quivers. Right panel: Non-equivalent reflections refined from raw integrated data. Bottom panels: model input, fitting parameters, plotting parameters…

Grazing-incidence x-ray diffraction measurement of the relaxations and elastic step interactions on vicinal Si(1 1 11) and Si(1 0 11) surfaces

F. Leroy[1], G. Prévot[2], B. Croset[2], F. Cheynis,[1] P. Müller[1], A. Coati[3] and Y. Garreau[3]
Local contact : G. Renaud
1 CINAM, Marseille
2 INSP, Paris
3 Synchrotron SOLEIL

Atomic steps are the most abundant structures/defects present at surfaces. They play a key role at surfaces of materials, e.g. attachment-detachment of ad-atoms at step edges or preferential diffusion at step edges. These elementary mechanims control the morphological evolutions during a thermal annealing or a growth process [1]. Therefore understanding atomic steps dynamics is crucial. In that perspective determining the elastic properties of steps and their mutual interactions is appealing [2]. We have focused on the determination by Grazing Incidence X-ray Diffraction (GIXD) measurements [3-6], of the elastic force distribution on vicinal surfaces close to Si(001). Due to the presence of an anisotropic surface reconstruction on terraces, alternatively (1x2) and (2x1), step interactions are expected to change drastically with the steps orientation [7]. In order to highlight this complex elastic behaviour, we have chosen two zone axis changing the miscut angle of the surface from Si(1 0 11) to Si(1 1 11).
The method consists in measuring by GIXD the diffracted intensity along the Crystal Truncation Rods (CTRs). Indeed it has been proposed [2] and recently measured [3-6] that step relaxations in the underlying volume can be attributed to a line of elastic force dipoles. These relaxations are responsible for modulations of intensity along the CTR and a detailed analysis of this intensity allows determining the value of the elastic force dipole equivalent to a step.
The first step was to be able to prepare vicinal Si surfaces of high enough quality (no contamination and long range order of steps). The approach consisted in preparing Si surfaces in two steps: (i) a *ex situ* wet cleaning by a 'shiraki' etching followed by a final 'Piranha' solution to get a surface with an oxide layer before the transfer into the UHV chamber. (ii) Then the remaining thin oxide layer (1-2 nm) was removed *in situ* by slow deposition of Si (1 ML/min) at 800°C. This low temperature cleaning procedure was enough to prevent the sample holder from contaminating the sample surface. However this approach had been inappropriate. Indeed, the surface roughness resulting from this process was too large. Therefore steps were not long-range ordered and it was impossible to measure the CTR far enough from the Bragg reflection to have a chance to extract intensity arising from elastic relaxations. The second approach, which was more successful, consisted in applying a very short thermal flash (10s; 1500 K) to desorb the thermal oxide capping and to promote the surface mobility in order to allow an ordering of the atomic steps. With this method we have been able to prepare high quality vicinal Si surfaces.

During this run we have focused on the characterization of the diffracted intensity from Si(1 1 n) surfaces. From the Si wafers available we had different Si surface orientations (3.5° to 7.3° -off from Si(001); <110> zone axis). Finally we have quantitatively measured the diffracted intensity from Si(1 1 11), Si(1 1 15) and Si(1 1 23) surfaces.

For each surface we have extracted more than ~500 structure factors arising from more than 15 CTRs. Clear modulations of intensity on satellite rods close to Bragg reflections indicate that elastic relaxations induced by steps are clearly measureable (see Figure). These large intensity variations are sufficiently reliable to propose a description of atomic steps in terms of elastic dipoles. The analysis is still in progress and will benefit from the codes developed by one of us to fit the elastic relaxations assuming step-step dipolar interactions.

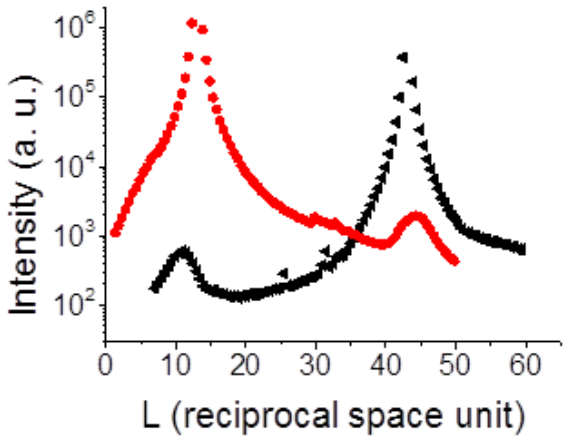

Fig: Non corrected intensity profiles along (16 0 L) (red) and (18 0 L) (black) CTRs. Intensity variations are measured each time a rod is coming close to a neighboring Bragg reflection. This effect is dominated by elastic relaxations and not by the diffuse scattering background of the Bragg peak.

The use of the beamline was successful and high quality data obtained. This proposal was part of a larger project aiming at addressing the elastic relaxations induced by steps on different faces of Si and to propose a model in terms of linear elastic dipoles. Already step interactions on vicinal Si surfaces close to Si(111) have been measured and published [5]. We pursue this research activity with vicinal Si surfaces close to Si(001).

[1] P. Müller, A. Saùl, Surf. Sci. Rep. 54, 157 (2004).
[2] V. I. Marchenko, Sov. Phys. JETP 54, 605 (1982).
[3] G. Prévot, P. Steadman, S. Ferrer, Phys. Rev. B 67, 245409 (2003)
[4] G. Prévot, A. Coati, Y. Garreau, Phys. Rev. B 70, 205406 (2004)
[5] G. Prévot, F. Leroy, B. Croset, Y. Garreau, A. Coati, P. Müller, Surf. Sci. 606, 209 (2012)
[6] G. Prévot, B. Croset, Phys. Rev. Lett. 92, 256104 (2004)
[7] F. K. Men, W. F. Packard, M. B. Webb, Phys. Rev. Lett. 61, 2469 (1988); F. Liu, M. Lagally, Phys. Rev. Lett 76, 3156 (1996).

Low pressure CO oxidation on AuCu nanoparticles supported on TiO_2(110)

A. Wilson[1], G. Prévot[1], R. Bernard[1], Y. Borensztein[1], B. Croset[1], Y. Garreau[2], A. Coati[2], A. Vlad[2], A. Bailly[3], M.-C. Saint Lager[3]
Local contact : G. Renaud
1 INSP, Paris
2 SOLEIL Synchrotron
3 Institut Néel, CBRS-Grenoble

Au-Cu nanoparticles (NP) attract a growing interest due to their specific catalytic properties for various reactions (CO oxidation, PROX, alcohol oxidation, propene epoxidation or methyl glycolate synthesis). For CO oxidation, it has been shown that the alloyed NPs display better performances than pure Au or Cu NPs. In all cases, bimetallic NPs are more thermally stable than monometallic ones, reflecting a decrease of the Ostwald ripening kinetics. If the synergetic effects between the two metals are clearly shown, the role of the support is not clearly understood. This is mainly due to a lack of precise structural characterization of the Au-Cu nanoparticles and their relationship with the oxide substrate, in particular during the reaction. In order to disentangle such effects from the role of the ligands (for NPs prepared by chemical way), it is necessary to work with NPs prepared by physical methods under UHV and on well characterized surfaces.

By evaporating Au and Cu on TiO_2(110), we have synthesized bimetallic Au-Cu NPs of controlled size and composition, namely pure Cu, $Au_{0.5}Cu_{0.5}$ and $Au_{0.7}Cu_{0.3}$ of size 1.5-2 nm. The sizes have been estimated from the fwhm of the diffraction peaks in the GIXD spectra, and the composition and deposited quantities from ex-situ RBS analysis.

These NPs are epitaxied on the substrate with various planar orientation (mostly Au-Cu(112)//TiO_2(110) or Au-Cu(111)//TiO_2(110)) but sharing all the Au-Cu[1-10]//TiO_2[001] epitaxial relationship. By GIXD and GISAXS, we have studied the structure and morphology of these NPs under O_2, CO and $CO+O_2$ low pressure (up to 10^{-4} mbar) gas environment and for temperature ranging from 300K to 700K.

We have first studied the stability of pure Cu NPs under O_2. STM studies show that small NPs disappear after exposure to 10^{-5} mbar oxygen, but that larger NPs are stable. Performing similar adsorption and following the evolution of the Cu NPs by GISAXS (mean size 2 nm, 2.5 10^{15} at/cm^2), we have observed that the lower tail of the particle size distribution is no more present after O_2 exposure. This confirms the STM observations. On the contrary, GIXD measurements do not evidence the formation of bulk Cu oxide. The intensity of the diffraction signal for various diffracting planes of the NPs does not show any significant variation during O_2 adsorption. However, a slight shift of the diffraction peak positions indicates that the mean lattice constant of the NPs increases (by 0.01Å). This is probably related to surface stress variation upon oxygen chemisorption.

Au-Cu NPs behave differently. For the same O_2 exposure as for pure Cu NPs, the GISAXS maps of $Au_{0.5}Cu_{0.5}$ (mean size 1.5 nm, 1.8 10^{15} at/cm^2) are identical after and before gas adsorption. Au stabilizes the small Cu NPs and prevents their dissociation upon oxygen adsorption. Contrary to the previous case, strong modification of the diffraction peak positions can be seen by GIXD. Upon oxygen adsorption, the mean lattice constant increases by 0.06Å. In that case, these variations must be attributed to Cu segregation at the surface of the NP (this has also been further confirmed by XPS on the TEMPO beamline of SOLEIL synchrotron).

Interestingly, the NPs do not evolve after pumping the oxygen, nor upon CO exposure (without O_2). Upon annealing up to 500 K, various changes are observed, but it is difficult to disentangle the effect of NP ripening, which are clearly evidenced on the GIXAXS map, from the effects of reverse segregation.
Finally, in a last experiment performed on $Au_{0.7}Cu_{0.3}$ NPs (mean size 1.4 nm, 1.2 10^{15} at/cm^2), we have evidenced that upon adsorption of a stoichiometric CO + O_2 mixture at room temperature, these NPs suffer a subsequent modification of their epitaxial relationship, in particular with a transformation to Au-Cu(001)//TiO_2(110).
Discussion
These experimental results are a first step to studies under higher gas pressure. The first important results obtained are that Au stabilizes Cu NPs, but that oxygen adsorption induces Cu surface segregation. The second important result obtained is that AuCu NPs are reactive at low pressure of reactant. This can be deduced from the change of epitaxial relationship of $Au_{0.7}Cu_{0.3}$ NPs observed at room temperature under CO+O_2 exposure which can only been explained by the heat released by the reaction (283 kJ/mol). A promising collaboration with *Laboratoire de chimie theorique* (ENS Lyon) will allow us to compare these results to DFT and DFT+U simulations of the model system for both UHV and *in-operando* conditions. The correlations of these two techniques (X-ray and DFT) shall bring us innovative results concerning heterogeneous catalyze with bimetallic NPs on reducible oxides.

Structure stress and strain at the CoO/Pt(111) interface

M. De Santis, A. Lamirand, H. Tolentino, A. Ramos, S. Grenier.

Ultrathin transition metal oxide (TMO) films are investigated mainly for their catalytic and magnetic properties. Similar to alumina films, the large supercells of epitaxial ultrathin TMO films grown on metals are also used as templates for self-assembling arrays of metal nanoclusters, as shown in the cases of the moiré or zigzag pattern resulting from the growth of a single FeO bilayer on Pt(111) and TiOx/Pt(111), as well as the (4 × 4) vanadium oxide mesh on Pd(111). These applications require understanding the surface structure of the oxide films.

Oxidization of 1 Co monolayer (ML) grown on top of Pt(111) results, under well defined growing conditions, in an almost-flawless moiré pattern of period about 2.7 nm. Fig. 1(a) and 1(b) show an STM image and the LEED pattern, respectively, of such a surface [M. De Santis, A. Buchsbaum, P. Varga and M. Schmid, Phys. Rev. **B** 84, 125430 (2011)].

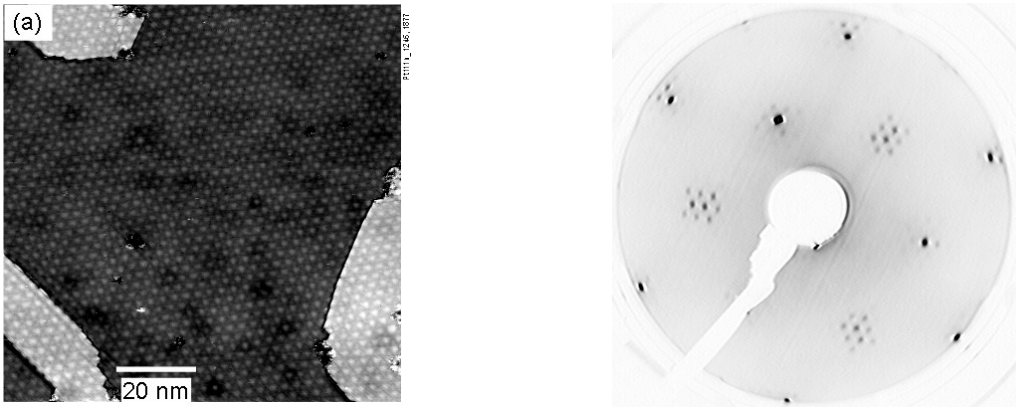

FIG. 1. (a) STM image (V_s= +0.5 V, I_t= 0.1 nA) and (b) LEED (E=120 eV) of 1 ML Co/Pt(111) deposited at RT, annealed and dosed with O2 at 570 K, then annealed under oxygen at 740 K.

STM at different bias put in evidence both the geometric corrugation of the cobalt oxide layer and surface electronic states (Fig.2).

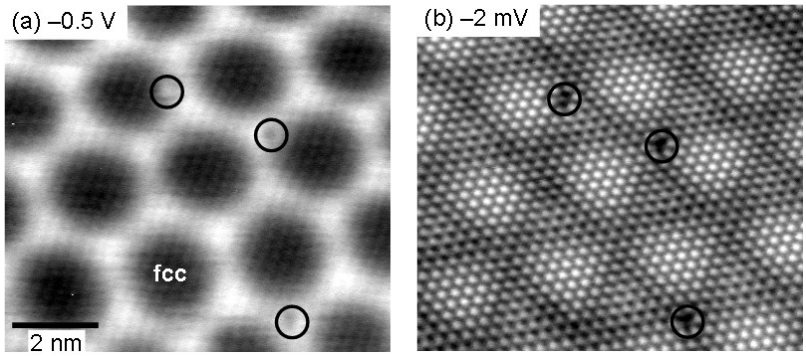

FIG. 2. STM images of the CoO/Pt(111) moiré structure. The same region is imaged with different sample bias (I_t= 1 nA).

The moiré pattern is supposed to be formed by a CoO(111) atomic bilayer oxygen terminated on top of the Pt(111), similar to that one observed for FeO/Pt(111). One of the tasks of the present experiment is to confirm such a structure. Other atomic configurations (like e. g. a trilayer O-Co-O structure, analogous to the surface structure of Rh(111) after oxidation) cannot be excluded a priori. The surface of this CoO(111) bilayer is polar, and atomic rearrangements are expected with respect to the bulk structure. A compression of the interlayer Co-O spacing would reduce the dipole energy, but it would result in an in-plane expansion and in an increase of the misfit stress with the substrate. The overlayer structure is then the result of a complex balance between the electrostatic and the elastic energy.

During the experiment, a full data set has been collected on a surface obtained by deposition of 1 ML Co/Pt(111), followed by annealing and dosing with O2 at 570 K, then by annealing under oxygen up to 870 K. Such a procedure avoids Co diffusion in Pt and results in a well ordered surface. The XRD data show the appearance of new diffraction rods besides the CTRs, which are located at in the hexagonal Pt(111) mesh reference. The observed Moiré pattern results then from the superimposition of CoO and Pt hexagonal mesh, with a period of . The resulting $d_{Co\text{-}Co}$ interatomic distance is of 312 pm, in good agreement with the value (309 ± 2 pm) obtained by STM. Further satellites peaks are observed at , which proves a modulation of the interatomic distances. Fig. 3 shows the structure factor modulus for CTRs, main CoO(111) rods and satellites rods extracted from the measured data.

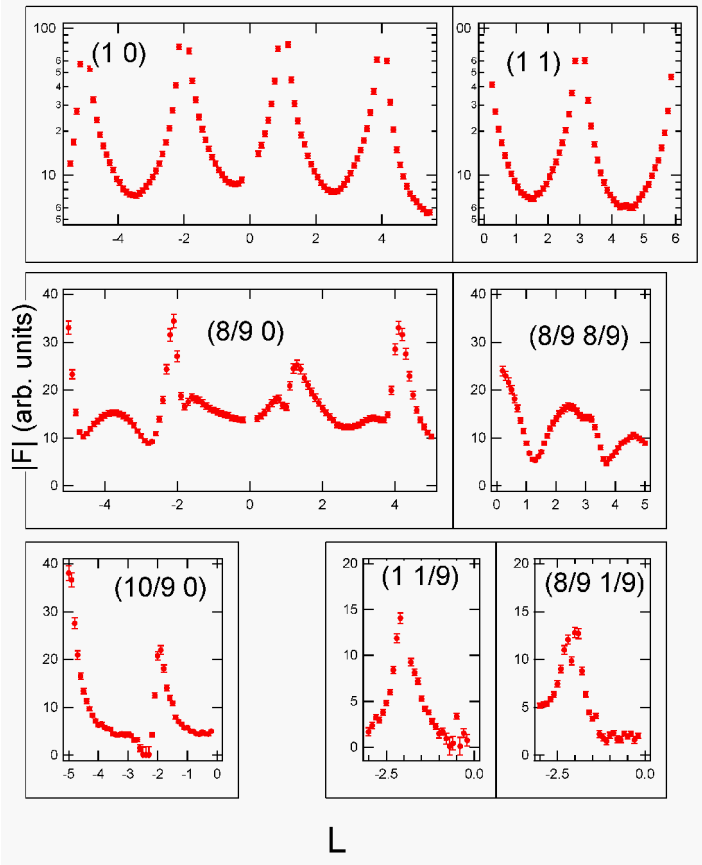

Fig. 3. Experimental rods.

The main CoO rods shows the superimposition of a smooth oscillation and of sharp peaks. The former comes from the 2D oxide structure, while the latter is due to the stress in Pt surface. GIXD is a powerful method for measuring the elastic displacement modes in bulk crystals close to the interface (G. Prévot, A. Coati, B. Croseta and Y. Garreau, J. Appl. Cryst. (2007). **40**, 874–882). Using Hooke's law, these displacements are related to the interface stress in the approximation of linear elasticity. This relationship between stress and strain is at the origin of nanostructuring at the N/Cu(001) and O/Cu(110) interface. In the present CoO/Pt(111) moiré the interface strain can be the origin of preferential nucleation sites which are the key for growing self-arranged nanostructures on top. The detailed structural analysis is in progress.

Structure, exchange coupling and spin orientation in ultrathin CoO/PtFe double-layers on Pt(001)

Anne D. Lamirand[1], Marcio M. Soares[1], Hélio C.N. Tolentino[1], Maurizio De Santis[1], Aline Y. Ramos[1], Julio C. Cezar[2], Abner de Siervo[3] and Matthieu Jamet[4]

[1] *Institut Néel, CNRS and UJF, BP166, 38042 Grenoble, France*

[2] *Laboratorio Nacional de Luz Sincrotron, LNLS, CNPEM, Campinas, Brazil*

[3] *Instituto de Fisica, UNICAMP, Campinas, Brazil*

[4] *Institut Nanosciences et Cryogénie, INAC, CEA, 38054 Grenoble, France*

This is a report on the growth, structure, exchange coupling properties and magnetic structure of ultrathin CoO/PtFe double-layer systems with perpendicular magnetic anisotropy on Pt(001) substrate. The growth and the structure have been studied by in situ surface x-ray diffraction at grazing incidence at the BM32 beamline at the ESRF, France. The growth by reactive molecular beam epitaxy of the cobalt oxide on a Pt-terminated PtFe/Pt(001) surface gives rise to an hexagonal (111)-like surface. The strain imposed by the substrate on the CoO layer leads to a monoclinic distorted structure at room temperature. This monoclinic distortion resembles that of the low temperature antiferromagnetic (AFM) phase of the bulk CoO compound [1] (fig.1-a).

To complement the studies with magnetic properties, soft x-ray absorption spectroscopy (XMCD and XMLD) experiments were performed at the PGM beamline of the Brazilian synchrotron radiation facility, LNLS, Brazil, and at the ID08 beamline at the ESRF. XMCD is sensitive to the ferromagnetic component of both Fe and Co, while XMLD provides information on the AFM spin orientation and on the transition temperature [2,3]. The study yielded an ordering temperature of T_N=293 K and demonstrated that the Co and Fe spins at the interface are coupled orthogonally to each other. The Fe spins are out-of-plane, with a strong perpendicular anisotropy, while the Co spins are oriented in-plane (fig.1-b). Magneto-optic Kerr effect in the polar geometry shows that the exchange coupling of such a distorted CoO layer with the PtFe(001) gives rise to a robust perpendicular exchange bias shift, which is kept up to the AFM ordering temperature T_N. This finding provides a unique example where the blocking and ordering temperatures of an ultrathin CoO layer are identical and match the bulk AFM transition temperature. Such exceptional behavior shares a close relationship with the good crystalline quality and the strain-induced monoclinic distortion of the CoO layer.

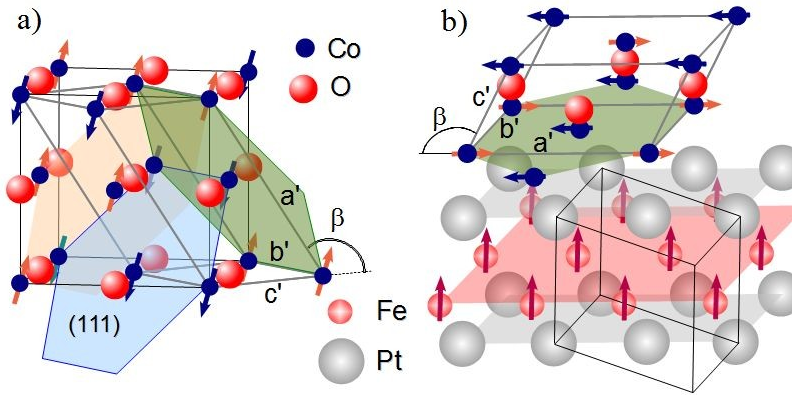

Fig.1: a) CoO crystallographic structure and b) CoO layer on PtFe(001) surface showing spin structure

These results have been published in a recent Physical Review B [5] (see attached paper). In complement to that study, we have studied the growth of the same CoO layer on Pt(001), but looking for an alternative synthesis pathway in order to change the crystallographic orientation of the CoO layer. By growing an initial defective layer of Co oxide (CoOx, x<1), we succeeded to change the (111) orientation to the (001) cubic CoO. Such a layer has no monoclinic distortion, which should affect the magnetic properties. This study is under way.

[1] Jauch et al, Phys. Rev. B 64, 052102 (2001)
[2] G. van der Laan et al, Phys. Rev. B 77, 064407 (2008)
[3] Csiszar et al, Phys. Rev. Lett. 95, 187205 (2005)
[4] F. Mittendorferet al, Phys. Rev. Lett. **109**, 015501 (2012).
[5] A. Lamirand et al., Phys. Rev. B 88, (2013)140401(R)

Structural properties of perpendicularly magnetized systems : CoO/Ni and Ni/CoO bilayers grown on Pd(001)

Anne D. Lamirand[1], Hélio C.N. Tolentino[1], Maurizio De Santis[1], Aline Y. Ramos[1], Marek Przybylski[2] ,Piotr Kuswik[2]
[1] Institut Néel, CNRS and UJF, BP166, 38042 Grenoble, France
[2] Max Plank Institut, Halle, Germany

Introduction

When a ferromagnetic (FM) thin film in contact with an antiferromagnetic (AFM) thin film is cooled through the Néel temperature of the AFM in an applied magnetic field the hysteresis loop of the FM shows enhanced coercive field and a loop-shift. This effect, called exchange bias, arises if the AFM order is established in the presence of the FM via the interfacial FM-AFM interaction. Exchange bias has been widely investigated in systems presenting in-plane anisotropy and has been applied in the magnetic recording (media) and in sensors such as spin-valves based devices, etc. Even more prominent candidates for developing new technologies are double-layer based systems combining magnetic out-of-plane anisotropy and perpendicular exchange bias effect. There is an interest also due to the fact that the phenomena of its magnetic interaction are still not yet entirely clear.

Fe-Co [1,2] and Ni [3,4] films grown on strongly mismatching fcc substrates like Pd, Ir and Rh(001) exhibit perpendicular easy magnetization axis induced by tetragonal distortion. In particular, Ni films grown on Pd(001) show perpendicular easy magnetization axis at RT, approximately up to a thickness of 15-17 ML [4]. The result confirms a volume character of perpendicular magnetic anisotropy of Ni films due to their tetragonal distortion [2,3]. Above the thickness of 17 ML of Ni the easy magnetization axis rotates towards the sample plane. A possible explanation of this change is the relaxation of the film structure which decrease the tetragonal distortion and so the perpendicular magnetic anisotropy.

Finally, it is relatively easy to grow an AFM layer, e.g., of CoO, on top of Ni(001) film. CoO seems to be a good candidate since its vertical expansion/contraction has a strong effect on electronic structure, and thus on magnetic anisotropy. Therefore, manipulation of the epitaxial strain, e.g. by growing CoO on a mismatching substrate, can change the spin axis from in-plane to out-of-plane [5]. For instance, a compressive in-plane strain (and thus the tetragonal distortion) by growing CoO on Ag(001) leads to a modified electronic structure, more precisely, to the overlap between the Co d_{xy} and oxygen orbitals different than for the bulk CoO. As a result, the orbital moment is expected to be not fully quenched, and a non-

zero in-plane orbital moment is expected to exist. Thus one can expect the preferable spin orientation in the sample plane. For a similar lattice distortion (as expected for CoO film grown on top of Pd(001)), a similar effect is expected. It should be noticed, however, that the expanded in-plane lattice experienced by CoO due to its growth on MnO results in spin axis perpendicular to the sample plane. It should be mentioned, that also preparation condition of CoO can influence the growth orientation [6] which may have a strong impact on the magnetic properties.

Our recent MOKE study shows that when CoO layer is deposited on Ni film on Pd(001) (which has in-plane magnetic anisotropy), it changes remarkably magnetic anisotropy of the system [4]. At temperatures lower than Neel temperature of CoO (T_N,CoO=293K), the CoO(001)/Ni bilayers show perpendicular magnetization and exchange bias effect up to the thickness of Ni much larger than the thickness up to which Ni films on Pd(001) show perpendicular anisotropy. We applied a simple method to prove whether the temperature at which the perpendicular anisotropy starts to decrease is related to the antiferromagnetism of CoO. We oxidized the topmost 1-2 atomic layers of Ni film and then covered with another 3ML of CoO (this results in the Neel temperature remarkably increased since T_N,NiO= 525K). The procedure causes perpendicular magnetization to be restored in the same thickness range but even at RT, which confirms the effect to be due the coupling to the antiferromagnetic film on top of Ni.

Results

The aim was to study the growth and the structural properties of both CoO and Ni on Pd(001) and then how the second layer stack on first one, i.e., how CoO grows on Ni/Pd(001) and Ni grows on CoO/Pd(001).

We used in situ grazing incidence x-ray diffraction (GI-XRD) at the French CRG BM32 beamline at the European Synchrotron Radiation Facility (ESRF, France) to study and optimize the growth of ultrathin Ni and CoO films on a clean Pd(001) substrate. The substrate was prepared by Ar sputtering and annealing cycles. The Ni layer was grown by thermal deposition at a rate of 0.25ML/min at a base pressure of 1x10-10 mbar on the clean Pd(001) substrate hold at 300 K. The layer grows at coherent epitaxy and displays a large tetragonal distortion up to about 6 ML. After that, it starts to relax the in-plane strain. From 15 to 23 ML it is almost completely relaxed with the epitaxial relation Ni(100)//Pd(100). The thickness measured by the period of the Kiessig oscillations in the final layer was found to be 22 ML, very close to the nominal one (23 ML) given by the quartz balance calibration. The lattice constant parallel and perpendicular to the surface are 3.59(2) Å and 3.47(2) Å, respectively, resulting in a c/a=0.97(1).

The CoO layer was grown by reactive thermal deposition on the ultrathin (22 ML)-Ni(001) layer hold at 375 K. First of all, 1 ML Co was deposited on top of the Ni film under ultra-high vacuum (2x10-10 mbar). The increase of the Ni truncation rods intensity and the decreasing of the peak width indicated that the Co layer is pseudomorph on the Ni(001) surface. Exposure to a partial oxygen pressure (8x10-7 mbar during 5 minutes) leads to the formation of an epitaxial (001) oriented rocksalt-like film with in-plane lattice constant of 4.15(2) Å. Its average thickness is estimated by the peak width perpendicular to the surface (perpendicular momentum transfer) and roughly corresponds to about 4 mixed atomic monolayers. However, the out-of-plane lattice parameter could not be measured precisely at this step. Both a decrease of the intensity of the metallic (Ni) rods and a widening of their peak were observed. This widening corresponds to a thickness reduction of 2 ML (1 Co + 1 Ni). Further deposition of 2 ML Co under a partial oxygen pressure (8x10-7 mbar) results in

an increase of the oxide layer thickness, while the Ni film remains unchanged. The lattice constant parallel and perpendicular to the surface are 4.18(2) Å and 4.31(1), respectively, indicating a slightly in-plane compressed oxide layer with c/a of about 1.03. The Ni lattice constants did not change during the whole oxide growth process. The average Co(Ni)O oxide layer thickness has been estimated to be 1.3 nm, i.e. about three CoO lattice parameters.

Reactive thermal deposition of CoO on pure Ni(001) oxidizes then about 1-2 ML of Ni. The interface between the Ni(001) and CoO layers shows a small Ni oxide contribution related to Ni atoms dispersed within the CoO layer and/or from Ni-O bounds at the interface. Such a Ni oxide component lead to the small increase in the Néel temperature of the Co(1-x)Ni(x)O layer observed by MOKE and XMLD studies. We show that the ferromagnetic properties are characteristic of metallic Ni and are not affected by the small oxide contribution. A short letter is being prepared to present the structural results along with the magnetic properties [4] (see attached draft).The detailed growth procedure and x-ray diffraction study of CoO on both Ni(001) and Pd(001) will be presented elsewhere.

References:

[1] "Strongly enhanced orbital moment by reduced lattice symmetry and varying composition of Fe1-xCox alloy films", F. Yildiz, F. Luo, C. Tieg, R.Abrudan, X. L. Fu, A.Winkelmann, M. Przybylski, J.Kirschner, Phys. Rev. Lett. **100**, 037205 (2008)

[2] "Volume contribution to perpendicular anisotropy in Fe0.5Co0.5 alloy films on Pd(001, Ir(001), and Rh(001)", F. Yildiz, M. Przybylski, J. Kirschner, Journal of Applied Physics **105**, (7), pp 07E129/1-3 (2009)

[3] "Magnetic anisotropy and magnetostriction in tetragonal and cubic Ni", O. Hjortstam, K.Baberschke, J.M. Wills, B. Johansson, O. Eriksson, Phys. Rev. B **55**, (1997) 15026.

[4] "Effect of CoO/Ni exchange coupling on perpendicular magnetization of Ni films on Pd(001)", P. Kuswik, P. L. Gastelois, H.C.N. Tolentino, M. De Santis, A.Y. Ramos, M.M. Ramos, M. Przybylski, J. Kirschner, Phys. Rev., submitted

[5] "Controlling Orbital Moment and Spin Orientation in CoO Layers by Strain", S. I. Csiszar, M. W. Haverkort, Z. Hu, A. Tanaka, H. H. Hsieh, , H.-J. Lin, C. T. Chen, T.Hibma, L. H. Tjeng, Phys. Rev. Lett. **95**, 187205 (2005).

*[6] "Tuning the Growth Orientation of Epitaxial Films by Interface Chemistry", M. Gubo, Ch. Ebensperger, W. Meyer, L. Hammer, K. Heinz, F. Mittendorfer, J. Redinger, Phys. Rev. Lett. **108**, 066101 (2012).*

Correlation between structural properties and magnetic behaviors of Fe1-xCox thin films grown on the Ir(001) surface

Anne D. Lamirand[1], Hélio C.N. Tolentino[1], Maurizio De Santis[1], Marek Przybylski[2], Rantej Bali [2], Fikret Yildiz [2]

[1] Institut Néel, CNRS and UJF, BP166, 38042 Grenoble, France

[2] Max Plank Institut, Halle, Germany

Background

Our aim was to correlate the structural properties and magnetic behavior of tetragonally distorted Fe1-xCox alloys grown on Rh(001) and Ir(001) surfaces. This work builds upon the ESRF-SI2092 proposal where we have obtained structure-property correlation for these alloys grown on the Rh(001) surface. Both Rh and Ir(001) surfaces induce tetragonal distortion in pseudomorphically grown Fe1-xCox layers [1,2]. This tetragonal distortion modifies the symmetry of the orbitals and the electronic structure around the Fermi level such that the spins are forced to align perpendicular to the film plane [3] (figure 1). The perpendicular magetic anisotropy depends on composition and thicknes (figure 2). Thus

structural distortion of the lattice induces perpendicular magnetic anisotropy (PMA). As the film thickness is increased structural relaxation can be expected leading to weakening of the PMA and at a critical thickness tc the spins reorient to lie within the film plane. A direct correlation of the spin reorientation transition (SRT) to the structural relaxation of the film is yet to be reported.

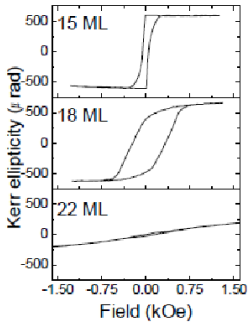

Figure-1 MOKE hysteresis loops of $Fe_{0.5}Co_{0.5}$ thin films for on Ir(001)

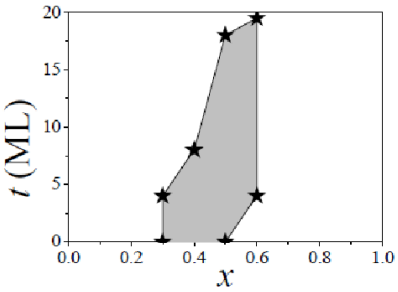

Figure-2 Dependence of the thickness of spin reorientation transition on composition. Shaded areas is the range with perpendicular easy axis.

Our results on the Rh(001) surface show that the SRT does not coincide with any abrupt structural relaxation: the film remains pseudomorphic well above tc, with a simultaneous c/a ratio and unit cell volume monotonous decrease.

Conversely, qualitative results on the Ir(001) surface show that the structural relaxation commences several monolayers (ML) below tc. This is counter-intuitive since magnetic measurements show that for a given composition the tc is larger for Ir(001) than for Rh(001) suggesting that the Ir(001) surface is better suited for pseudomorphic growth of Fe1-xCox. Comparison of the relaxation mechanisms and magnetic properties of Fe1-xCox alloys on Rh and Ir(001) will help explaining this contradiction and provide fundamental insight into the mechanism of PMA.

Experimental results

We have used the surface preparation and electron beam deposition techniques at the UHV X-ray diffractometer at BM32 beamline to gather information on the growth of Fe1-xCox ($0 < x < 0.5$) alloys. Grazing incidence X-ray diffraction (GIXRD) using 22 keV photons has been employed to optimize the growth route and to measure the crystallographic structure (in-plane and out-of-plane lattice parameters) as function of the coverage and composition on Rh(001) and Ir(001).

In the case of the Rh(001) substrate, we were able to study three different compositions (x=0, 0.25, 0.5). A short experiment was done, in addition, on the Ir(001) crystal for the composition x=0.5.

The deposition rate was calibrated for both Fe and Co using a quartz balance. For the x=0.5 sample the calibration was at about 1ML/18min. At each stage of the growth the c/a ratio was determined. At the end of each thin layer preparation, the composition was checked by Auger spectroscopy. A summary of the main results that has been found up to now (further analysis is required) are given below (figure 3).

For the deposition of Fe1-xCox alloys on Rh(001), we have obtained:

x=0.5 (red squares): There is no in plane layer relaxation at all, i.e., the in-plane parameter of the Fe50Co50 alloy is strictly the same as that of Rh crystal up to 19 ML. The interlayer spacing decreases with increasing thickness and reaches the nearly saturated value of c=3.181A above 12-14 ML. This gives a c/a=1.18A and a cell volume of 11.50A^3. The analysis has been based on a model where the d-spacing – or c/2 – is the same for the whole thin layer, except for the d-spacing between the Rh surface and the first alloy layer. The blue point (figure) at 1 ML represents that value, which is almost independent on the layer thickness.

x=0.25 (green circles): The thin layer displays a similar behavior at that composition. However, the layer starts to relax around 8-10 ML, where the (c/a) is about 1.20. One can observe that the (c/a) (green circles) is larger for all unrelaxed (up to 10 ML) thickness compared to x=0.5 (red squares) which is expected because there is more Fe in the composition.

x=0.00 : Qualitatively, we observed a similar behavior with a decreasing (c/a) as thickness increases. In addition, a clear relaxation process starts around 6 to 8 ML. As for x=0.25, the relaxation process is gradual. A quantitative fitting involving both relaxed and unrelaxed phases has to be done.

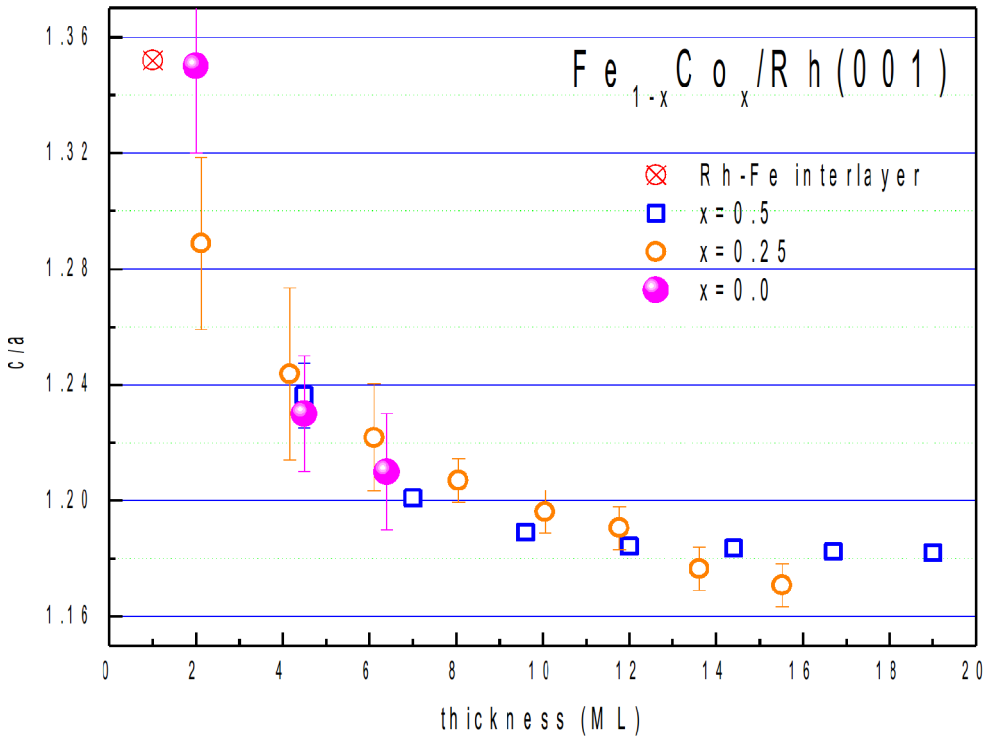

Figure 3: c/a variation as function of the layer thickness for different Fe/Co compositions on Rh(001).

For the Fe1-xCox/Ir(001), the crystal quality was not good and we had, in addition, many problems of source unstability. We have obtained some preliminary qualitative results:

First of all, we checked that the Ir reconstruction is washed out after 0.4 to 0.5 ML deposit.

x=0

Pure Fe grows pseudomorph up to 8 ML and starts to relax around 9-10 ML;
in-plane parameter relaxes to 2.745A (a_Ir=2.715A) and the out-plane parameter to 3.16A, giving (c/a)=1.15 after relaxation around 8ML.
in-plane parameter relaxes to 2.770 A (a_Ir=2.715A) and the out-plane parameter to 3.074A, giving (c/a)=1.11 after relaxation around 13MLs.

X=0.5

During the deposition of the x=0.5 alloy, the Co deposition rate was extremely stable. However, the Fe source decreased slowly, giving a composition with an excess in Co.

x=0.5 (first experiment)
The film started to relax around 12-13 ML. The final sample with about 18 ML gave an in-plane parameter of 2.753A (a_Ir=2.715A) and an out-plane of 3.012A, giving a (c/a)=1.09.

x=0.55 (second experiment)
relaxation around 10 to 12 ML, but in both sources deposition rates decreased, with probably the largest variation in the Fe source. Up to 8 ML, Fe source flux decreased from 5.4 nA to 2.2 nA and Co source decreased from 31% to 27% of 30nA. Probably, we have got an excess in Co larger than 55%.
(c/a) relaxed to 1.15 at 12 ML

x=0.50 (third experiment)
during this deposition, the Co source was extremely stable. Nevertheless, the Fe source decreased slowly: starting flux 3.7 nA; flux at about 8-9 ML 2.9 nA (20% less). The film started to relax again around 12-13 ML (nominal). After reajusting Fe source conditions, we deposited up to about 18 ML and measured the relaxed film: in-plane parameter relaxes to 2.753A (a_Ir=2.715A) and the out-plane parameter to 3.012A, giving (c/a)=1.09

At the end we checked the source: Co gave the same figures as from the beginning; Fe showed a deposition rate close to half the initial value. So, we probably have less Fe then Co. We checked the Fe/Co composition by X-ray fluorescence spectroscopy in this final sample, covered by 10 ML of Ir, and found that the composition was close to 50/50 within an error bar of 10%.

References

[1] “Giant magnetic anisotropy in tetragonal FeCo alloys”, T. Burkert, L. Nordstrom, O. Eriksson, and O.
Heinonen, Phys. Rev. Lett. **93**, 027203 (2004).
[2] “Tight-binding approach to the orbital magnetic moment and magnetocrystalline anisotropy of transition-metal monolayers”, P. Bruno, Phys. Rev. B **39**, 865 (1989)
[3] “Strongly enhanced orbital moment by reduced lattice symmetry and varying composition of Fe1-xCox alloy films”, F. Yildiz, F. Luo, C. Tieg, R.Abrudan, X. L. Lu, A.Winkelmann, M. Przybylski, J.Kirschner, Phys. Rev. Lett. **100**, 037205 (2008)
[4] “Volume contribution to perpendicular anisotropy in Fe0.5Co0.5 alloy films on Pd(001, Ir(001), and Rh(001)”, F. Yildiz, M. Przybylski, J. Kirschner, Journal of Applied Physics **105**, (7), pp 07E129/1-3 (2009)

4 Publications

4.1 Synthèse

Nombre de publications (avec comité de lecture) et facteur d'impact moyen (sur les cinq dernières années) par année :

2013	20	[4.5]
2012	23	[3.3]
2011	25	[3.6]

Articles publiés au cours des trois dernières années (2011-2013) classés par leur facteur d'impact (>2):

Acta Cryst. A	30.6	1
Nano Letters	14.1	1
Proc. Nat. Acad. Sci. USA	10.6	1
Phys. Rev. Lett.	7.4	1
Chem. Comm.	6.2	1
J. Phys. Chem	**5.2**	**3**
Elect. Comm.	5.0	1
J. Appl. Cryst.	**4.5**	**4**
Acta Mater.	**4.4**	**3**
Faraday Disc.	4.1	2
Nanotechnology	4.0	1
Appl. Phys. Lett.	**3.8**	**8**
Phys. Rev. B	**3.4**	**11**
J. Elect. Soc.	**2.8**	**3**
Nanoscale Res. Lett	2.5	1
Eur. Biophys. J.	2.4	1
J. Appl. Phys.	**2.2**	**8**

Articles (publiés depuis moins de 5 ans) les plus cités (nombre de citations entre paranthèses) :

[22.3] (138) *Probing surface and interface morphology with Grazing Incidence Small Angle X-Ray Scattering*
G. Renaud, R. Lazzari and F. Leroy
Surf. Sci. Rep. **64** pp 255-380 (2009)

[7.4] (59) Enhanced Relaxation and Intermixing in Ge Islands Grown on Pit-Patterned Si(001)

Substrates
T. U. Schülli, G. Vastola, M.-I. Richard, A. Malachias, G. Renaud, F. Uhlik, F. Montalenti, G. Chen,
L.Miglio, F. Schäffler, G. Bauer
Phys. Rev. Lett. **102**, 025502 (2009)

[4.0] (41) Nucleation mechanism of GaN nanowires grown on (111) Si by molecular beam epitaxy
O. Landré, C. Bougerol, H. Renevier and B. Daudin
Nanotechnology **20** 415602 (2009)

[5.2] (27) *Size and Catalytic Activity of Supported Gold Nanoparticles: An in operando Study During CO Oxidation*
I. Laoufi, M.-C. Saint-Lager, R. Lazzari, J. Jupille, O. Robach, S. Garaudee, G. Cabailh, P. Dolle, H. Cruguel, A. Bailly
J. Phys. Chem. **C 115** (11) pp 4673-4679 (2011)

[36.2] (26) *Substrate-enhanced supercooling in AuSi eutectic droplets*
T.U. Schülli, R. Daudin, G. Renaud, A. Vaysset, O. Geaymond and A. Pasturel,
Nature **464**, 1174 (2010)

[3.4] (23) Adhesion of growing nanoparticles at a glance: Surface differential reflectivity spectroscopy and grazing incidence small angle x-ray scattering
R. Lazzari, G. Renaud, C. Revenant , J. Jupille and Y. Borensztein
Phys. Rev. **B 79**, 125428 (2009)

Articles (publiés depuis moins de 3 ans) les plus cités (nombre de citations entre paranthèses) :

[5.2] (27) *Size and Catalytic Activity of Supported Gold Nanoparticles: An in operando Study During CO Oxidation*
I. Laoufi, M.-C. Saint-Lager, R. Lazzari, J. Jupille, O. Robach, S. Garaudee, G. Cabailh, P. Dolle, H. Cruguel, A. Bailly
J. Phys. Chem. **C 115** (11) pp 4673-4679 (2011)

[1.5] (15) *Dislocation storage in single slip-oriented Cu micro-tensile samples: New insights via X-ray*
microdiffraction
C. Kirchlechner, D. Kiener, C. Motz, S. Labat, N. Vaxelaire, O. Perroud, J. -S. Micha, O. Ulrich, O.
Thomas, G. Dehm, and J. Keckes
Phil. Mag. **91** (7-9) Special Issue p 1256-1264 (2011)

[5.2] (11) *Competition between polar and nonpolar growth of MgO films on Au(111)*
S. Benedetti , N. Nilius, P. Myrach, P. Torelli, G. Renaud, H.-J. Freund, S. Valeri
J. Phys. Chem. **C 115,** 23043 (2011)

[1.7] (11) *A new white beam x-ray microdiffraction setup on the BM32 beamline at the European Synchrotron Radiation Facility*
O. Ulrich, X. Biquard, P. Bleuet, O. Geaymond, P. Gergaud, J. S. Micha, O. Robach, and F. Rieutord
Rev. Sci. Instrum. **82**, 033908 (2011)

[2.2] (8) *Structural and optical analyses of GaP/Si and (GaAsPN/GaPN)/GaP/Si nanolayers for integrated photonics on silicon*
T. Nguyen Thanh, C. Robert, W. Guo, A. Letoublon, C. Cornet, G. Elias, A. Ponchet, T. Rohel, N. Bertru, A. Balocchi, O. Durand, J.-S. Micha, M. Perrin, S. Loualiche, X. Marie and A. Le Corre
J. Appl. Phys. **112**, 053521 (2012)
Publisher erratum: J. Appl. Phys. **112**, 079904 (2012)

5 Données sur l'utilisation du temps de faisceau

Les données présentées sont relatives aux expériences allouées sur BM32 pendant les périodes couvertes par les comités de programmes d'octobre 2012 et avril 2013 et donc réalisées entre le 01/03/2013 et le 28/02/2014. Le comité Français a alloué 240 shifts de 8 heures et le comité international de l'ESRF 145 shifts.

La figure 1 présente le nombre de shifts demandés et alloués sur la période d'exploitation. Le rapport du temps demandé sur le temps attribué est de 1.3 sur le comité français et 3.3 sur le comité international, pour un taux de pression global de 2.1. La tendance est à une stagnation de la pression sur le comité français et une augmentation sur le comité international. La répartition du temps de faisceau sur les trois instruments est donnée sur la figure 2. On constate l'équilibre entre les deux cabanes d'expérience INS et GMT, cette dernière accueillant le goniomètre multi-technique et l'instrument de micro-diffraction en faisceau blanc.

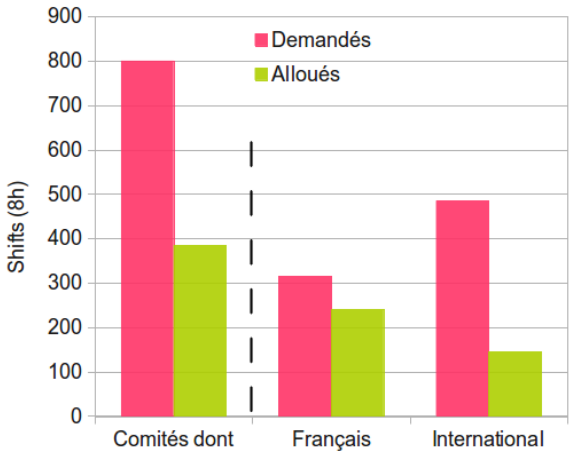

Figure 1 : Nombre de shifts demandés et alloués par les comités de programmes du 10/2012 et 4/2013

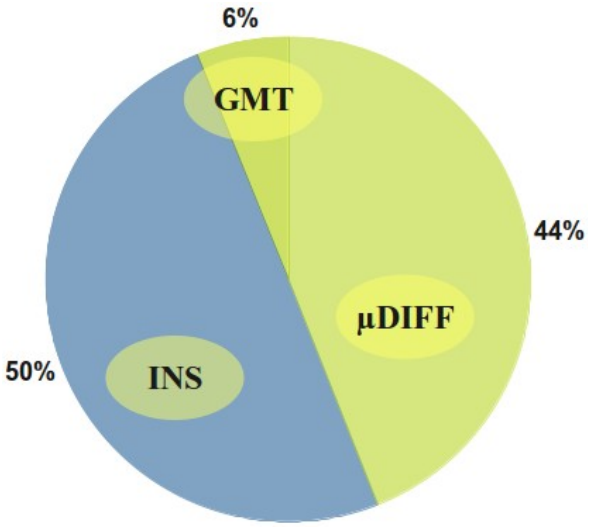

Figure 2 : Répartition par instrument des shifts alloués par les comités GMT : goniomètre multitechnique, INS : In Situ nanostructure Surface, µdiff : micro diffraction Laue.

La répartition par comité de programme (figure 3) indique toujours la prépondérance des sciences des Surfaces et Interfaces (SI) pour lesquelles la ligne BM32 est optimisée. Si 100% des expériences sur l'instrument INS concernent ce domaine, le goniomètre multi-technique de par sa flexibilité, reçoit lui des expériences plus variées retenues par les comités SI et MA (Matériaux appliqués et pour l'ingénierie). L'installation de micro-diffraction répond

largement aux thématiques de MA (par exemple mécanique fondamentale etmétallurgie) grâce à sa capacité à mesurer des déformations à l'échelle sub-micronique.

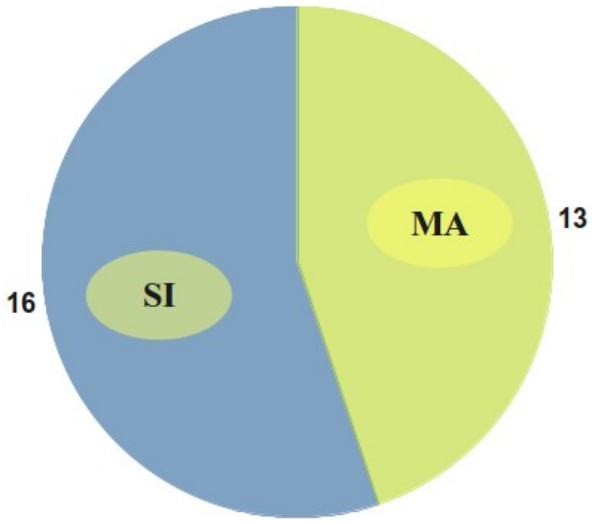

Figure 3 : Répartition par comité de programme (équivalent ESRF) des expériences réalisées sur BM32 CRG-IF

SI: Surface and Interface

MA: Applied Materials Engineering + Instrumental

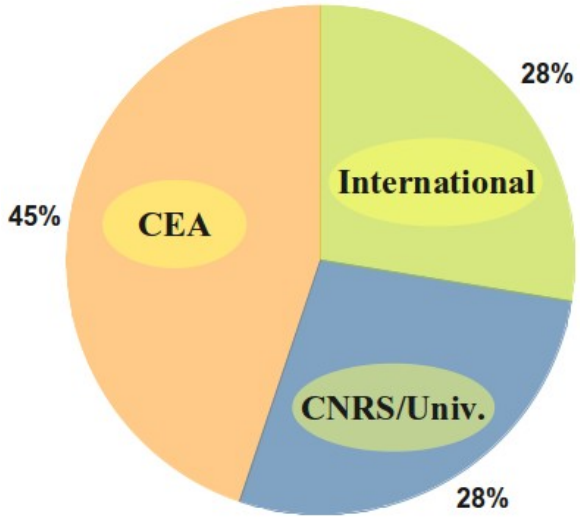

Figure 4 : Répartition du temps de faisceau par le laboratoire d'origine des utilisateurs pour les expériences réalisées sur BM32 CRG-IF.

CEA : DEN+DRT+DSM

CNRS/Univ :CNRS + Université,

UE : International (Allemagne, Autriche, Suède).

La figure 4 présente l'origine des utilisateurs classée selon 3 catégories. La part internationale, très majoritairement de l'Union Européenne, prouve une fois de plus la pertinence des choix faits sur BM32 ces dernières années pour développer une instrumentation performante. L'instrument de micro-diffraction en faisceau blanc reste à ce jour unique en Europe et attire une majorité de groupe de recherche étrangers. Le cloisonnement entre CEA et CNRS n'est qu'apparent puisque très souvent les équipes sont mixtes. Enfin pour compléter, le figure 6 montre la connexion de la ligne de lumière avec les laboratoires grenoblois, avec une utilisation majoritaire de 50 % (CEA/INAC, LITEN, LETI, CNRS/Institut Néel).

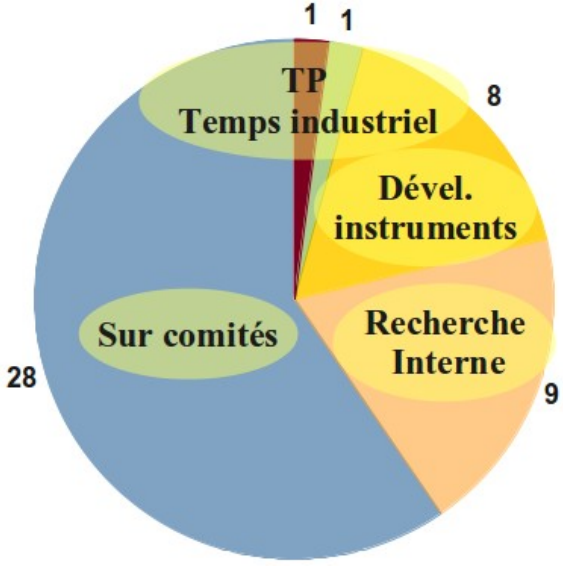

Figure 5 : Répartition des expériences sur la ligne Interfaces

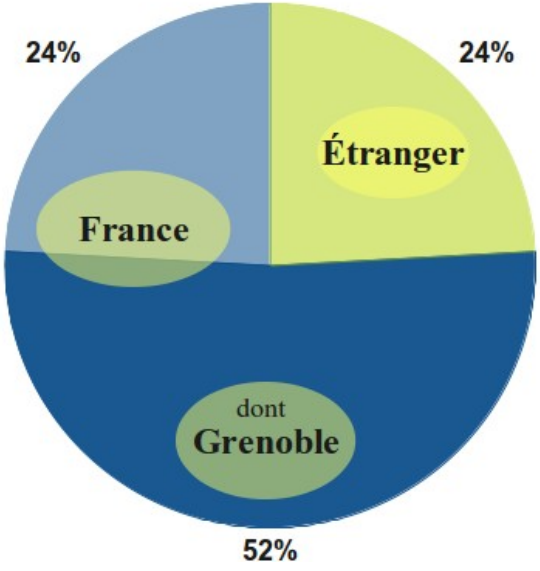

Figure 6 : Origine géographique des équipes de recherche ayant des expériences acceptées par les comités de programmes

La figure 5 illustre l'utilisation du faisceau sur la ligne IF. Il faut noter que dans le cadre de la formation HERCULES (Higher European Research Course for Users of Large Experimental Systems) la ligne accueille toujours plusieurs groupes d'étudiants et chercheurs pour des travaux pratiques, et que de plus cette année 6 shifts ont été vendus à des industriels.

7 Liste des publications, thèses et conférences

Les publications relatives à l'utilisation de BM32 sur la période 2012-2013 sont classées par année et par ordre décroissant du facteur d'impact de la revue.

[] facteur d'impact de la revue au 13/01/2014
() nombre de citations de l'article au 13/01/2014

7.1 2013

[30.6] *A tunable multicolour 'rainbow' filter for improved stress and dislocation density field mapping in polycrystals using X-ray Laue microdiffraction*
O. Robach, J.-S. Micha, O. Ulrich, O. Geaymond, O. sicardy, L. Haertwig, F. Rieutord
Acta Cryst **A 69**, 164-170 (2013)

[7.4] *Point defect-induced strains in epitaxial graphene*
N. Blanc, F. Jean, A. V. Krasheninnikov, G. Renaud, and J. Coraux
Phys. Rev. Lett., 111, 085501 (2013).

[4.5] *Integration techniques for SXRD data obtained with a 2D detector*
J. Drnec, T. Zhou, S. Pintea, W. Onderwaater, E. Vlieg, G. Renaud and R. Felici,
J. appl. Cryst., In press. (2013)

[4.1] *Operando atomic structure and active sites of TiO2(110)-supported gold nanoparticles during carbon monoxide oxidation*
M.C. Saint-Lager, I. Laoufi and A. Bailly
Faraday Discussions 162, 179-190 (2013)

[3.8] *In-situ observation of stress-induced stochastic twin boundary motion in off stoichiometric NiMnGa single crystals*
R.I. Barabash, C. Kirchlechner, O. Robach, Odile; O. Ulrich, J.-S. Micha, A. Sozinov and O.M. Barabash
Appl. Phys. Lett. **103** (2), 021909 (2013)

[3.8] *Interface Accommodation Mechanism for Weakly Interacting Epitaxial Systems*

A. Danescu, B. Gobaut, J. Penuelas, G. Grenet, V. Favre-Nicolin, N. Blanc, T. Zhou, G. Renaud, and G. Saint-Girons
Appl. Phys. Lett. **103**, 021602 (2013).

[3.8] *Effect of H-implantation in the local elastic properties of silicon crystals*
S. Reboh, F. Rieutord, L. Vignoud, F. Mazen, D. Landru, M. Zussy, and C. Deguet
Appl. Phys. Lett. **103**, 181911 (2013)

[3.8] *Agglomeration dynamics of germanium islands on a silicon oxide substrate: A grazing incidence small-angle x-ray scattering study*
F. Cheynis, F. Leroy, T. Passanante *et al.*
Appl. Phys. Lett. **102** (16), 161603 (2013)

[3.6] *Robust perpendicular exchange coupling in an ultrathin CoO/PtFe double layer: Strain and spin orientation*
A. D. Lamirand, M. M. Soares, A.Y. Ramos, H.C.N. Tolentino, M. De Santis, J. C. Cezar, A. de Siervo and M. Jamet
Phys. Rev. **B 88**, 140401 (2013)

[3.6] *Different commensurabilities and 10-1300 K thermal expansion of graphene on Ir(111) as a function of preparation*
F. Jean, T. Zhou, N. Blanc, J. Coraux and G. Renaud,
Phys. Rev. **B 88**, 165406 (2013)

[3.6] Local band bending and grain-to-grain interaction induced strain nonuniformity in polycrystalline CdTe films
V. Consonni, N. Baier, O. Robach, C. Cayron, F. Donatini and G. Feuillet
accepted in Phys Rev. B.

[2.6] *Treatments of deposited SiOx surfaces enabling low temperature direct bonding*
C. Rauer, H. Moriceau, F. Fournel, A.-M. Charvet, C. Morales, N. Rochat, L. Vandroux, F. Rieutord, T. Mc Cormick, and I. Radu
J. Electrochem. Soc., (2013)

[2.5] *Metal organic vapour-phase epitaxy growth of GaN wires on Si (111) for light-emitting diode applications*
D. Salomon, A. Dussaigne, M. Lafossas, C. Durand, C. Bougerol, P. and J. Eymery
Nanoscale Res. Lett. **8**, 61-1 (2013)

[2.2] *Lattice strain of hydrogen-implanted silicon : correlation between X-ray scattering analysis and ab-initio simulations.*
F. Rieutord, F. Mazen, S. Reboh, J. D. Penot, L. Bilteanu, J. P. Crocombette, V. Vales, V. Holy, and L. Capello
J. Appl. Phys. **113**, 153511, (2013)

[2.2] *Nanoscale organization by elastic interactions between H and He platelets in Si*
S. Reboh, F. Rieutord, F. Mazen, N. Cherkashin, M. F. Beaufort, J.-F. Barbot, M. Vallet, P. F. P. Fichtner, and J. Grilhé
J. Appl. Phys. **114**, 073517 (2013)

[2.2] *Development of microcracks in hydrogen-implanted silicon substrates*

J. D. Penot, D. Massy, F. Rieutord, F. Mazen, S. Reboh, F. Madeira, L. Capello, D. Landru, and O. Kononchuk
J. Appl. Phys. **114**, 123513, (2013)

[2.0] *Mechanism of Edge Bonding Void Formation in Hydrophilic Direct Wafer Bonding*
A. Castex, B. M., F. Rieutord, K. Landry, and C. Lagahe-Blanchard
Electrochem. Sol. State Lett. **2**, 47-50, (2013)

[1.6] Quantitative study of microtwins in GaP/Si thin film and GaAsPN quantum wells grown on silicon substrates
T. Nguyen Thanh, C. Robert, E. Giudicelli, A. Létoublon, C. Cornet, A. Ponchet, T. Rohel, A. Balocchi, J.S. Micha, M. Perrin, S. Loualiche, X. Marie, N. Bertru, O. Durand, A. Le Corre
J. Crystal Growth **378**, 25-28 (2013)

[1.3] *Structural investigation of nanoporous alumina film with grazing incidence small angle X-ray scattering*
D. Buttard, T. Schülli and R. Lazzari
Phys. Stat. Solid. **A** 210, 2521-2525 (2013)

[1.1] *Thermal bump removal of a Crystal Monochromator by designing an optimal shape*
J.-S. Micha, O. Geaymond, F. Rieutord
4th international workshop on Metrology for X-ray Optics, Mirror Design, and Fabrication
Barcelona, 4th to 6th July 2012
Nucl. Instr. Methods **A 710**, 155-160 (2013)

[0.9] *Hydrophobic direct bonding of silicon reconstructed surfaces*
C. Rauer, F. Rieutord, J. M. Hartmann, A.-M. Charvet, F. Fournel, D. Mariolle, C. Morales, and H. Moriceau
Microsystem Technologies, **19**, 675 (2013)

Energetic Structure of μLaue Peaks from a Plastically-Deformed Cu Cantilever Revealed by a Three-Dimensional X-ray Detector
A. Abboud, C. Kirchlechner, J.-S. Micha, O. Ulrich, S. Send, N. Pashniak, R. Hartmann, L. Struder, J. Keckes and U. Pietsch
submitted to J. Appl. Cryst.

Chapître:
Nanostructures observed by surface sensitive x-ray scattering and highly focused beams
T. Schulli, V. Favre-Nicolin M.-I. Richard and G. Renaud,
in „Characterization of Semiconductor Heterostructures and Nanostructures“, C. Lamberti ed.; second edition, 2013, pp 113-173., Elsevier.

Grazing incidence diffraction anomalous fine structure in the study of structural properties of nanostructures
H. Renevier and M.G. Proietti
In: "Characterization of Semiconductor Heterostructures and Nanostructures. 2. Edition", Lamberti C. (Eds.)Agostini G. (Eds.) (Elsevier, 2013) pp.311-359

Article de vulgarisation:

-« *Propriétés structurales de surfaces, interfaces et nanostructures étudiées à l'aide des rayons X* »
G. Renaud,
Reflets de la Physique n°34-35 et Le BUP, Hors Série N°1 , pp 65-69, 2013

Conférences

Strain-stress determination in copper filled TSVs using X-Rays diffraction : average and local approach
Christopher Krauss, Stéphane Labat , Stéphanie Escoubas, Olivier Thomas, Alexis Farcy, Jean-Sébastion Micha, Odile Robach
Materials for Advanced Metallization 10-13 March 2013, Leuven

Multi-scale X-ray diffraction study of strains induced by the implantation in UO2 polycrystals
A. Richard, E. Castelier, H. Palancher, J.S. Micha, H. Rouquette, A. Ambard, Ph. Garcia, Ph. Goudeau
17th Radiation Effects In Insulator (REI-2013) Helsinki 30th June- 5th July)
accepted in Nucl. Instr. Methods. B Proceedings

La Microdiffraction Laue des rayons X : un outil de métrologie locale
invited : Odile Robach et al
RX et matière 2013, Nantes 12-15 Novembre 2013

X-ray Laue Microdiffraction : a local metrology tool
invited : Odile Robach et al
Small Scale Plasticity, Cargese, Octobre 2013

Mesures 3D micrométriques de la microstructure et du champ des déformations élastiques par DAXM à BM32 (ESRF)
J.-B. Marijon, F. Grennerat, O. Robach, O. Castelnau, J.-S. Micha
RX et matière 2013, Nantes 12-15 Novembre 2013

Laue micro-beam tomography on Through-Silicon-Via
Dario Ferreira Sanchez et al
RX et matière 2013, Nantes 12-15 Novembre 2013

Analyse quantitative de la perfection cristalline de nanocouches épitaxiales GaP/Si
Antoine Létoublon et al
RX et matière 2013, Nantes 12-15 Novembre 2013

Influence of dislocation pile-ups on mechanical properties of microcantilevers: New insights via in situ μLaue and in situ SEM bending experiments.
M.Kapp et al
EUROMAT 2013, Seville, 8-13 september 2013

Gallium nitride single-wires studied by X-ray diffraction: homogeneous wires and core-shell heterostructures
J. Eymery, C. Durand, D. Salomon, V. Favre-Nicolin, F. Rieutord, O. Robach, J.S. Micha, M. Burghammer, E. Di Cola, M. Reynolds

E-MRS, strasbourg, May 2013

A tunable multi-color "rainbow" filter for improved stress and dislocation field mapping in polycrystals using x-ray Laue microdiffraction
O. Robach, J.-S. Micha, Olivier Ulrich, Olivier Geaymond, Olivier Sicardy, Jürgend Härtwig, François Rieutord
TMS 2013, San Antonio (US/TX), 3rd – 7th march 2013

Prix

T. Zhou: prix de la meilleure présentation Science Days ESRF Oct 2013
A. Lamirand: prix du meilleur poster Science Days ESRF Oct 2013

Thèse

K. Hestroffer
Croissance et caractérisation de nanofils de GaN et d'hétérostructures - Growth and characterization of GaN nanowires and GaN/AlN heterostructure nanowires
Université de Grenoble, France (PhD Thesis, 2013)

C. Leclere
Spectroscopies X et diffraction anomale de boîtes quantiques GaN et d'hétéro-structures III-N : inter-diffusion et ordre à courte distance
Université de Grenoble, France (PhD Thesis, 2013)

7.2 2012

[10.6] (1) Controlling *Interactions in supported bilayers from weak electrostatic repulsion to high osmotic pressure*
A. Hemmerle, L. Malaquin , T. Charitat,, S. Lecuyer, G. Fragneto and J. Daillant
Proc. Nat. Acad. Sciences USA **109** (49) 19938-19942 (2013)

[6.2] (3) *From metastable to stable modifications—in situ Laue diffraction investigation of diffusion processes during the phase transitions of (GeTe)nSb2Te3 (6 <= n <= 15) crystals*
M. N. Schneider, X. Biquard, C. Stiewe, T. Schröder, P. Urban and O. Oeckler
Chemical Communications **48** (16) 2192-2194 (2012)

[5.2] (3) CO-Induced Scavenging of Supported Pt Nanoclusters: A GISAXS Study
N. Chaabane, R. Lazzari, J. Jupille, G. Renaud, and E. A. Soares
J. Phys. Chem. **C, 116** (44), 23361-23370 (2012)

[4.5] (1) *Strains in light ion implanted polycrystals: influence of grain orientation*
A. Richard, H. Palancher, E. Castelier, J. S. Micha, M. Gamaleri, G. Carlot, H. Rouquette, P. Goudeau, G. Martin, F. Rieutord, J. P. Piron and P. Garcia
J. Appl. Cryst. **45** (4) 826-833 (2012)

[4.5] (1) *Multi scale measurements of residual strains in stabilized zirconia layer*
J. Villanova, C. Maurice, J.-S. Micha, P. Bleuet, O. Sicardy and R. Fortunier
J. Appl. Cryst. **45** (5) p 926-935. (2012)

[4.4] (3) *Expected and unexpected plastic behavior at the micron scale: An in situ Laue tensile study*
C. Kirchlechner , P.J. Imrich, W. Grosinger, M.W. Kapp, J. Keckes, J.S. Micha, O. Ulrich, O. Thomas, S. Labat, C. Motz, and G. Dehm
Acta Mater. **60** (3) 1252-1258 (2012)

[3.8] (5) In situ study of self-assembled GaN nanowires nucleation on Si(111) by plasma-assisted molecular beam epitaxy
K. Hestroffer, C. Leclere, V. Cantelli, C. Bougerol, H. Renevier and B. Daudin
Appl. Phys. Lett. **100** (21) 212107 (2012)

[3.6] (4) *Interface-driven phase separation in multifunctional materials: The case of the ferromagnetic semiconductor GeMn*
E. Arras, F. Lançon, I. Slipukhina, É. Prestat, M. Rovezzi, S. Tardif, A. Titov, P. Bayle-Guillemaud, F. d'Acapito, A. Barski, V. Favre-Nicolin, M. Jamet, J. Cibert, and P. Pochet
Phys. Rev. B **85,** 115204 (2012)

[3.6] (1) *Chemically ordered MnPt ultrathin films on Pt(001) substrate: Growth, atomic structure, and magnetic properties*
M. M. Soares, M. De Santis, H. C. N. Tolentino, A. Y. Ramos, M. El Jawad and Y. Gauthier
Phys. Rev. B **85**, 205417 (2012)

[3.6] (1) *Epitaxial orientation changes in a dewetting gold film on Si(111)*
R. Daudin, T. Nogaret, T.-U. Schülli, N. Jakse, A. Pasturel and G. Renaud
Phys. Rev. **B 86**, 094103 (2012)

[3.6] *Dynamics, anisotropy, and stability of silicon-on-insulator dewetting fronts*
F. Leroy, F. Cheynis, T. Passanante, and P. Müller
Phys. Rev. **B 85**, 195414 (2012) and erratum **85** 239901 (2012)

[3.6] (2) *Local deformations and incommensurability of high quality epitaxial graphene on a weakly interacting transition metal*
N. Blanc, J. Coraux, C. Vo-Van, A. T. N'Diaye, O. Geaymond, and G. Renaud
Phys. Rev. **B 86**, 235439 (2012)

[2.4] (5) *Floating lipid bilayers: Models for physics and biology*
Fragneto G. Charitat T. Daillant J. -
European Biophysics Journal 41, 863-874 (2012)

[2.2] (1) *Measurement of bonding energy in an anhydrous nitrogen atmosphere and its application to silicon direct bonding technology*
F. Fournel, L. Contini, C. Morales, J. Da Fonseca, H. Moriceau, F. Rieutord, A. Barthelemy and I. Radu

J. Appl. Phys. **111** (10) 104907 (2012)

[2.2] (8) *Structural and optical analyses of GaP/Si and (GaAsPN/GaPN)/GaP/Si nanolayers for integrated photonics on silicon*
T. Nguyen Thanh, C. Robert, W. Guo, A. Letoublon, C. Cornet, G. Elias, A. Ponchet, T. Rohel, N. Bertru, A. Balocchi, O. Durand, J.-S. Micha, M. Perrin, S. Loualiche, X. Marie and A. Le Corre
J. Appl. Phys. **112**, 053521 (2012)
Publisher erratum: J. Appl. Phys. **112**, 079904 (2012)

[2.2] *Low temperature direct bonding mechanisms of tetraethyl orthosilicate based silicon oxide films deposited by plasma enhanced chemical vapor deposition*
C. Sabbione, L. Di Cioccio, L. Vandroux, J.-P. Nieto, and F. Rieutord
J. Appl. Phys. **112**, 063501 (2012)

[1.7] (2) Advances in martensitic transformations in Cu-based shape memory alloys achieved by in situ neutron and synchrotron X-ray diffraction methods
B. Malard, P. Sittner, S. Berveiller, E. Patoor
Compt. Rend. Physique **13** (2012) 280–292

[1.5] Investigation of reversible plasticity in a micron-sized, single crystalline copper bending beam by X-ray μLaue diffraction
C. Kirchlechner, W. Grosinger, M.W. Kapp, P.J. Imrich, J.-S. Micha, O. Ulrich, J. Keckes, G. Dehm and C. Motz
Philosophical Magazine **92** (25-27), 3231-3242 (2012)

[1.4] (4) *Growth and dewetting of gold on Si(1 1 1) investigated in situ by grazing incidence small angle x-ray scattering*
R. Daudin, C. Revenant, G. Davi and G. Renaud
Physica **E 44**, 1905 (2012)

[1.2] *Low temperature direct bonding: an attractive technique for heterostructures build-up*
H. Moriceau, F. Rieutord, F. Fournel, C. Moulet, L. Libralesso, P. Gueguen, R. Taibi and C. Deguet
Microelectronics Reliability **52** (2) p 331-341 (2012)

[1.2] Regular arrays of palladium and palladium-gold clusters supported on ultrathin alumina films: stability under oxygen
G. Sitja, M. Marsault, F. Leroy *et al.*
Int. J. Nanotech. **9** (3-7) 567-575 (2012)

[1.1] (3) *Si exfoliation by MeV proton implantation*
C. Braley, F. Mazen, A. Tauzin, F. Rieutord, C. Deguet and E. Ntsoenzok
Nucl. Instr. Methods ***B 277, 93-97 (2012)***

[1.1] (1) *Smart Cut™: review on an attractive process for innovative substrate elaboration*
H. Moriceau, F. Mazen, C. Braley, F. Rieutord, A. Tauzin, and C. Deguet,
Nucl. Instrum. Meth. **B 277**, p 84-92 (2012)

chapitre:
"Laue microdiffraction at ESRF, chapter 5"
Robach, O., Kirchlechner, C., Micha, J.-S., Ulrich, O., Biquard, X., Geaymond, O., Castelnau, O., Bornert, M., Petit, J., Berveiller, S., Sicardy, O., Villanova, J., and Rieutord, F.
in Strain and dislocation gradients from diffraction (2012)
Imperial College Press and World Scientific Publishing.
R. I. Barabash and G. E. Ice editors

proceedings

Bio-materials characterization across multiple scales at Oxford HEX-lab
Sui T. Hofmann F. Song X. Tao L. Zeng K. Korsunsky A.M.
Lecture Notes in Engineering and Computer Sciences 2199, 1657-1662 (2012)
In: "Proceedings of the World Congress on Engineering, International Association of Engineers", 2012) pp.1657-1662

Combining Laue microdiffraction and digital image correlation for improved measurements of the elastic strain
field with micrometer spatial resolution
J. Petit, M. Bornert, F. Hofmann, O. Robach, J.-S. Micha, O. Ulrich, C. Le Bourlot, D. Faurie, A.M. Korsunsky and O. Castelnau
Procedia IUTAM 4 (2012) 133 – 143

Daudin B. Bougerol C. Camacho D. Cros A. Gayral B. Hestroffer K. Leclere C. Mata R. Niquet Y.M. Renevier H. Sam-Giao D. Tourbot G. - Growth, structural and optical properties of GaN/AlN and GaN/GaInN nanowire heterostructures
Physics Procedia 28, 5-16 (2012)
15th Brazilian Workshop On Semiconductors

Coherent integration of photonics on silicon through the growth of nanostructures on GaP/Si
Thanh, TN ; Robert, C ; Cornet, C; Guo, W ; Letoublon, A ; Perrin, M ; Bertru, N ; Even, J ; Chevalier, N ; Folliot, H; Loualiche, S ; Ponchet, A ; Elias, G; Micha, JS; Durand, O ; Le Corre, A
Quantum Sensing and Nanophotonic devices IX Book Series: Proceedings of SPIE
8268 , 82681H (2012)

Fracture in (100)Si after high energy protons implantation
Braley C. Mazen F. Papon A.M. Charvet A.M. Rieutord F. Ntsoenzok E.
Special Issue: E-MRS 2012 Spring Meeting – Symposium A
Physica Status Solidi (c) 9, 2023-2026 (2012)

Thèses :

Mathieu Guerain , Université de La Rochelle , 05 Octobre 2012, Sciences des Matériaux
Contribution à l'étude des mécanismes de relaxation de contraintes dans les films de chromine formés sur Ni-30Cr et Fe-47Cr : approche multi-échelle par spectroscopie Raman et microdiffraction Synchrotron

Gael Daveau, Ecole Centrale Paris, 19 septembre 2012, Mécanique et Matériaux
Interaction dislocations - joints de grains en déormation plastique monotone : éude expérimentale et modélisations numériques

Axel Richard, Université de Poitiers, 22 Novembre 2012,
Etude par diffraction des rayons X des déformations induites par iraadiation/implantation d'ions dans le dioxyde d'uranium

Jean-Claude Bastien
Étude des matériaux à changement de phase pour application dans le domaine des PCRAM

Audrey Bastard
Analyse théorique et physique de matériaux pour application aux Mémoires à Changement de Phases (PCRAM)

Rémi Daudin, Février 2012
"Formation and supercooling of AuSi eutectic droplets on Si substrates: an in-situ study using synchrotron radiation"

Conférences:

Relations contraintes résiduelles – endommagement dans des systèmes oxydes thermiques sur métal : apports de la spectroscopie Raman et de la micro-diffraction Synchrotron
M. Guerain, J.L. Grosseau-Pouyssard, P. Goudeau, B. Panucaud, N. Tamura, M. Kunz, J.-S. Micha.,
Colloque GFAC-SF2M, St Nazaire, 3-4/04/2012
and
8th International Symposium on High-Temperature Corrosion and Protection of Materials 2012, 20-25 Mai 2012, Les Embiez

Use of Raman Spectroscopy and Synchrotron micro-Diffraction to investigate stress in thermal oxide films : a multiscale approach
FAC: Déformations élastiques dans des échantillons polycristallins d'UO2 implantés en hélium : mesures par micro diffraction Laue et modélisation élastique
É. Castelier, H. Palancher, A. Richard, J.-S. Micha, P. Goudeau

Combining Laue microdiffraction and digital image correlation for improved stress field measurements
with micrometer spatial resolution
F. Zhang, O. Castelnau, M. Bornert, J. Petit, O. Robach, J.S. Micha, F. Hofmann, A. Korsunsky
Int. Conf. of Residual Stresses (oct 2012)

Strain-stress determination in silicon around copper filled TSVs using Laue microdiffraction
C. Krauss, S. Labat, S. Escoubas, O. Thomas, M. Bouchoucha, L.-L. Chapelon, P. Chausse, J.-S. Micha and O. Ulrich

12th Workshop on Stress-Induced Phenomena in Microelectronics.
Kyoto du 28 au 30 Mai 2012

Measuring energy profiles of Laue spots : a third method RSI
O. Robach et al
oral communication RSI 2012

Combined Analysis of Delamination Process at the Surface of Cr2O3 Thermal Oxide Films
P. Goudeau , M. Guerain , J.-L. Grosseau- Poussard, N. Tamura , M. Kunz , J.-S. Micha ,
oral communication MRS Fall

Influence of Grain Orientation on Radiation Induced Strains in UO2 Polycrystals
P. Goudeau , E. Castelier , H. Palancher , A. Richard, J.-S. Micha ,
oral communication MRS Fall

μ-XRD study of strains in light ion implanted polycrystals: influence of grain orientation
H. Palancher, A. Richard, E. Castelier, J.S Micha, Ph. Goudeau, Ph. Garcia
oral communication JMC13

ESRF Highlights

An alternative pathway for understanding plasticity at the micron scale
C. Kirchlechner et al
ESRF Highlight 2012

7.3 2011

[14.1] (25) *M-plane core-shell InGaN/GaN multiple-quantum-well on GaN wires for electroluminescent device*
R. Koester, J. S. Hwang, D. Salomon, X. Chen, C. Bougerol, J.-P. Barnes, D. Le Si Dang, L. Rigutti, M. Tchernycheva, C. Durand and J. Eymery
Nano Letters **11**, p 4839-4845 (2011)

[4.5] (7) *Full local elastic strain tensor from Laue microdiffraction: simultaneous Laue pattern and spot energy measurement*
O. Robach, J.-S. Micha, O. Ulrich and P. Gergaud
J. Appl. Cryst.. **44** p 688–696 (2011)

[5.2] (27) *Size and Catalytic Activity of Supported Gold Nanoparticles: An in operando Study During CO Oxidation*
I. Laoufi, M.-C. Saint-Lager, R. Lazzari, J. Jupille, O. Robach, S. Garaudee, G. Cabailh, P. Dolle, H. Cruguel, A. Bailly
J. Phys. Chem. **C 115** (11) pp 4673-4679 (2011)

[5.2] (11) *Competition between polar and nonpolar growth of MgO films on Au(111)*
S. Benedetti , N. Nilius, P. Myrach, P. Torelli, G. Renaud, H.-J. Freund, S. Valeri
J. Phys. Chem. **C 115,** 23043 (2011)

[5.0] (3) *In situ grazing-incidence X-ray diffraction during electrodeposition of birnessite thin films: Identification of solid precursors*
M. Ndjeri, S. Peulon, M.L. Schlegel, A. Chaussé
Electrochem. Commun. **13**, (5) p 491-494 (2011)

[4.4] (3) *In situ synchrotron analysis of lattice rotations in individual grains during stress-induced martensitic transformations in a polycrystalline CuAlBe shape memory alloy*
Berveiller S., Malard B., Wright J., et al.
Acta Mater. **59** (9) p 3636-3645 (2011)

[4.4] (4) *Impact of instrumental constraints and imperfections on the dislocation structure in micron-sized Cu compression pillars*
Kirchlechner C., Keckes J., Motz C., Grosinger W., Kapp M.W., Micha J.S., Ulrich O. and Dehm G.
Acta Mater. **59** (14) p 5618-5626 (2011)

[4.1] (6) *Catalytic properties of supported gold nanoparticles: new insights into the size-activity relationship gained from in operando measurements*
M.-C. Saint-Lager, I. Laoufi, A. Bailly, O. Robach, S. Garaudée and P. Dolle
Faraday Discuss., **152**, p253–265 (2011)

[3.8] (3) *Effect of doping on global and local order in crystalline GeTe*
Biquard X., Krbal M., Kolobov A. V. *et al*
Appl. Phys. Lett. **98** (23) 231907 (2011)

[3.8] (1) *In situ x-ray study of the formation of defects in Ge islands on Si(001)*
M.-I. Richard, T. U. Schülli, and G. Renaud
Appl. Phys. Lett. **99** 161905 (2011)

[3.8] (7) *Catalyst-free growth of high-optical quality GaN nanowires by metal-organic vapor phase epitaxy*
X.J. Chen, B. Gayral, D. Sam-Giao, C. Bougerol, C. Durand and J. Eymery
Appl. Phys. Lett. **99** (25) 251910 (2011)

[4.0] *Metal positioning using dislocation arrays.*
A. Bavard, F. Fournel and J. Eymery
Nanotechnology **22**, 215301(2011)

[3.6] (2) *Twins and their boundaries during homoepitaxy on Ir(111)*
S. Bleikamp, J. Coraux, O. Robach, G. Renaud and T. Michely,
Phys. Rev. **B 83** 064103 (2011)

[3.6] (4) Tracking defect type and strain relaxation in patterned Ge/Si(001) islands by x-ray forbidden reflection analysis
M.I. Richard, A. Malachias, J.-L. Rouvière, T.-S. Yoon, E. Holmström, Y.-H. Xie, V. Favre-Nicolin, V. Holy, K. Nordlund, G. Renaud, T.-H. Metzger
Phys. Rev. **B 84**, 075314 (2011)

[3.6] (4) *Atomic structure and composition of the 2 × N reconstruction of the Ge wetting layer on Si(001) investigated by surface x-ray diffraction*
T. Zhou, G. Renaud, J. Issartel, C. Revenant, T.U. Schülli, R. Felici and A. Malachias,
Phys. Rev. **B 83**, 195426 (2011)

[2.6] *H_2O diffusion barriers at Si-Si Direct bonding interfaces for low temperature anneals*
H. Moriceau, F. Rieutord, L. Libralesso, C. Ventosa, F. Fournel, C. Morales, T. Mc Cormick, T. Chevolleau and I. Radu
J. Electrochem. Soc. **158** (9) H919 (2011)

[2.6] (1) An overview of patterned metal/dielectric surface bonding: mechanism, alignment and characterization
L. Di Cioccio, P. Gueguen, R. Taibi, D. Landru, G. Gaudin, C. Chappaz, F. Rieutord, F. de Crecy, I. Radu, L.-L. Chapelon, and L. Clavelier
J. Electrochemical Soc. 158 (6) P81-86 (2011)

[2.2] (1) *Highly anisotropic epitaxial (L1)0 FePt on Pt(001)*
Soares M.M., Tolentino H.C.N., De Santis M., Ramos A.Y., Cezar J.C.
J. Appl. Phys. **109** p.07D725-1-07D725-3 (2011)

[2.2] *(4) Structure and magnetism of Ge3Mn5 clusters*
A. Jain, M. Jamet, A. Barski, T. Devillers, I.-S. Yu, C. Porret, P. Bayle-Guillemaud, V. Favre-Nicolin, S. Gambarelli, V. Maurel, G. Desfonds, J. F. Jacquot, and S. Tardif
*J. Appl. Phys. **109**, 013911 (2011)*

[1.8] (5) *In Situ μLaue: Instrumental Setup for the Deformation of Micron Sized Samples*
C. Kirchlechner, J. Keckes, J.-S.Micha and G. Dehm
Advanced Engineering Materials **13** (8) p 837-844 (2011)

[1.7] (11) *A new white beam x-ray microdiffraction setup on the BM32 beamline at the European Synchrotron Radiation Facility*
O. Ulrich, X. Biquard, P. Bleuet, O. Geaymond, P. Gergaud, J. S. Micha, O. Robach, and F. Rieutord
Rev. Sci. Instrum. **82**, 033908 (2011)

[1.5] (15) *Dislocation storage in single slip-oriented Cu micro-tensile samples: New insights via X-ray*
microdiffraction
C. Kirchlechner, D. Kiener, C. Motz, S. Labat, N. Vaxelaire, O. Perroud, J. -S. Micha, O. Ulrich, O.
Thomas, G. Dehm, and J. Keckes
Phil. Mag. **91** (7-9) Special Issue p 1256-1264 (2011)

[1.3] *Water management on semiconductor surfaces*
Y. Le Tiec, C. Ventosa, N. Rochat, F. Fournel, H. Moriceau, L. Clavelier, F. Rieutord, J. Butterbaugh, and I. Radu
Microelectronic Engineering **88**, p3432-3436 (2011)

[1.2] Combined In Situ Grazing Incidence Small Angle X-Ray Scattering and Grazing Incidence X-Ray Diffraction Study of the Growth of Ge Islands on Pit-Patterned Si(001) Substrates
M.-I. Richard, T. Schülli, G. Renaud, Z.-Z. Zhong and G. Bauer
J. Nanoscience & Nanotechnology **11**, 9123 (2011)

[1.1] (4) *Analysis of strain error sources in micro-beam Laue diffraction*
F. Hofmann, S. Eve, J. Belnoue, J.-S. Micha, and A.M. Korsunsky
Nucl. Instrum. Meth. A **660** (1) p 130-137 (2011)

(1) X-Ray diffraction determination of macro and micro stresses in SOFC electrolyte and evolution with redox cycling of the anode
Villanova J., Sicardy O., Fortunier R., Micha J.S., Bleuet P.
Materials Science Forum, vol. **681**, p.25-30 (2011)

chapitre

X-ray Diffraction analysis of elastic strains at the nanoscale
O. Thomas, O. Robach, S. Escoubas, JS. Micha, N. Vaxelaire, O. Perroud
Chapter in "Mechanical stress on the nanoscale : simulation, material systems and characterization techniques"
Ed. : M. Hanbücken, P. Müller, U. Gösele, R. B. Wehrspohn, Wiley-VCH Books, 2011

Conférences:

Growth and structure of cobalt oxide on an ultrathin PtFe epitaxial ferromagnetic layer by GIXRD
A. Lamirand, M. De Santis, H.C.N. Tolentino, M.M. Soares, A.Y. Ramos,
ECOSS-28, 28 Aug.-2 Sep., 2011, Wroclaw.

Thèses :

Plasticity at the Micron Scale: a µLaue Study
PhD Thesis, University Leoben, Autria, 2011
Christoph Kirchlechner

Grain level deformation studied by micro diffraction techniques
PhD Thesis, Oxford University, United-Kingdom, 2011
Felix Hofmann

Croissance, structure et magnétisme dans les systèmes à décalage d'échange FM/AFM : approche fondamentale par la physique des surfaces
Thèse, Université Joseph Fourier Grenoble, France, 2011
Marcio M. Soares

Nanocolonnes de GeMn : propriétés magnétiques et structurales à la lumière du synchrotron
Thèse de l'Université de Grenoble, 2011.

S. Tardif

HDR:

Etudes in situ par GISAXS de la croissance de nanoparticules
Renaud G.
Université de Grenoble, France (Diplôme d'Habilitation à Diriger des Recherches), 2011

Les publications relatives à l'utilisation de BM32 sur la période 2012-2013 sont classées par année et par ordre décroissant du facteur d'impact de la revue.

[] facteur d'impact de la revue au 13/01/2014
() nombre de citations de l'article au 13/01/2014

[30.6] *A tunable multicolour 'rainbow' filter for improved stress and dislocation density field mapping in polycrystals using X-ray Laue microdiffraction*
O. Robach, J.-S. Micha, O. Ulrich, O. Geaymond, O. sicardy, L. Haertwig, F. Rieutord
Acta Cryst **A 69**, 164-170 (2013)

[7.4] *Point defect-induced strains in epitaxial graphene*
N. Blanc, F. Jean, A. V. Krasheninnikov, G. Renaud, and J. Coraux
Phys. Rev. Lett., 111, 085501 (2013).

[4.5] *Integration techniques for SXRD data obtained with a 2D detector*
J. Drnec, T. Zhou, S. Pintea, W. Onderwaater, E. Vlieg, G. Renaud and R. Felici,
J. appl. Cryst., In press. (2013)

[4.1] *Operando atomic structure and active sites of TiO2(110)-supported gold nanoparticles during carbon monoxide oxidation*
M.C. Saint-Lager, I. Laoufi and A. Bailly
Faraday Discussions 162, 179-190 (2013)

[3.8] *In-situ observation of stress-induced stochastic twin boundary motion in off stoichiometric NiMnGa single crystals*
R.I. Barabash, C. Kirchlechner, O. Robach, Odile; O. Ulrich, J.-S. Micha, A. Sozinov and O.M. Barabash
Appl. Phys. Lett. **103** (2), 021909 (2013)

[3.8] *Interface Accommodation Mechanism for Weakly Interacting Epitaxial Systems*
A. Danescu, B. Gobaut, J. Penuelas, G. Grenet, V. Favre-Nicolin, N. Blanc, T. Zhou, G. Renaud, and G. Saint-Girons
Appl. Phys. Lett. **103**, 021602 (2013).

[3.8] *Effect of H-implantation in the local elastic properties of silicon crystals*
S. Reboh, F. Rieutord, L. Vignoud, F. Mazen, D. Landru, M. Zussy, and C. Deguet
Appl. Phys. Lett. **103**, 181911 (2013)

[3.8] *Agglomeration dynamics of germanium islands on a silicon oxide substrate: A grazing incidence small-angle x-ray scattering study*
F. Cheynis, F. Leroy, T. Passanante *et al.*
Appl. Phys. Lett. **102** (16), 161603 (2013)

[3.6] *Robust perpendicular exchange coupling in an ultrathin CoO/PtFe double layer: Strain and spin orientation*
A. D. Lamirand, M. M. Soares, A.Y. Ramos, H.C.N. Tolentino, M. De Santis, J. C. Cezar, A. de Siervo and M. Jamet
Phys. Rev. **B 88**, 140401 (2013)

[3.6] *Different commensurabilities and 10-1300 K thermal expansion of graphene on Ir(111) as a function of preparation*
F. Jean, T. Zhou, N. Blanc, J. Coraux and G. Renaud,
Phys. Rev. **B 88**, 165406 (2013)

[3.6] Local band bending and grain-to-grain interaction induced strain nonuniformity in polycrystalline CdTe films
V. Consonni, N. Baier, O. Robach, C. Cayron, F. Donatini and G. Feuillet
accepted in Phys Rev. B.

[2.6] *Treatments of deposited SiOx surfaces enabling low temperature direct bonding*
C. Rauer, H. Moriceau, F. Fournel, A.-M. Charvet, C. Morales, N. Rochat, L. Vandroux, F. Rieutord, T. Mc Cormick, and I. Radu
J. Electrochem. Soc., (2013)

[2.5] *Metal organic vapour-phase epitaxy growth of GaN wires on Si (111) for light-emitting diode applications*
D. Salomon, A. Dussaigne, M. Lafossas, C. Durand, C. Bougerol, P. and J. Eymery
Nanoscale Res. Lett. **8**, 61-1 (2013)

[2.2] *Lattice strain of hydrogen-implanted silicon : correlation between X-ray scattering analysis and ab-initio simulations.*
F. Rieutord, F. Mazen, S. Reboh, J. D. Penot, L. Bilteanu, J. P. Crocombette, V. Vales, V. Holy, and L. Capello
J. Appl. Phys. **113**, 153511, (2013)

[2.2] *Nanoscale organization by elastic interactions between H and He platelets in Si*
S. Reboh, F. Rieutord, F. Mazen, N. Cherkashin, M. F. Beaufort, J.-F. Barbot, M. Vallet, P. F. P. Fichtner, and J. Grilhé
J. Appl. Phys. **114**, 073517 (2013)

[2.2] *Development of microcracks in hydrogen-implanted silicon substrates*
J. D. Penot, D. Massy, F. Rieutord, F. Mazen, S. Reboh, F. Madeira, L. Capello, D. Landru, and O. Kononchuk
J. Appl. Phys. **114**, 123513, (2013)

[2.0] *Mechanism of Edge Bonding Void Formation in Hydrophilic Direct Wafer Bonding*
A. Castex, B. M., F. Rieutord, K. Landry, and C. Lagahe-Blanchard
Electrochem. Sol. State Lett. **2**, 47-50, (2013)

[1.6] Quantitative study of microtwins in GaP/Si thin film and GaAsPN quantum wells grown on silicon substrates
T. Nguyen Thanh, C. Robert, E. Giudicelli, A. Létoublon, C. Cornet, A. Ponchet, T. Rohel, A. Balocchi, J.S. Micha, M. Perrin, S. Loualiche, X. Marie, N. Bertru, O. Durand, A. Le Corre
J. Crystal Growth **378**, 25-28 (2013)

[1.3] *Structural investigation of nanoporous alumina film with grazing incidence small angle X-ray scattering*
D. Buttard, T. Schülli and R. Lazzari
Phys. Stat. Solid. **A** 210, 2521-2525 (2013)

[1.1] *Thermal bump removal of a Crystal Monochromator by designing an optimal shape*

J.-S. Micha, O. Geaymond, F. Rieutord
4th international workshop on Metrology for X-ray Optics, Mirror Design, and Fabrication
Barcelona, 4th to 6th July 2012
Nucl. Instr. Methods **A 710**, 155-160 (2013)

[0.9] *Hydrophobic direct bonding of silicon reconstructed surfaces*
C. Rauer, F. Rieutord, J. M. Hartmann, A.-M. Charvet, F. Fournel, D. Mariolle, C. Morales, and H. Moriceau
Microsystem Technologies, **19**, 675 (2013)

Energetic Structure of µLaue Peaks from a Plastically-Deformed Cu Cantilever Revealed by a Three-Dimensional X-ray Detector
A. Abboud, C. Kirchlechner, J.-S. Micha, O. Ulrich, S. Send, N. Pashniak, R. Hartmann, L. Struder, J. Keckes and U. Pietsch
submitted to J. Appl. Cryst.

Chapître:
Nanostructures observed by surface sensitive x-ray scattering and highly focused beams
T. Schulli, V. Favre-Nicolin M.-I. Richard and G. Renaud,
in „Characterization of Semiconductor Heterostructures and Nanostructures“, C. Lamberti ed.; second edition, 2013, pp 113-173., Elsevier.

Grazing incidence diffraction anomalous fine structure in the study of structural properties of nanostructures
H. Renevier and M.G. Proietti
In: "Characterization of Semiconductor Heterostructures and Nanostructures. 2. Edition", Lamberti C. (Eds.)Agostini G. (Eds.) (Elsevier, 2013) pp.311-359

Article de vulgarisation:
-« *Propriétés structurales de surfaces, interfaces et nanostructures étudiées à l'aide des rayons X* »
G. Renaud,
Reflets de la Physique n°34-35 et Le BUP, Hors Série N°1 , pp 65-69, 2013

Conférences
Strain-stress determination in copper filled TSVs using X-Rays diffraction : average and local approach
Christopher Krauss, Stéphane Labat , Stéphanie Escoubas, Olivier Thomas, Alexis Farcy, Jean-Sébastion Micha, Odile Robach
Materials for Advanced Metallization 10-13 March 2013, Leuven

Multi-scale X-ray diffraction study of strains induced by the implantation in UO2 polycrystals
A. Richard, E. Castelier, H. Palancher, J.S. Micha, H. Rouquette, A. Ambard, Ph. Garcia, Ph. Goudeau
17th Radiation Effects In Insulator (REI-2013) Helsinki 30th June- 5th July)
accepted in Nucl. Instr. Methods. B Proceedings

La Microdiffraction Laue des rayons X : un outil de métrologie locale
invited : Odile Robach et al

RX et matière 2013, Nantes 12-15 Novembre 2013

Mesures 3D micrométriques de la microstructure et du champ des déformations élastiques par DAXM à BM32 (ESRF)
J.-B. Marijon, F. Grennerat, O. Robach, O. Castelnau, J.-S. Micha
RX et matière 2013, Nantes 12-15 Novembre 2013

Laue micro-beam tomography on Through-Silicon-Via
Dario Ferreira Sanchez et al
RX et matière 2013, Nantes 12-15 Novembre 2013

Analyse quantitative de la perfection cristalline de nanocouches épitaxiales GaP/Si
Antoine Létoublon et al
RX et matière 2013, Nantes 12-15 Novembre 2013

Influence of dislocation pile-ups on mechanical properties of microcantilevers: New insights via in situ μLaue and in situ SEM bending experiments.
M.Kapp et al
EUROMAT 2013, Seville, 8-13 september 2013

Gallium nitride single-wires studied by X-ray diffraction: homogeneous wires and core-shell heterostructures
J. Eymery, C. Durand, D. Salomon, V. Favre-Nicolin, F. Rieutord, O. Robach, J.S. Micha, M. Burghammer, E. Di Cola, M. Reynolds
E-MRS, strasbourg, May 2013

A tunable multi-color "rainbow" filter for improved stress and dislocation field mapping in polycrystals using x-ray Laue microdiffraction
O. Robach, J.-S. Micha, Olivier Ulrich, Olivier Geaymond, Olivier Sicardy, Jürgend Härtwig, François Rieutord
TMS 2013, San Antonio (US/TX), 3rd – 7th march 2013

Prix

T. Zhou: prix de la meilleure présentation Science Days ESRF Oct 2013
A. Lamirand: prix du meilleur poster Science Days ESRF Oct 2013

Thèse

K. Hestroffer
Croissance et caractérisation de nanofils de GaN et d'hétérostructures - Growth and characterization of GaN nanowires and GaN/AlN heterostructure nanowires
Université de Grenoble, France (PhD Thesis, 2013)

C. Leclere
Spectroscopies X et diffraction anomale de boîtes quantiques GaN et d'hétéro-structures III-N : inter-diffusion et ordre à courte distance

Université de Grenoble, France (PhD Thesis, 2013)

2012

[10.6] (1) Controlling *Interactions in supported bilayers from weak electrostatic repulsion to high osmotic pressure*
A. Hemmerle, L. Malaquin , T. Charitat,, S. Lecuyer, G. Fragneto and J. Daillant
Proc. Nat. Acad. Sciences USA **109** (49) 19938-19942 (2012)

[6.2] (3) *From metastable to stable modifications—in situ Laue diffraction investigation of diffusion processes during the phase transitions of (GeTe)nSb2Te3 (6 <= n <= 15) crystals*
M. N. Schneider, X. Biquard, C. Stiewe, T. Schröder, P. Urban and O. Oeckler
Chemical Communications **48** (16) 2192-2194 (2012)

[5.2] (3) CO-Induced Scavenging of Supported Pt Nanoclusters: A GISAXS Study
N. Chaabane, R. Lazzari, J. Jupille, G. Renaud, and E. A. Soares
J. Phys. Chem. **C, 116** (44), 23361-23370 (2012)

[4.5] (1) *Strains in light ion implanted polycrystals: influence of grain orientation*
A. Richard, H. Palancher, E. Castelier, J. S. Micha, M. Gamaleri, G. Carlot, H. Rouquette, P. Goudeau, G. Martin, F. Rieutord, J. P. Piron and P. Garcia
J. Appl. Cryst. **45** (4) 826-833 (2012)

[4.5] (1) *Multi scale measurements of residual strains in stabilized zirconia layer*
J. Villanova, C. Maurice, J.-S. Micha, P. Bleuet, O. Sicardy and R. Fortunier
J. Appl. Cryst. **45** (5) p 926-935. (2012)

[4.4] (3) *Expected and unexpected plastic behavior at the micron scale: An in situ Laue tensile study*
C. Kirchlechner , P.J. Imrich, W. Grosinger, M.W. Kapp, J. Keckes, J.S. Micha, O. Ulrich, O. Thomas, S. Labat, C. Motz, and G. Dehm
Acta Mater. **60** (3) 1252-1258 (2012)

[3.8] (5) In situ study of self-assembled GaN nanowires nucleation on Si(111) by plasma-assisted molecular beam epitaxy
K. Hestroffer, C. Leclere, V. Cantelli, C. Bougerol, H. Renevier and B. Daudin
Appl. Phys. Lett. **100** (21) 212107 (2012)

[3.6] (4) *Interface-driven phase separation in multifunctional materials: The case of the ferromagnetic semiconductor GeMn*
E. Arras, F. Lançon, I. Slipukhina, É. Prestat, M. Rovezzi, S. Tardif, A. Titov, P. Bayle-Guillemaud, F. d'Acapito, A. Barski, V. Favre-Nicolin, M. Jamet, J. Cibert, and P. Pochet
Phys. Rev. B **85,** 115204 (2012)

[3.6] (1) *Chemically ordered MnPt ultrathin films on Pt(001) substrate: Growth, atomic structure, and magnetic properties*
M. M. Soares, M. De Santis, H. C. N. Tolentino, A. Y. Ramos, M. El Jawad and Y. Gauthier

Phys. Rev. B **85**, 205417 (2012)

[3.6] (1) *Epitaxial orientation changes in a dewetting gold film on Si(111)*
R. Daudin, T. Nogaret, T.-U. Schülli, N. Jakse, A. Pasturel and G. Renaud
Phys. Rev. **B 86**, 094103 (2012)

[3.6] *Dynamics, anisotropy, and stability of silicon-on-insulator dewetting fronts*
F. Leroy, F. Cheynis, T. Passanante, and P. Müller
Phys. Rev. **B 85**, 195414 (2012) and erratum **85** 239901 (2012)

[3.6] (2) *Local deformations and incommensurability of high quality epitaxial graphene on a weakly interacting transition metal*
N. Blanc, J. Coraux, C. Vo-Van, A. T. N'Diaye, O. Geaymond, and G. Renaud
Phys. Rev. **B 86**, 235439 (2012)

[2.4] (5) *Floating lipid bilayers: Models for physics and biology*
Fragneto G. Charitat T. Daillant J. -
European Biophysics Journal 41, 863-874 (2012)

[2.2] (1) *Measurement of bonding energy in an anhydrous nitrogen atmosphere and its application to silicon direct bonding technology*
F. Fournel, L. Contini, C. Morales, J. Da Fonseca, H. Moriceau, F. Rieutord, A. Barthelemy and I. Radu
J. Appl. Phys. **111** (10) 104907 (2012)

[2.2] (8) *Structural and optical analyses of GaP/Si and (GaAsPN/GaPN)/GaP/Si nanolayers for integrated photonics on silicon*
T. Nguyen Thanh, C. Robert, W. Guo, A. Letoublon, C. Cornet, G. Elias, A. Ponchet, T. Rohel, N. Bertru, A. Balocchi, O. Durand, J.-S. Micha, M. Perrin, S. Loualiche, X. Marie and A. Le Corre
J. Appl. Phys. **112**, 053521 (2012)
Publisher erratum: J. Appl. Phys. **112**, 079904 (2012)

[2.2] *Low temperature direct bonding mechanisms of tetraethyl orthosilicate based silicon oxide films deposited by plasma enhanced chemical vapor deposition*
C. Sabbione, L. Di Cioccio, L. Vandroux, J.-P. Nieto, and F. Rieutord
J. Appl. Phys. **112**, 063501 (2012)

[1.7] (2) Advances in martensitic transformations in Cu-based shape memory alloys achieved by in situ neutron and synchrotron X-ray diffraction methods
B. Malard, P. Sittner, S. Berveiller, E. Patoor
Compt. Rend. Physique **13** (2012) 280–292

[1.5] Investigation of reversible plasticity in a micron-sized, single crystalline copper bending beam by X-ray μLaue diffraction
C. Kirchlechner, W. Grosinger, M.W. Kapp, P.J. Imrich, J.-S. Micha, O. Ulrich, J. Keckes, G. Dehm and C. Motz
Philosophical Magazine **92** (25-27), 3231-3242 (2012)

[1.4] (4) *Growth and dewetting of gold on Si(1 1 1) investigated in situ by grazing incidence small angle x-ray scattering*
R. Daudin, C. Revenant, G. Davi and G. Renaud
Physica **E 44**, 1905 (2012)

[1.2] *Low temperature direct bonding: an attractive technique for heterostructures build-up*
H. Moriceau, F. Rieutord, F. Fournel, C. Moulet, L. Libralesso, P. Gueguen, R. Taibi and C. Deguet
Microelectronics Reliability **52** (2) p 331-341 (2012)

[1.2] Regular arrays of palladium and palladium-gold clusters supported on ultrathin alumina films: stability under oxygen
G. Sitja, M. Marsault, F. Leroy *et al.*
Int. J. Nanotech. **9** (3-7) 567-575 (2012)

[1.1] (3) *Si exfoliation by MeV proton implantation*
C. Braley, F. Mazen, A. Tauzin, F. Rieutord, C. Deguet and E. Ntsoenzok
Nucl. Instr. Methods ***B 277, 93-97 (2012)***

[1.1] (1) *Smart Cut™: review on an attractive process for innovative substrate elaboration*
H. Moriceau, F. Mazen, C. Braley, F. Rieutord, A. Tauzin, and C. Deguet,
Nucl. Instrum. Meth. **B 277**, p 84-92 (2012)

chapitre:
"Strain and dislocation gradients from diffraction : Spatially-resolved local structure and defects, chapter 5"
Robach, O., Kirchlechner, C., Micha, J.-S., Ulrich, O., Biquard, X., Geaymond, O., Castelnau, O., Bornert, M., Petit, J., Berveiller, S., Sicardy, O., Villanova, J., and Rieutord, F.
in Strain and dislocation gradients from diffraction (2012)
Imperial College Press and World Scientific Publishing.
R. I. Barabash and G. E. Ice editors

proceedings

Bio-materials characterization across multiple scales at Oxford HEX-lab
Sui T. Hofmann F. Song X. Tao L. Zeng K. Korsunsky A.M.
Lecture Notes in Engineering and Computer Sciences 2199, 1657-1662 (2012)
In: "Proceedings of the World Congress on Engineering, International Association of Engineers", 2012) pp.1657-1662

Combining Laue microdiffraction and digital image correlation for improved measurements of the elastic strain
field with micrometer spatial resolution
J. Petit, M. Bornert, F. Hofmann, O. Robach, J.-S. Micha, O. Ulrich, C. Le Bourlot, D. Faurie, A.M. Korsunsky and O. Castelnau
Procedia IUTAM 4 (2012) 133 – 143

Daudin B. Bougerol C. Camacho D. Cros A. Gayral B. Hestroffer K. Leclere C. Mata R. Niquet Y.M. Renevier H. Sam-Giao D. Tourbot G. - Growth, structural and optical properties of GaN/AlN and GaN/GaInN nanowire heterostructures
Physics Procedia 28, 5-16 (2012)
15th Brazilian Workshop On Semiconductors

Coherent integration of photonics on silicon through the growth of nanostructures on GaP/Si
Thanh, TN ; Robert, C ; Cornet, C; Guo, W ; Letoublon, A ; Perrin, M ; Bertru, N ; Even, J ; Chevalier, N ; Folliot, H; Loualiche, S ; Ponchet, A ; Elias, G; Micha, JS; Durand, O ; Le Corre, A
Quantum Sensing and Nanophotonic devices IX Book Series: Proceedings of SPIE
8268 , 82681H (2012)

Fracture in (100)Si after high energy protons implantation
Braley C. Mazen F. Papon A.M. Charvet A.M. Rieutord F. Ntsoenzok E.
Special Issue: E-MRS 2012 Spring Meeting – Symposium A
Physica Status Solidi (c) 9, 2023-2026 (2012)

Thèses :

Mathieu Guerain , Université de La Rochelle , 05 Octobre 2012, Sciences des Matériaux
Contribution à l'étude des mécanismes de relaxation de contraintes dans les films de chromine formés sur Ni-30Cr et Fe-47Cr : approche multi-échelle par spectroscopie Raman et microdiffraction Synchrotron

Gael Daveau, Ecole Centrale Paris, 19 septembre 2012, Mécanique et Matériaux
Interaction dislocations - joints de grains en déormation plastique monotone : éude expérimentale et modélisations numériques

Axel Richard, Université de Poitiers, 22 Novembre 2012,
Etude par diffraction des rayons X des déformations induites par iraadiation/implantation d'ions dans le dioxyde d'uranium

Jean-Claude Bastien
Étude des matériaux à changement de phase pour application dans le domaine des PCRAM

Audrey Bastard
Analyse théorique et physique de matériaux pour application aux Mémoires à Changement de Phases (PCRAM)

Rémi Daudin, Février 2012
"Formation and supercooling of AuSi eutectic droplets on Si substrates: an in-situ study using synchrotron radiation"

Conférences:

Relations contraintes résiduelles – endommagement dans des systèmes oxydes thermiques sur métal : apports de la spectroscopie Raman et de la micro-diffraction Synchrotron
M. Guerain, J.L. Grosseau-Pouyssard, P. Goudeau, B. Panucaud, N. Tamura, M. Kunz, J.-S. Micha.,
Colloque GFAC-SF2M, St Nazaire, 3-4/04/2012
and
8th International Symposium on High-Temperature Corrosion and Protection of Materials 2012, 20-25 Mai 2012, Les Embiez

Use of Raman Spectroscopy and Synchrotron micro-Diffraction to investigate stress in thermal oxide films : a multiscale approach
FAC: Déformations élastiques dans des échantillons polycristallins d'UO2 implantés en hélium : mesures par micro diffraction Laue et modélisation élastique
É. Castelier, H. Palancher, A. Richard, J.-S. Micha, P. Goudeau

Combining Laue microdiffraction and digital image correlation for improved stress field measurements
with micrometer spatial resolution
F. Zhang, O. Castelnau, M. Bornert, J. Petit, O. Robach, J.S. Micha, F. Hofmann, A. Korsunsky
Int. Conf. of Residual Stresses (oct 2012)

Strain-stress determination in silicon around copper filled TSVs using Laue microdiffraction
C. Krauss, S. Labat, S. Escoubas, O. Thomas, M. Bouchoucha, L.-L. Chapelon, P. Chausse, J.-S. Micha and O. Ulrich
12th Workshop on Stress-Induced Phenomena in Microelectronics.
Kyoto du 28 au 30 Mai 2012

Measuring energy profiles of Laue spots : a third method RSI
O. Robach et al
oral communication RSI 2012

Combined Analysis of Delamination Process at the Surface of Cr2O3 Thermal Oxide Films
P. Goudeau , M. Guerain , J.-L. Grosseau- Poussard, N. Tamura , M. Kunz , J.-S. Micha ,
oral communication MRS Fall

Influence of Grain Orientation on Radiation Induced Strains in UO2 Polycrystals
P. Goudeau , E. Castelier , H. Palancher , A. Richard, J.-S. Micha ,
oral communication MRS Fall

μ-XRD study of strains in light ion implanted polycrystals: influence of grain orientation
H. Palancher, A. Richard, E. Castelier, J.S Micha, Ph. Goudeau, Ph. Garcia
oral communication JMC13

ESRF Highlights

An alternative pathway for understanding plasticity at the micron scale
C. Kirchlechner et al

2011

[14.1] (25) *M-plane core-shell InGaN/GaN multiple-quantum-well on GaN wires for electroluminescent device*
R. Koester, J. S. Hwang, D. Salomon, X. Chen, C. Bougerol, J.-P. Barnes, D. Le Si Dang, L. Rigutti, M. Tchernycheva, C. Durand and J. Eymery
Nano Letters **11**, p 4839-4845 (2011)

[4.5] (7) *Full local elastic strain tensor from Laue microdiffraction: simultaneous Laue pattern and spot energy measurement*
O. Robach, J.-S. Micha, O. Ulrich and P. Gergaud
J. Appl. Cryst.. **44** p 688–696 (2011)

[5.2] (27) *Size and Catalytic Activity of Supported Gold Nanoparticles: An in operando Study During CO Oxidation*
I. Laoufi, M.-C. Saint-Lager, R. Lazzari, J. Jupille, O. Robach, S. Garaudee, G. Cabailh, P. Dolle, H. Cruguel, A. Bailly
J. Phys. Chem. **C 115** (11) pp 4673-4679 (2011)

[5.2] (11) *Competition between polar and nonpolar growth of MgO films on Au(111)*
S. Benedetti , N. Nilius, P. Myrach, P. Torelli, G. Renaud, H.-J. Freund, S. Valeri
J. Phys. Chem. **C 115,** 23043 (2011)

[5.0] (3) *In situ grazing-incidence X-ray diffraction during electrodeposition of birnessite thin films: Identification of solid precursors*
M. Ndjeri, S. Peulon, M.L. Schlegel, A. Chaussé
Electrochem. Commun. **13**, (5) p 491-494 (2011)

[4.4] (3) *In situ synchrotron analysis of lattice rotations in individual grains during stress-induced martensitic transformations in a polycrystalline CuAlBe shape memory alloy*
Berveiller S., Malard B., Wright J., et al.
Acta Mater. **59** (9) p 3636-3645 (2011)

[4.4] (4) *Impact of instrumental constraints and imperfections on the dislocation structure in micron-sized Cu compression pillars*
Kirchlechner C., Keckes J., Motz C., Grosinger W., Kapp M.W., Micha J.S., Ulrich O. and Dehm G.
Acta Mater. **59** (14) p 5618-5626 (2011)

[4.1] (6) *Catalytic properties of supported gold nanoparticles: new insights into the size-activity relationship gained from in operando measurements*
M.-C. Saint-Lager, I. Laoufi, A. Bailly, O. Robach, S. Garaudée and P. Dolle
Faraday Discuss., **152**, p253–265 (2011)

[3.8] (3) *Effect of doping on global and local order in crystalline GeTe*
Biquard X., Krbal M., Kolobov A. V. *et al*

Appl. Phys. Lett. **98** (23) 231907 (2011)

[3.8] (1) *In situ x-ray study of the formation of defects in Ge islands on Si(001)*
M.-I. Richard, T. U. Schülli, and G. Renaud
Appl. Phys. Lett. **99** 161905 (2011)

[3.8] (7) *Catalyst-free growth of high-optical quality GaN nanowires by metal-organic vapor phase epitaxy*
X.J. Chen, B. Gayral, D. Sam-Giao, C. Bougerol, C. Durand and J. Eymery
Appl. Phys. Lett. **99** (25) 251910 (2011)

[4.0] *Metal positioning using dislocation arrays.*
A. Bavard, F. Fournel and J. Eymery
Nanotechnology **22**, 215301(2011)

[3.6] (2) *Twins and their boundaries during homoepitaxy on Ir(111)*
S. Bleikamp, J. Coraux, O. Robach, G. Renaud and T. Michely,
Phys. Rev. **B 83** 064103 (2011)

[3.6] (4) Tracking defect type and strain relaxation in patterned Ge/Si(001) islands by x-ray forbidden reflection analysis
M.I. Richard, A. Malachias, J.-L. Rouvière, T.-S. Yoon, E. Holmström, Y.-H. Xie, V. Favre-Nicolin, V. Holy, K. Nordlund, G. Renaud, T.-H. Metzger
Phys. Rev. **B 84**, 075314 (2011)

[3.6] (4) *Atomic structure and composition of the 2 × N reconstruction of the Ge wetting layer on Si(001) investigated by surface x-ray diffraction*
T. Zhou, G. Renaud, J. Issartel, C. Revenant, T.U. Schülli, R. Felici and A. Malachias,
Phys. Rev. **B 83**, 195426 (2011)

[2.6] *H_2O diffusion barriers at Si-Si Direct bonding interfaces for low temperature anneals*
H. Moriceau, F. Rieutord, L. Libralesso, C. Ventosa, F. Fournel, C. Morales, T. Mc Cormick, T. Chevolleau and I. Radu
J. Electrochem. Soc. **158** (9) H919 (2011)

[2.6] (1) An overview of patterned metal/dielectric surface bonding: mechanism, alignment and characterization
L. Di Cioccio, P. Gueguen, R. Taibi, D. Landru, G. Gaudin, C. Chappaz, F. Rieutord, F. de Crecy, I. Radu, L.-L. Chapelon, and L. Clavelier
J. Electrochemical Soc. 158 (6) P81-86 (2011)

[2.2] (1) *Highly anisotropic epitaxial (L1)0 FePt on Pt(001)*
Soares M.M., Tolentino H.C.N., De Santis M., Ramos A.Y., Cezar J.C.
J. Appl. Phys. **109** p.07D725-1-07D725-3 (2011)

[2.2] *(4) Structure and magnetism of Ge3Mn5 clusters*
A. Jain, M. Jamet, A. Barski, T. Devillers, I.-S. Yu, C. Porret, P. Bayle-Guillemaud, V. Favre-Nicolin, S. Gambarelli, V. Maurel, G. Desfonds, J. F. Jacquot, and S. Tardif

J. Appl. Phys. ***109****, 013911 (2011)*

[1.8] (5) *In Situ μLaue: Instrumental Setup for the Deformation of Micron Sized Samples*
C. Kirchlechner, J. Keckes, J.-S.Micha and G. Dehm
Advanced Engineering Materials **13** (8) p 837-844 (2011)

[1.7] (11) *A new white beam x-ray microdiffraction setup on the BM32 beamline at the European Synchrotron Radiation Facility*
O. Ulrich, X. Biquard, P. Bleuet, O. Geaymond, P. Gergaud, J. S. Micha, O. Robach, and F. Rieutord
Rev. Sci. Instrum. **82**, 033908 (2011)

[1.5] (15) *Dislocation storage in single slip-oriented Cu micro-tensile samples: New insights via X-ray*
microdiffraction
C. Kirchlechner, D. Kiener, C. Motz, S. Labat, N. Vaxelaire, O. Perroud, J. -S. Micha, O. Ulrich, O.
Thomas, G. Dehm, and J. Keckes
Phil. Mag. **91** (7-9) Special Issue p 1256-1264 (2011)

[1.3] *Water management on semiconductor surfaces*
Y. Le Tiec, C. Ventosa, N. Rochat, F. Fournel, H. Moriceau, L. Clavelier, F. Rieutord, J. Butterbaugh, and I. Radu
Microelectronic Engineering **88**, p3432-3436 (2011)

[1.2] Combined In Situ Grazing Incidence Small Angle X-Ray Scattering and Grazing Incidence X-Ray Diffraction Study of the Growth of Ge Islands on Pit-Patterned Si(001) Substrates
M.-I. Richard, T. Schülli, G. Renaud, Z.-Z. Zhong and G. Bauer
J. Nanoscience & Nanotechnology **11**, 9123 (2011)

[1.1] (4) *Analysis of strain error sources in micro-beam Laue diffraction*
F. Hofmann, S. Eve, J. Belnoue, J.-S. Micha, and A.M. Korsunsky
Nucl. Instrum. Meth. A **660** (1) p 130-137 (2011)

(1) X-Ray diffraction determination of macro and micro stresses in SOFC electrolyte and evolution with redox cycling of the anode
Villanova J., Sicardy O., Fortunier R., Micha J.S., Bleuet P.
Materials Science Forum, vol. **681**, p.25-30 (2011)

chapitre

X-ray Diffraction analysis of elastic strains at the nanoscale
O. Thomas, O. Robach, S. Escoubas, JS. Micha, N. Vaxelaire, O. Perroud
Chapter in “Mechanical stress on the nanoscale : simulation, material systems and characterization techniques”
Ed. : M. Hanbücken, P. Müller, U. Gösele, R. B. Wehrspohn, Wiley-VCH Books, 2011

Conférences:

Growth and structure of cobalt oxide on an ultrathin PtFe epitaxial ferromagnetic layer by GIXRD
A. Lamirand, M. De Santis, H.C.N. Tolentino, M.M. Soares, A.Y. Ramos,
ECOSS-28, 28 Aug.-2 Sep., 2011, Wroclaw.

Thèses :

Plasticity at the Micron Scale: a µLaue Study
PhD Thesis, University Leoben, Autria, 2011
Christoph Kirchlechner

Grain level deformation studied by micro diffraction techniques
PhD Thesis, Oxford University, United-Kingdom, 2011
Felix Hofmann

Croissance, structure et magnétisme dans les systèmes à décalage d'échange FM/AFM : approche fondamentale par la physique des surfaces
Thèse, Université Joseph Fourier Grenoble, France, 2011
Marcio M. Soares

Nanocolonnes de GeMn : propriétés magnétiques et structurales à la lumière du synchrotron
Thèse de l'Université de Grenoble, 2011.
S. Tardif

HDR:

Etudes in situ par GISAXS de la croissance de nanoparticules
Renaud G.
Université de Grenoble, France (Diplôme d'Habilitation à Diriger des Recherches), 2011